REMOVAL OF EMERGING CONTAMINANTS FROM URBAN WATER SYSTEMS BY USING TiO_2 COATED $CuWO_4$ NANOCATALYST



By

Md. Mahfujur Rahman

ID-20MSCHEM013F

A thesis submitted in partial fulfillment of the requirements for the degree of

MASTER of SCIENCE in Chemistry

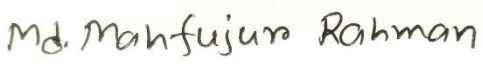
Department of Chemistry

CHITTAGONG UNIVERSITY OF ENGINEERING AND TECHNOLOGY

September 2025

Declaration

I hereby declare that the work contained in this thesis has not been previously submitted to meet requirements for an award at this or any other higher education institution. To the best of my knowledge and belief, the Thesis contains no material previously published or written by another person except where due reference is cited. Furthermore, the Thesis complies with PLAGIARISM and ACADEMIC INTEGRITY regulations of CUET.



Md. Mahfujur Rahman

ID-20MSCHEM013F

Department of Chemistry

Chittagong University of Engineering & Technology (CUET)

Copyright © Md. Mahfujur Rahman, 2025.

This work may not be copied without the permission of the author or Chittagong University of Engineering & Technology.

Dedication

To my beloved parents

List Of Publications

Journal Articles:

- "Harnessing neural network model with optimization for enhanced ciprofloxacin antibiotic adsorption from contaminated water: A transparent and objective framework" Yunus Ahmed, **Md. Mahfujur Rahman**, Md. Shafiul Alam, Mohammad Islam Miah, Md. Shamimul Haque Choudhury, Obaid A. Alharbi, Parul Akhtar, Syed Masiur Rahman, Journal of Water Process Engineering DOI: https://doi.org/10.1016/j.jwpe.2024.105724. (IF: 6.3, Q1)

- "Synthesis, Characterization, Optimization, and Application of Nano-adsorbent for the Removal of Antibiotics and Textile Dye from Aqueous Solutions" **Md. Mahfujur Rahman**, Md. Arif Hossen, Akser Alam Siddiqua Maya, Keya Rani Dutta, Tahmina Akter and Yunus Ahmed. (Draft Manuscript)

Conferences:

- "Modeling and optimization of $CuWO_4@TiO_2$ nanocatalyst for the removal of ciprofloxacin and methylene blue." **Md. Mahfujur Rahman**, Tahmina Akter, Akser Alam Siddiqua Maya, Keya Dutta, and Dr. Yunus Ahmed. 7th ICNST, Asian University for Women, 02-03 March 2023.

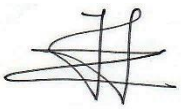
- "Photocatalytic Activity of $CuWO_4@TiO_2$ Nanocomposites: Synthesis, Optimization, and Application in Wastewater Treatment." Keya Rani Dutta, **Md. Mahfujur Rahman**, Akser Alam Siddiqua Maya and Yunus Ahmed. 2nd ICRAC-2024, Jagannath University, 31 January – 02 February 2025.

- "Synthesis, Characterization, Optimization, and Application of $CuWO_4@TiO_2$ Nanoadsorbent for the Removal of Antibiotic from Aqueous Solution." Yunus Ahmed, **Md. Mahfujur Rahman**, Akser Alam Siddiqua Maya, Tahmina Akter, Keya Rani Dutta, Obaide Alharbi. 19th IWA-LET, Essen, Germany, 24-28 June 2024.

- "Antibiotic-Resistant Bacteria and its Genes in Urban Water: Making the Invisible Visible." Akser Alam Siddiqua Maya**, Md. Mahfujur Rahman**, Yunus Ahmed. BCSIR Congress 2022, BCSIR, 01-03 December 2022.

Approval/Declaration by the Supervisor(s)

This is to certify that **Md. Mahfujur Rahman** has carried out this research work under our supervision, and that he has fulfilled the relevant Academic Ordinance of the Chittagong University of Engineering and Technology, so that he is qualified to submit the following Thesis in the application for the degree of MASTER of SCIENCE in Chemistry. Furthermore, the Thesis complies with the PLAGIARISM and ACADEMIC INTEGRITY regulations of CUET.

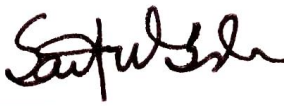


Dr. Yunus Ahmed (Supervisor)

Professor

Department of Chemistry

Chittagong University of Engineering & Technology



Dr. Saiful Islam (Co-supervisor)

Principal Scientific Officer

Industrial Microbiology and Research Division

Bangladesh Council of Scientific and Industrial Research, Chattogram.

Acknowledgment

All praise to Merciful and Almighty Allah (SWT), who gave me the capability and opportunity to complete the research and submit this thesis for the degree of Master of Science (M.Sc.) in Chemistry.

I am deeply grateful to my principal supervisor, Dr. Yunus Ahmed, Professor, Department of Chemistry, CUET, for his invaluable guidance, unwavering support, and continuous encouragement throughout my research. His insightful supervision and dedication played a vital role in the successful completion of this thesis. I would like to express my sincere gratitude to my co-supervisor, Dr. Saiful Islam, Principal Scientific Officer, IMRD, BCSIR, Chattogram, for granting me the opportunity to work in the microbiology laboratory at BCSIR and for his valuable guidance, mentorship, and support throughout my research.

I am also thankful to all the respected teachers and staff of the Department of Chemistry, CUET, for their collaboration, continual inspiration, and constant encouragement during this journey.

My heartfelt thanks go to my friends from the Department of Chemistry, CUET, for their valuable discussions and cooperation, especially Akser Alam, Siddiqua Maya, and Syed Julkar Nine. I would also like to acknowledge my juniors—Keya Rani Dutta, Tahmina Akter, Meherunnesa Prima, Sharmin Nahar Chowdhury Nepu, and Afrin Sultana—for their kind assistance, encouragement, and support. A special note of appreciation goes to my student, Abdullah Bin Sohel, for his helpful cooperation during this work.

I express my deepest gratitude to my beloved parents, Md. Zakir Hossain and Mst. Mahfuja Khatun, for their unconditional love, unwavering support, continuous encouragement, and countless sacrifices throughout the course of my academic life.

Finally, I gratefully acknowledge the Planning and Development (P&D) Office, CUET, for providing financial support through a scholarship that significantly contributed to the completion of this research.

CERTIFICATION

The thesis titled **"REMOVAL OF EMERGING CONTAMINANTS FROM URBAN WATER SYSTEMS USING TiO_2 COATED $CuWO_4$ NANOCATALYST"** submitted by **Md. Mahfujur Rahman** (Student ID: **20MSCHEM013F** of Session: 2020-2021) has been accepted as satisfactory in partial fulfilment of the requirement for the degree of **Master of Science in Chemistry** on 8th July, 2025.

BOARD OF EXAMINERS

1. 8/7/2025
Professor Dr. Yunus Ahmed
Department of Chemistry, CUET
Chattogram-4349, Bangladesh.
Chairman
(Supervisor)

2. 08.07.25
Dr. Saiful Islam
Principal Scientific Officer, IMRD, BCSIR
Chattogram-4220, Bangladesh.
Member
(Co-Supervisor)

3. _____
Professor Dr. Mst. Roksana Khatun
Head, Department of Chemistry, CUET
Chattogram-4349, Bangladesh.
Member
(Ex-Officio)

4. 08.07.25
Professor Dr. Md. Rezaul Karim
Department of Chemistry, CUET
Chattogram-4349, Bangladesh.
Member

5. 8.7.25
Professor Dr. M. K. Mohammad Ziaul Hyder
Department of Chemistry, CUET
Chattogram-4349, Bangladesh.
Member

6. _____
Professor Dr. Newaz Mohammed Bahadur
Department of Chemistry
Noakhali Science and Technology University
Noakhali-3814, Bangladesh.
Member
(External)

Mahfuj (20MSCHEM013F).docx

ORIGINALITY REPORT

19%	11%	18%	4%
SIMILARITY INDEX	INTERNET SOURCES	PUBLICATIONS	STUDENT PAPERS

PRIMARY SOURCES

1	Submitted to University of Mosul Student Paper	1%
2	www.mdpi.com Internet Source	1%
3	Chinenye Adaobi Igwegbe, Stephen N. Oba, Chukwunonso O. Aniagor, Adewale George Adeniyi, Joshua O. Ighalo. "Adsorption of Ciprofloxacin from Water: A Comprehensive Review", Journal of Industrial and Engineering Chemistry, 2020 Publication	1%
4	Amirhossein Khazaie, Hirsa Kia, Elham Moniri, Amir Hessam Hassani, Mahsasadat Miralinaghi. "Adsorption modeling of tetracycline removal by multi-walled carbon nanotube functionalized with aspartic acid and poly-pyrrole using Bayesian optimized artificial neural network", Journal of the Taiwan Institute of Chemical Engineers, 2023 Publication	1%
5	Submitted to University of Warwick Student Paper	<1%
6	mdpi-res.com Internet Source	<1%
7	Nafisur Rahman, Poornima Varshney. " Assessment of ampicillin removal efficiency	<1%

Abstract

The growing presence of antibiotics in urban water systems poses serious risks to environmental and human health. This thesis presents a comprehensive approach to remove ciprofloxacin (CIP), a widely used and persistent antibiotic, using a TiO_2-coated $CuWO_4$ ($CuWO_4$@TiO_2) core-shell nanocatalyst. The nanomaterial was synthesized via a two-step hydrothermal method and thoroughly characterized using FTIR, XRD, FESEM, XPS, and BET techniques, confirming its core-shell architecture, surface properties, and active sites. Batch adsorption experiments, optimized through Response Surface Methodology (RSM), demonstrated over 99% CIP removal under neutral pH conditions with optimal parameters including 10 mg/L initial CIP concentration, 300 mg/L adsorbent dose, and 40 minutes of contact time. The adsorption process followed the Langmuir isotherm and pseudo-second-order kinetic models, with a maximum theoretical adsorption capacity of 109.58 mg/g. The material showed strong reusability, retaining high removal efficiency after five adsorption–desorption cycles. Complementing the experimental study, a multilayer perceptron (MLP) neural network model was developed using experimental data to predict CIP removal efficiency. Hyperparameter tuning via Bayesian and Random Search, coupled with Particle Swarm Optimization (PSO), yielded highly accurate predictions, with R^2 values up to 0.9985 for training and R^2 0.9856 for testing. Feature importance analysis identified contact time and adsorbent dosage as the most influential factors. This work provides a robust and transparent machine learning-integrated framework for optimizing nanomaterial-based antibiotic removal, contributing to the advancement of sustainable water treatment technologies.

বিমূর্ত

নগরজীবনের জলাধারগুলিতে অ্যান্টিবায়োটিকের ক্রমবর্ধমান উপস্থিতি পরিবেশ এবং মানব স্বাস্থ্যের জন্য গুরুতর হুমকি সৃষ্টি করছে। এই থিসিসে সিপ্রোফ্লক্সাসিন (CIP) নামক একটি বহুল ব্যবহৃত এবং স্থায়ী অ্যান্টিবায়োটিক অপসারণের জন্য TiO_2-কোটিংকৃত $CuWO_4$ ($CuWO_4@TiO_2$) কোর-শেল ন্যানোক্যাটালিস্ট ব্যবহারের একটি সমন্বিত পদ্ধতি উপস্থাপন করা হয়েছে। কোর-শেল ন্যানোক্যাটালিস্টটি দুই ধাপে হাইড্রোথার্মাল পদ্ধতিতে সংশ্লেষিত হয় এবং FTIR, XRD, FESEM, XPS ও BET বিশ্লেষণের মাধ্যমে চরিত্রায়িত করা হয়, যা এর কোর-শেল গঠন, পৃষ্ঠ বৈশিষ্ট্য ও সক্রিয় সাইট নিশ্চিত করে। রেসপন্স সারফেস মেথডোলজি (RSM) দ্বারা অপ্টিমাইজ করা ব্যাচ অ্যাডসোরপশন পরীক্ষায় নিরপেক্ষ pH অবস্থায় ১০ mg/L CIP, ৩০০ mg/L অ্যাডসোরবেন্ট ডোজ ও ৪০ মিনিট প্রতিক্রিয়া সময়ে ৯৯% এর বেশি CIP অপসারণ দেখানো হয়েছে। অ্যাডসোরপশন প্রক্রিয়া Langmuir আইসোথার্ম এবং pseudo second order কাইনেটিক মডেল অনুসরণ করে, যার সর্বোচ্চ তাত্ত্বিক অ্যাডসোরপশন ক্ষমতা ১০৯.৫৮ mg/g। সংশ্লেষিত উপাদানটি পাঁচটি পুন: চক্রের পরেও উচ্চ অপসারণ দক্ষতা ধরে রাখে, যা এর পুনঃব্যবহারযোগ্যতা নিশ্চিত করে। পরীক্ষামূলক তথ্য ব্যবহার করে একটি মাল্টি-লেয়ার পার্সেপট্রন (MLP) নিউরাল নেটওয়ার্ক মডেল তৈরি করা হয় এবং CIP অপসারণ দক্ষতা পূর্বাভাসের জন্য। বাইয়েসিয়ান ও র‍্যান্ডম সার্চ এবং পার্টিকেল সোয়ার্ম অপটিমাইজেশন (PSO) এর মাধ্যমে হাইপারপ্যারামিটার টিউনিং করে অত্যন্ত নির্ভুল পূর্বাভাস অর্জন করা হয়, যেখানে প্রশিক্ষণ ও পরীক্ষণ সেটে R^2 মান যথাক্রমে ০.৯৯৮৫ এবং ০.৯৮৫৬ হয়। ফিচার ইম্পর্টেন্স বিশ্লেষণে দেখা যায়, প্রতিক্রিয়া সময় এবং অ্যাডসোরবেন্ট ডোজ CIP অপসারণে সবচেয়ে প্রভাবশালী ভূমিকা পালন করে। এই গবেষণাটি একটি শক্তিশালী ও স্বচ্ছ মেশিন লার্নিং-ভিত্তিক কাঠামো উপস্থাপন করে যা ন্যানোম্যাটেরিয়াল ব্যবহার করে টেকসই পানি পরিশোধন প্রযুক্তির উন্নয়নে সহায়ক হবে।

Table of Contents

Declaration i

Dedication ii

List Of Publications iii

Approval/Declaration by the Supervisor(s) v

Acknowledgment vi

Abstract vii

বিমূর্ত… viii

Table of Contents ix

List of Figures xii

List of Tables xv

Nomenclature xvi

Acronyms and Abbreviations xvii

Chapter 1: INTRODUCTION 1

1.1 Background 1

1.2 Statement of the Problem 7

1.3 Research Gaps 8

1.4 Aims and Objectives 9

1.5 Significance of This Study 10

1.6 Thesis Outline 11

Chapter 2: LITERATURE REVIEW 12

2.1 Overview of Antibiotics in Aquatic Environments 12

2.2 Adsorption Techniques for Remediation of Contaminants from Water 12

2.3 Ecotoxicology of CIP 16

2.4 Overview of Mitigation Strategies of CIP 18

2.5 Adsorption of Ciprofloxacin from Water 22

2.6 CIP Adsorption Mechanism 29

Chapter 3: MATERIALS AND METHODOLOGY 37

3.1 Chemicals and Reagents 37

3.2 Instruments 37

3.3 Synthesis 37

3.3.1 Synthesis of $CuWO_4$ 37

3.3.2 Synthesis of $CuWO_4@TiO_2$ 38

3.4 Characterization 39

3.5 Adsorption Studies 39

3.6 RSM-Based Modelling and Optimization 40

3.7 Machine Learning-Based Modelling and Optimization 43

3.7.1 Design of Predictive Model and Evaluation 43

3.7.2 Multilayer Perceptron (MLP) Neural Network Design 45

3.7.3 Model Optimization and Its Importance 47

3.8 Adsorption Isotherms 48

3.9 Adsorption Kinetics 50

3.10 Reusability Test 51

Chapter 4: RESULTS AND DISCUSSION 52

4.1 Characterization 52

4.1.1 X-ray Diffraction (XRD) 52

4.1.2 Fourier Transform Infrared Spectroscopy (FTIR) 52
4.1.3 Field Emission Scanning Electron Microscopy (FESEM) and Average Particle Size 54
4.1.4 X-ray Photoelectron Spectroscopy (XPS) 55
4.1.5 Surface Analysis of Brunauer–Emmett–Teller (BET) 57
4.2 Response Surface Methodology-Based Optimization Results 59
4.2.1 Box Behnken Statistical Analysis and Model Fitting 59
4.2.2 Verification of the Model Using the Desirability Function 63
4.2.3 Interaction Effects of Variables and Response Surface 64
4.3 Machine Learning-Based Optimization Result 68
4.3.1 Data Processing and Analysis 68
4.3.2 Performance of Prediction Model and Optimization 69
4.3.3 PSO Optimization of Input Parameters and Experimental Validations 78
4.3.4 Effect of Factors on Adsorption and Comparison with the MLP Optimized Model 80
4.4 Adsorption Isotherms 85
4.5 Adsorption Kinetics 88
4.6 Reusability Test 89
Chapter 5: CONCLUSION 90
5.1 General 90
5.2 Key Findings 90
5.3 Limitations of the Study 91
5.4 Recommendation for Further Study 92
REFERENCES 93

List of Figures

Figure No. **Caption** **Page No.**

Figure 2.1 General chemical structure of Ciprofloxacin. 16

Figure 2.2 Ionic forms of CIP based on the pK_a (showing the positions of the protonation and deprotonation functional groups) [157].....31

Figure 3.1 Schematic diagram of the four-layer MLP model with four input and one output layer used in this study.....46

Figure 3.2 Scatter plot matrix for input and outcome variables. Red and blue circle tones indicate a positive and negative correlation with proportion, respectively.....46

Figure 4.1 FESEM and average particle size **(a)** core $CuWO_4$ **(b)** hollow TiO_2 **(c)** TiO_2 coated $CuWO_4$ ($CuWO_4$@TiO_2).....54

Figure 4.2 High-resolution XPS spectra of **(a)** Ti 2p, **(b)** O 1s, **(c)** Cu 2p and **(d)** W 4f for $CuWO_4$@TiO_2 56

Figure 4.3 N_2 adsorption and desorption isotherms and BJH pore size distribution curves (insets) for **(a)** core $CuWO_4$ and **(b)** core-shell $CuWO_4$@TiO_2.....58

Figure 4.4 Plot of actual vs. predicted responses for removal of CIP by $CuWO_4$@TiO_2.....61

Figure 4.5 (a) Plot of the internally studentized residual with normal probability, **(b)** plot of the predicted value against the internally studentized residuals of the CIP adsorption by $CuWO_4$@TiO_2.....62

Figure 4.6 The graph of optimization displays the best-predicted values for the maximum removal of CIP (%) and desirability function. 62

Figure 4.7 3D surface plots illustrating the impact of four factors on the adsorption of CIP by using $CuWO_4$@TiO_2 (a-f). 64

Figure 4.8 Training and testing loss (a) Bayesian optimization (b) Random search optimization. 71

Figure 4.9 Feature importance of MLP model (a) Bayesian optimization (b) Random search optimization 72

Figure 4.10 The scatter plot represents the predictive results of the MLP model with training and testing dataset (a) Training dataset with Bayesian optimization (b) Training dataset with random search optimization (c) Testing dataset with Bayesian optimization (d) Testing dataset with random search optimization. 73

Figure 4.11 Radar plots illustrating the statistical performance of the MLP model on (a) the training dataset utilizing Bayesian optimization, (b) the training dataset employing random search optimization, (c) the testing dataset with Bayesian optimization, and (d) the testing dataset with random search optimization. 75

Figure 4.12 Regression error characteristic curves illustrating the performance of the MLP model under (a) Bayesian optimization and (b) Random search optimization. 76

Figure 4.13 Model performance realization for full dataset with Bayesian optimization.....77

Figure 4.14 Model performance realization for full dataset with Random search optimization. 77

Figure 4.15 PSO algorithm convergence for optimal input parameters design under (a) Bayesian optimization and (b) Random search optimization MLP model 78

Figure 4.16 Experimental validation for removal of ciprofloxacin under optimum condition (9.6 mg/L of initial CIP, 400 mg/L of $CuWO_4@TiO_2$ adsorbent, 40 minutes of adsorption time at room temperature and neutral pH). 80

Figure 4.17 The effect of antibiotic concentration on the removal of ciprofloxacin with the $CuWO_4@TiO_2$ adsorbent at a dosage of 400 mg/L and pH 7, and the comparison of the experimental data with a) Bayesian optimisation and b) Random search optimisation MLP model. 81

Figure 4.18 The effect of adsorbent dosage ($CuWO_4@TiO_2$) on the removal of ciprofloxacin with an initial ciprofloxacin concentration of 10 mg/L and pH 7, and the comparison of the experimental data with a) Bayesian optimisation and b) Random search optimisation MLP model. 82

Figure 4.19 The effect of the pH of the solution on the removal of ciprofloxacin, with an initial antibiotic concentration of 10 mg/L and 400 mg/L of $CuWO_4@TiO_2$ adsorbent, and the comparison of the experimental data with a) Bayesian optimisation and b) Random search optimisation MLP model. 84

Figure 4.20 (a–c) Isotherm models: Langmuir, Freundlich, and Temkin; (d–e) kinetic models: pseudo-first and pseudo-second order; (f) reusability of the TiO_2-coated $CuWO_4$ nanocatalyst. 87

List of Tables

Table No. **Caption** **Page No.**

Table 2.1 Adsorption techniques for the remediation of contaminants.....14

Table 2.2 Adsorption of CIP From Water 25

Table 2.3 Mechanism of ciprofloxacin (CIP) uptake from aqueous media.....32

Table 3.1 Levels of experimental variables in Box-Behnken design. 41

Table 3.2 Box-Behnken design matrix with actual and predicted response..42

Table 3.3 Isotherm models of Langmuir, Freundlich, and Temkin 49

Table 3.4 pseudo-first-order model and pseudo-second-order kinetics models 51

Table 4.1 Physiochemical properties of $CuWO_4$ and $CuWO_4@TiO_2$ 58

Table 4.2 Model statistics for the removal of CIP using $CuWO_4$ $@TiO_2$. 59

Table 4.3 ANOVA for the response surface quadratic model for removal of CIP by $CuWO_4@TiO_2$ 60

Table 4.4 Summarized results of the statistics of the experimental data 69

Table 4.5 Hyper-parameters' range and optimal values 71

Table 4.6 Statistical performance measures for training and testing data with two algorithms 76

Table 4.7 Input parameters optimization using the novel framework.....78

Table 4.8 Non-linear fitting of the adsorption of CIP onto $CuWO_4@TiO_2$ yielded the adsorption isotherm values. pH=7, contact period of 40 minutes, CIP concentration of 5–25 mg/L, and adsorbent dose of 300 mg/L.....86

Table 4.9 Non-linear fitting was employed to figure out the adsorption kinetics parameters for CIP on $CuWO_4@TiO_2$ (adsorbent dose 300 mg/L, CIP concentration 10 mg/L, and pH 7).....88

Nomenclature

Symbols	Elaborations
e.g.	For example
etc.	Etcetera
et al.	And Others
Fig.	Figure
E. coli	*Escherichia coli*

Acronyms and Abbreviations

ANOVA	Analysis of variance
ARB	Antibiotic Resistance Bacteria
BCSIR	Bangladesh Council of Scientific and Industrial Research
CIP	Ciprofloxacin
CCD	Central Composite Design
CV	Cyclic Voltammetry
EIS	Electrochemical Impedance Spectroscopy
FE-SEM	Field Emission Scanning Electron Microscopy
IMRD	Industrial Microbiology Research Division
RSM	Response Surface Methodology
UV-VIS	Ultraviolet-visible Spectroscopy
WHO	World Health Organization
WWTP	Waste Water Treatment Plant
XRD	X-ray Diffraction
XPS	X-ray Photoelectron Spectroscopy

Chapter 1: INTRODUCTION

1.1 Background

Urban water systems, frequently contaminated with antibiotics, pose a significant environmental and public health threat. To stop the spread of antibiotic-resistant bacteria and protect water quality, it is essential to remove antibiotic pollutants rapidly, especially with the help of advanced nanotechnology-based solutions. Antibiotics play a fundamental role in contemporary medicine and have significantly transformed the treatment of bacterial infections since their discovery. The overuse, misuse, and improper disposal of antibiotics have contributed to the emergence and spread of antibiotic-resistant bacteria [1-4], posing a significant threat to global public health [5]. Antibiotics, even at concentrations ranging from nanograms per liter to milligrams per liter in water and low to moderate milligrams per kilogram in sediments, can accumulate and persist in the environment, posing risks to both aquatic and terrestrial ecosystems [6]. The European Commission's science and knowledge service put out a technical report in 2018 that said it was worried about antibiotics being in the environment [7]. This report indicates that most antibiotics in wastewater treatment plant (WWTP) effluents have maximum concentrations between 0.1 and 1 μg/L. The maximum concentration for thirteen antibiotics ranges from 1 to 10 μg/L, and for just three antibiotics (ciprofloxacin, sulfamethoxazole, and ofloxacin), it is almost 10 μg/L [7]. Ciprofloxacin, a fluoroquinolone antibiotic that works on a wide range of bacteria, is often found in polluted water sources because it is used a lot and remains in the environment for a long time [8]. Ciprofloxacin in aquatic habitats offers substantial concerns, including the spread of antibiotic resistance, disruption of microbial populations, and potential harm to aquatic creatures. In order to alleviate these effects, it is imperative to employ effective wastewater treatment procedures to eliminate

antibiotics prior to releasing the effluent into aquatic environments [9]. Furthermore, using enhanced strategies in healthcare, agriculture, and pharmaceutical manufacturing can effectively mitigate the discharge of antibiotics into the environment.

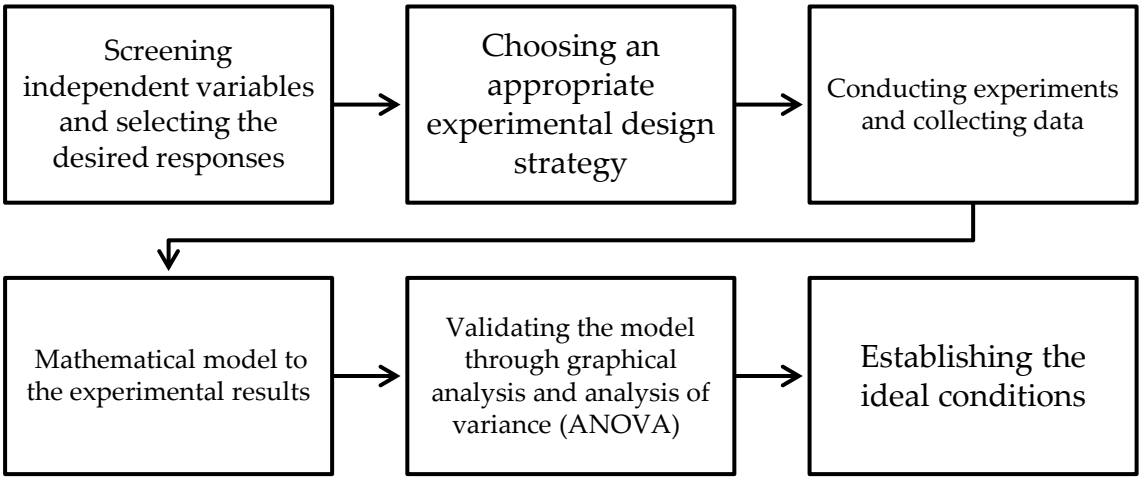
It is very important to reduce the amount of antibiotics in the environment because they can harm ecosystems and human health. Ciprofloxacin, similar to other antibiotics, can be introduced into the environment by many routes, such as wastewater discharges, agricultural runoff, and incorrect disposal of unused drugs [10-12]. Multiple antibiotic treatment processes exist for this purpose, each possessing distinct benefits and drawbacks. Advanced oxidation processes (AOPs) offer effective degradation of ciprofloxacin and other antibiotics. These processes have the ability to selectively eliminate a broad spectrum of pollutants and exhibit notably rapid reaction rates. Nevertheless, they entail substantial operational expenses because of energy and chemical prerequisites, and the generation of potentially hazardous by-products is a matter of worry [13, 14]. Membrane filtration procedures efficiently eliminate ciprofloxacin and other micropollutants, achieving high water quality standards. They possess the ability to be easily adjusted in size and are well-suited for applications on a grand scale. However, membrane fouling, cleaning demands, and elevated energy and maintenance expenses pose substantial obstacles linked to this approach [15, 16]. Biological treatment offers a sustainable and eco-friendly method for eliminating ciprofloxacin, converting it into harmless metabolites by mineralization. It is economically efficient for extended periods of operation. Nevertheless, the rate at which biodegradation occurs might differ, and the presence of elevated levels of ciprofloxacin can hinder the process [17]. Photocatalysis can effectively degrade ciprofloxacin utilizing either visible or UV light, leading to complete mineralization. Although it exhibits reduced operational expenses in comparison to certain AOPs, the presence of light sources and the retrieval of catalysts

provide significant obstacles [18]. Electrochemical techniques efficiently break down ciprofloxacin and other contaminants, offering high energy efficiency and minimum sludge generation. However, there are limitations to consider, such as the significant upfront expenses, the issue of electrode fouling, and the limited suitability for specific water compositions [19]. Ion exchange provides a method for specifically eliminating ciprofloxacin and other charged impurities using ion exchange resins that may be regenerated and reused. Nevertheless, there are problems with resin saturation, regeneration chemicals, and the poor removal efficacy for neutral substances [20]. Adsorption techniques demonstrate a notable ability to adsorb ciprofloxacin and other pharmaceutical drugs are frequently cost-efficient, particularly when utilizing low-cost adsorbents such as activated carbon [21-24]. Their simplicity and ease of implementation render them appealing alternatives. Nevertheless, the effectiveness of adsorbents can be hindered by factors like as saturation, regeneration, and disposal, especially when dealing with low concentrations or intricate matrices.

Using titanium dioxide (TiO_2) coated copper tungstate ($CuWO_4$) nano adsorbent is a big step forward in water treatment, especially for the removal of antibiotics in contaminated water. This novel nanomaterial synergistically combines the exceptional adsorption capacity of copper tungstate with the catalytic capabilities of titanium dioxide. This makes it a very effective and eco-friendly way to deal with the problems caused by antibiotic pollution. The main part of the hybrid nanocomposite is $CuWO_4$ nano adsorbent. This adsorbent has a lot of active sites and a large surface area, which makes it good at taking up antibiotic compounds from contaminated water. Adding copper ions to the surface of the nano adsorbent makes it easier for antibiotics to stick to it through electrostatic interactions and surface complexation. This traps the antibiotics and then removes them from the water. This dual-action mechanism not only makes it

easier to remove antibiotics, but it could also make the pollutants that are already stuck to the surface stronger, which would make water purification easier.

One-factor-at-a-time (OFAT) is a traditional optimization method that is costly and time-consuming, as it tests variables individually while overlooking their interactions and combined effects on the response [25, 26]. To overcome these limitations, Response Surface Methodology (RSM) develops the relationships between multiple factors and the response using a second-degree polynomial [27-30]. Moreover, it aims to identify optimal or desirable operational conditions [31, 32]. The RSM process involves six key steps to simulate and optimize physicochemical processes.



RSM provides a comprehensive framework for optimizing complex processes and understanding the interplay between various factors [33]. Based on this approach, Prior research has shown the effective utilization of RSM for the adsorption of diverse pollutants, including heavy metals [34, 35], dyes [36, 37], antibiotics [38, 39] and many other wastes from water. In particular, the successful application of RSM in modelling the adsorption of CIP using different adsorbents such as VO_2 [40], CoFe-MOF [39], $HoFeO_3/Ho_3Fe_5O_{12}$ [41], FMWCNTs-Fe_3O_4 [42], etc. To optimize parameters (contact time, pH, adsorbent dosage, initial concentration, etc.) for enhancing the adsorption capacity of the

materials, the effectiveness of RSM in modelling CIP adsorption processes is an important factor.

Machine learning models have become invaluable tools for predicting the concentration of pollutants in contaminated water, providing crucial insights for environmental monitoring, risk evaluation, and remediation plans [43, 44]. To ensure the protection of human health and ecosystem integrity, it is essential to develop accurate models due to the growing occurrence of antibiotic pollution in water sources. The implementation of artificial neural network (ANN)-based machine learning models signifies a substantial advancement in the predictive analysis of antibiotics and antibiotic resistance genes in wastewater systems. The multilayer perceptron neural network framework (MLPNNF) is an ANN that is recognized for its capacity to acquire complex patterns and connections from data. Multi-layer perceptron neural networks (MLPNNs) are highly effective at representing complex connections between input variables and output responses [45, 46]. The combination of a multilayer perceptron neural network (MLPNNF) model with a novel nanoadsorbent represents a major advancement in accurately predicting ciprofloxacin concentrations in wastewater. This makes them particularly suitable for accurately forecasting concentrations of ciprofloxacin by considering several characteristics such as using ciprofloxacin concentrations, adsorbent dosages, solution pH, adsorption time etc. The conventional methods for monitoring ciprofloxacin concentration in wastewater frequently lack the accuracy and effectiveness required for efficient environmental management. Researchers have successfully increased the prediction capabilities and detection accuracy by merging MLPNNF models with advanced nano adsorbents.

Over the past few years, the utilization of ANNs has become increasingly popular due to their convenient and reliable capabilities in addressing nonlinear interactions between variables, particularly in complex systems. ANNs offer significant benefits for data analysis and function approximation, particularly in

scenarios where uncovering statistical and mathematical relationships between dependent and independent variables proves challenging [47]. In the last decade, artificial neural networks (ANNs) have been extensively applied across diverse domains of adsorption research. For instance, studies have investigated the adsorption of metronidazole by graphene oxide [48] and the removal of ciprofloxacin and ofloxacin using a combination of graphene oxide (GO), chitosan (CS), and polydopamine (PDA) nano adsorbent [24]; sorption of amoxicillin by magnetic activated carbon of Palm kernel, tetracycline removal by modified zeolite [49]; multi-walled carbon nanotube functionalized with aspartic acid and poly-pyrrole [50]; The degradation of ofloxacin has been investigated using a TS-1/C_3N_4 composite photocatalyst, composed of titanium–silicon molecular sieves loaded onto carbon nitride [51]; adsorption of sarafloxacin by magnetized metal-organic framework [52]; photocatalytic degradation of oxytetracycline by TiO_2 [53]. Despite its potential significance, the primary knowledge gap addressed in this study pertains to the development and validation of predictive models for measuring ciprofloxacin concentrations in contaminated water using nano adsorbents. To my knowledge, no previous studies have documented the application of $CuWO_4$@TiO_2 nanoadsorbent for the removal of ciprofloxacin. This study presents an innovative $CuWO_4$@TiO_2 nano adsorbent for the effective removal of ciprofloxacin from aqueous solutions, supported by predictive modeling methodologies. The lack of previous research in this area underscores the importance of my findings, which not only enhance the field of water treatment but also lay the groundwork for subsequent investigations into data-driven adsorption system design. The combined use of experimental validation and computational prediction ensures a robust understanding of adsorption dynamics. This integrative approach can be extended to other emerging contaminants, advancing the development of next-generation water purification technologies.

1.2 Statement of the Problem

There are a lot of worries about the bad effects that antibiotics might have on human health and aquatic ecosystems because they are being used more and more in water. Drugs in water can help antibiotic-resistant bacteria grow and spread, which is a big risk to public health.

Even though these problems have been recognized, there is still a great need for long-term and effective ways to get antibiotics out of the water. Traditional methods for treating water may not be enough to get rid of these pollutants and the environmental risks that come with them. Also, the development of new adsorbents that are specifically made to perform well in neutral conditions is a promising way to mitigate the effects of these pollutants on water quality and ecosystem health.

Therefore, this research seeks to address the following key challenges:

- The need for new materials and technologies that can effectively remove ciprofloxacin (CIP) from water at neutral pH levels.
- The optimization of adsorbent doses using RSM to achieve efficient removal while minimizing resource consumption.
- The implementation of a machine learning-based approach for predictive modelling and optimization of CIP removal efficiency.
- . The prepared adsorbent was carefully studied to find out about its morphological, structural, and surface properties
- Reusability tests were conducted over multiple cycles to assess their practicality and sustainability in water treatment applications.

1.3 Research Gaps

In the context of devising an effective technique for the elimination of antibiotics from aqueous solutions utilizing a CuWO4@TiO2 nano adsorbent under neutral circumstances, several prospective research gaps may exist:

- **Limited Studies on Neutral pH Conditions:** Many existing studies focus on adsorption processes under specific pH conditions, often neglecting the importance of neutral pH, which is more representative of natural water bodies. Investigating the performance of nano adsorbents under neutral pH conditions presents a research gap that this study seeks to address.
- **Lack of Reusability Assessment:** Water treatment research often focuses on creating new adsorbents, but there isn't always a thorough evaluation of how well they can be reused. Evaluating the reusability of the CuWO4@TiO2 nano adsorbent addresses a research gap that this study seeks to fill, as it is essential for practical and sustainable water treatment applications.
- **Limited Application of RSM:** RSM has been extensively utilized across diverse domains; however, its effectiveness in optimizing adsorbent dosages for the elimination of antibiotics under neutral conditions may be constrained. This study aims to fill this research gap by using RSM to improve removal efficiency while using fewer resources.
- **Need for Comprehensive Characterization:** Numerous studies exhibit insufficient comprehensive characterization of newly developed adsorbents, which is crucial for elucidating their properties and performance. This study aims to fill the gap by employing various characterization techniques, such as FTIR, FESEM, XRD, BET, and XPS, to thoroughly analyze the synthesized $CuWO_4@TiO_2$ nano adsorbent.
- **Lack of Advanced Predictive Modelling Approaches:** The use of machine learning methods to model and improve adsorption processes is still not very

common in this field. Incorporating machine learning can enhance the understanding of complex nonlinear relationships among process variables and support more robust predictive modelling.

- **Limited Application of Metal WO_4@TiO_2 in Water Treatment:** Despite their potential, the combined use of metal tungstate and TiO_2 composites in water purification is not extensively studied. Their dual adsorption and photocatalytic properties under neutral conditions remain underutilized. This study addresses the gap by exploring $CuWO_4$@TiO_2 for effective pollutant removal.

1.4 Aims and Objectives

- Synthesizing the $CuWO_4$@TiO_2 nano adsorbent using a two-step hydrothermal method and comprehensively characterizing its morphological, structural, and compositional properties through advanced techniques including FTIR, FESEM, XRD, BET and XPS.
- Investigating the efficacy of the $CuWO_4$@TiO_2 nano adsorbent in eliminating ciprofloxacin (CIP) from synthetic aqueous samples under neutral conditions.
- Optimizing key parameters, including adsorbent dose, pH, CIP concentration, and reaction time, utilizing Response Surface Methodology (RSM) and Machine Learning application for achieving maximum removal efficiency under neutral pH conditions.
- Evaluating the adsorption isotherms of CIP on $CuWO_4$@TiO_2 by models including Langmuir, Freundlich, and Temkin to reveal the adsorption mechanism and surface behavior.

- To elucidate the rate and mechanism of the adsorption process, adsorption kinetics were analyzed using pseudo-first-order and pseudo-second-order models.
- Assessing the reusability of the $CuWO_4@TiO_2$ nano adsorbent over multiple adsorption cycles, providing insights into its stability and performance for potential long-term applications.

1.5 Significance of This Study

1. **Innovative Water Treatment Approach:**
    - This study introduces an innovative approach to water treatment by synthesizing and exploring the potential of the $CuWO_4@TiO_2$ nano-adsorbent. The effective removal of antibiotics addresses a critical need for efficient and targeted water treatment strategies.
2. **Advanced Nanomaterial Characterization:**
    - The comprehensive characterization of the nano adsorbent contributes to the understanding of advanced nanomaterials, their structural features, and how these characteristics influence pollutant removal efficiency. The study advances knowledge in the synthesis and application of nanostructured materials for environmental remediation.
3. **Optimization Strategies:**
    - The application of RSM in optimizing adsorbent doses and key parameters represents a significant contribution. This methodology enhances the precision of experimental design, providing a systematic approach for achieving optimal conditions for pollutant removal.
    - The application of Machine Learning (ML) techniques offers a powerful approach for optimizing adsorption processes. By using data-driven

models, ML can predict the adsorption efficiency based on key variables, improving the accuracy and efficiency of the optimization process.

4. **Reusability and Sustainable Water Treatment:**
    - The investigation into the reusability of the nano adsorbent addresses the sustainability aspect of water treatment technologies. Assessing the material's stability across multiple cycles provides valuable insights for developing environmentally sustainable and cost-effective treatment solutions.

1.6 Thesis Outline

Chapter 2 provides a concise review of antibiotic contamination in urban waters, the limitations of treatment plants, CIP-related ecotoxicity and resistance, and the use of adsorption techniques, especially for ciprofloxacin removal.

Chapter 3 for developing the TiO_2-coated $CuWO_4$ nano catalyst, along with the experimental setup for adsorption studies and the modelling approaches applied for optimization.

Chapter 4 presents and discusses the characterization results of the synthesized nano catalyst, adsorption performance for ciprofloxacin removal, kinetic and isotherm modelling, reusability analysis, and optimization outcomes using RSM and machine learning approaches.

Chapter 5 summarizes the key findings of the research, highlights the effectiveness of TiO_2-coated $CuWO_4$ nano catalysts in ciprofloxacin removal, discusses the implications for water treatment, and provides recommendations for future research and practical applications.

Chapter 2: LITERATURE REVIEW

2.1 Overview of Antibiotics in Aquatic Environments

The rising use of antibiotics in both human and veterinary medicine has greatly polluted water sources all over the world [54]. This pollutant in water bodies causes major issues for the environment. Their presence makes it more difficult to treat water and includes to the problem of antibiotic resistance and toxic chemical exposure in aquatic life [55]. Effluents from pharmaceutical manufacturing, excretion from humans and animals, hospitals, and livestock farms significantly increase antibiotic concentration in water [56]. Antibiotic usage worldwide ranges from 100,000 to 200,000 tons annually, encompassing both human medical treatments and veterinary applications, which contributes significantly to environmental contamination. Nearly 90% of antibiotics administered are eliminated from the body in their original form, subsequently contaminating water sources [11].

The following section will discuss adsorption techniques for removing contaminants from water.

2.2 Adsorption Techniques for Remediation of Contaminants from Water

Adsorption is a widely used technique utilized in water treatment, where impurities are captured on the surface of solid adsorbent materials. This method effectively removes a diverse array of inorganic and organic contaminants from water, such as pesticides, dyes, heavy metals, and antibiotics. It is particularly beneficial for eliminating trace contaminants, even at low concentrations. In addition, adsorption is a straightforward and cost-effective treatment procedure that does not necessitate sophisticated equipment or substantial pre-treatment. In general, adsorption is a flexible and extensively utilized water treatment method that can serve as a vital element of a comprehensive water treatment system. **Table 2.1** provides a comprehensive overview of sophisticated materials

and their abilities to adsorb or remove diverse contaminants in water treatment, along with their corresponding capacities or efficiencies. The materials consist of carbon-based, metal oxide-based, and nanocomposites, all of which have proven to be successful in adsorbing a diverse array of pollutants, such as pharmaceuticals, heavy metals, dyes, etc.

According to Ren, Lin [57], Fe_3O_4@carbon has demonstrated adsorption capabilities of 262.72 mg/g for Congo red dye and 33.35 mg/g for Cr(VI). $CoFe_2O_4$ exhibits high adsorption capacities for heavy metals, such as 109.89 mg/g for Pb(II) and 294.12 mg/g for U(VI), and shows effectiveness in removing EBT dye, achieving a removal efficiency of 59.3% [58, 59]. $CoFe_2O_4$ combined with multi-walled carbon nanotubes (MWCNT) increased the ability to adsorb U(VI) and Pb(II), resulting in capacities of 500 mg/g and 217.39 mg/g, respectively [59]. $Fe^0/Fe^{3+}C/\gamma$-Fe_2O_3 carbon demonstrated efficient adsorption of 169.49 mg/g for sulfamethoxazole [60] whereas another novel method utilizes $ZnFe_2O_4$:Ce^{3+}/carbon fibers, which achieved a removal efficiency of 265.2 mg/g for Congo red [61]. As reported by Patra, Mohanty [62], MnO_2 nanoparticles have shown for Reactive Blue 21 (RB-21) dye an adsorption capacity of 705 mg/g and a removal effectiveness of 98%. Irawan, Nata [63] discovered that montmorillonite coated with magnetic nanoparticles had remarkable efficacy in the removal of As(V) with an adsorption capacity of 19.10 mg/g and Pb(II) with an adsorption capacity of 38.15 mg/g. Levofloxacin was efficiently removed using mesoporous Fe_2O_3, demonstrating an adsorption capacity of 33.1 mg/g [64], whereas 98% of rhodamine B was effectively removed using AC-CdS nanoflowers [65]. On the other hand, ZIF-8/MWCNTs-COOH nano adsorbents are capable of removing 70.68% of tetracycline (471.22 mg/g) and 97.93% of Congo red (1185.58 mg/g) as reported by Zhang, Yuan [66]. 70.96% of methylene blue was successfully removed using nano-aluminum oxide [67], but γ-AlOOH adorned 3D-reduced graphene oxide demonstrates a significant adsorption capacity of 930.0889 mg/g for the same dye [68]. The studies conducted by

Rajendran, Panneerselvam [69] and Eyni Gavabari, Goudarzi [70] Nanocomposite films consisting of polyurethane, activated carbon, and cellulose nano-whiskers, as well as the magnetic nanocomposites activated carbon, were found to remove 95% and 88.9% of methylene blue, respectively. Graphene oxide and chitosan composite material, along with nano-graphene oxide, have been found to have high adsorption capabilities for methylene blue (117.16 ± 0.03 mg/g), while nano-graphene oxide can adsorb 96.84% of it [71, 72]. The Co-doped Fe-MOF bimetallic organic framework demonstrated a methylene blue dye adsorption capacity of 562.10 mg/g [73]. At the same time, Khooni, Ahmadzadeh [74] reported that the magnetic graphene oxide/Mg-Al layered double hydroxide nanocomposite exhibits an efficiency of 93.8% in removing the same dye. salah omer, A.El Naeem [75] noted that treated sugarcane bagasse (TSCB) demonstrates an impressive (96%) removal of methylene blue, while the Iron Oxide/MOF nanocomposite has an adsorption capacity of 32.46 mg/g for the same dye [76].

Table 2.1 Adsorption techniques for the remediation of contaminants

Pollutant	**Adsorbent**	**Results** **Adsorption capacity (mg/g)** **Removal Efficiency (%)**	**Reference**
Cr (VI)	Fe_3O_4@carbon	33.35 mg/g	[57]
Congo red	Fe_3O_4@carbon	262.72 mg/g	[57]
EBT dye	$CoFe_2O_4$	59.30%	[58]
Pb (II) U(VI)	$CoFe_2O_4$	U (VI) = 294.12 mg/g Pb (II) = 109.89 mg/g	[59]
U(VI) Pb (II)	$CoFe_2O_4$/MWCNT	U (VI) =500 mg/g Pb (II) = 217.39 mg/g	[59]
Congo red	$ZnFe_2O_4$:Ce^{3+}/carbon fibers	265.20 mg/g	[61]
Sulfamethoxazole	$Fe^0/Fe^{3+}C/\gamma$-Fe_2O_3 Carbon	169.50 mg/g	[60]
Levofloxacin	Mesoporous Fe_2O_3	33.10 mg/g	[64]
EBT dye	$CoFe_2O_4$	59.30%	[58]

BRB dye	$CoFe_2O_4$	61.40%	[58]
RB-21 dye	MnO_2 nanoparticles	705 mg/g and 98%	[62]
Pb (II)	Magnetic nanoparticles- coated montmorillonite	38.15 mg/g	[63]
As (V)	Magnetic nanoparticles-coated montmorillonite	19.10 mg/g	[63]
Rhodamine B	AC-CdS nanoflowers	98%	[65]
Congo red	ZIF-8/MWCNTs-COOH nanoadsorbents	97.93% and 1185.58 mg/g	[66]
Tetracycline	ZIF-8/MWCNTs-COOH nanoadsorbents	70.68% and 471.22 mg/g,	[66]
Methylene Blue	Polyurethane/activatd (AC)/cellulose nanowhisker nanocomposite film	88.90 %	[70]
Methylene Blue	Magnetic nanocomposites activated carbon	95%	[69]
Methylene Blue	Polyurethane/activated carbon (AC)/cellulose nanowhisker nanocomposite film	88.90 %	[70]
Methylene Blue	Graphene oxide and chitosan composite materia	117.16 ± 0.03 mg/g	[71]
Methylene Blue	nano graphene oxide	96.84%	[72]
Methylene Blue	nano-aluminum oxide	70.96%.	[67]
Methylene Blue	γ-AlOOH decorated 3D-reduce graphene oxide	930.0889 mg/g	[68]
Methylene Blue	Magnetic graphene oxide/Mg-Al layered double hydroxide nanocomposite	93.80 %	[74]
Methylene Blue	Co-doped Fe-MOF bimetallic organic framework	562.10 mg/g	[73]

Methylene Blue	Treated sugarcane bagasse (TSCB)	96.00%	[75]
Methylene Blue	Iron Oxide/MOF nanocomposite	32.46 mg/g	[76]

In short, the table shows how well different advanced materials work for water treatment by adsorption. These materials have high adsorption capacities and removal efficiencies, making them promising options for getting rid of a wide range of pollutants from water sources. This is a step toward more sustainable water treatment practices.

2.3 Ecotoxicology of CIP

An outline of Ciprofloxacin's (CIP) ecotoxicology is provided in this section, highlighting the detrimental effects of CIP contamination in aquatic ecosystems. It also emphasizes the importance of efficiently removing CIP from water sources. CIP is predominantly utilized in human medicine, particularly for the treatment of urinary tract infections in males. [77, 78]. The general chemical structure of CIP is depicted in **Figure 2.1**

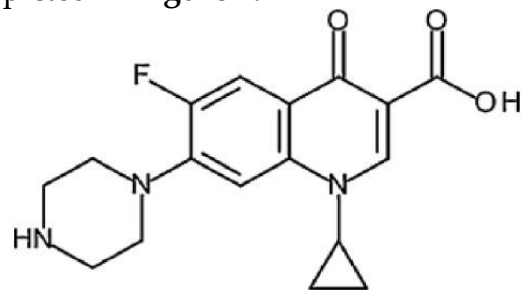


Figure 2.1 General chemical structure of Ciprofloxacin.

Wastewater treatment is critical to safeguarding ecosystems, protecting public health, and promoting sustainable water management practices. This process is essential for purifying water by eliminating contaminants, decreasing pollutants, and ensuring that the treated water is suitable for safe discharge or reuse in natural water bodies. Nonetheless, these pharmaceutical compounds frequently persist through conventional treatment systems, ultimately contributing to the

pollution of surface and groundwater via natural water circulation [79, 80]. Ciprofloxacin (CIP), a prevalent pharmaceutical active component (PhAC), is frequently identified as a pollutant in wastewater from the pharmaceutical sector [81]. The presence of CIP in the aquatic environment could indicate significant toxicity to the species of aquatic flora and fauna. Several sources have reported groundwater pollution caused by pharmaceuticals and personal care products (PhACs) [82, 83]. After 11 days of cultivation, a growth inhibition of 88±3%, 75±3%, and 36±1% in *C. mexicana* after exposure to CIP doses of 100, 60, and 40 mg/L, respectively. The study conducted by Nie, Wang [84] demonstrated that at concentrations between 2 and 39.5 mg/L, CIP effectively hindered the growth of *Chlorella vulgaris* following a 96-hour incubation period. The presence of aqueous quinolones had a notable inhibitory effect on the growth of *P. subcapitata*, as observed in the study conducted by González-Pleiter, Gonzalo [85]. Magdaleno, Saenz [86] identified Ciprofloxacin (CIP) has been recognized as one of the most harmful antibiotics to *P. subcapitata*. Cardiac dysfunction or injury has also been reported in zebrafish following 24 hours of exposure to CIP-contaminated water [87]. Furthermore, exposure to a CIP concentration of 301.8 nmol/L resulted in notable alterations in the decomposition patterns of microbial and macroinvertebrate communities [88, 89]. Näslund, Hedman [90] also shows that 1700 nmol/L CIP concentration resulted in a 50% reduction in the degradation of pyrene. One study examined the growth inhibition of photoautotrophic aquatic organisms exposed to aqueous ciprofloxacin (CIP). Notable toxic effects were observed in the monocotyledonous macrophyte *Lemna minor* and the cyanobacterium *Anabaena flos-aquae*, with EC_{50} values of 62.5 mg/L and 10.2 mg/L, respectively [80]. The results findings indicate that CIP adversely impacts the environment upon its discharge into the ecosystem. Consequently, the removal of effluents via adsorption is essential, rendering this section especially relevant.

2.4 Overview of Mitigation Strategies of CIP

Additionally, chemical methods include advanced oxidation processes [13, 91], ion exchange [92-94], electrocoagulation [95], and chemical oxidation [96]. Biological treatment methods have also been investigated [97-101]. The membrane-based filtration techniques—such as microfiltration, ultrafiltration, nanofiltration, and hyperfiltration—utilize microporous membranes composed of metallic, polymeric, or ceramic materials to effectively remove dissolved compounds, fine particles, and colloidal matter from aqueous solutions [102]. Using ceramic UF (ultrafiltration) membranes, Banerjee, Jana [103] removed over 99% of CIP at an initial concentration of 1 mg/L and a transmembrane pressure of 4.5 kg/cm². The reverse osmosis (RO) membrane demonstrated high efficacy in removing ciprofloxacin (CIP), reaching a maximum removal efficiency of 99.96%, which exceeds 90% [104]. Due to their convenient magnetic separation capability, magnetic resins have also gained widespread application as effective adsorbents in water treatment [105]. According to a study, both with and without humic acid, the use of five different magnetic multifunctional resins did not effectively reduce CIP. The investment, installation, and operation expenses of membrane separation techniques such as nanofiltration, ultrafiltration (UF) and reverse osmosis (RO) are substantial [106-108]. Advanced oxidation processes (AOPs) are recognized as highly effective techniques for the removal of pollutants; The significant degrading effectiveness of several advanced oxidation processes (AOPs) can be attributed to their synergetic ability to produce various ROS ($HO^{\bullet}$, $O_2^{\bullet-}$, $^1O_2$, H_2O_2, $SO_4^{\cdot-}$, $^{\cdot}N_3$) and subsequent radicals reactions [109, 110]. The effectiveness of AOPs depends on the efficacy of the oxidant [111]. They may involve Fenton/electro-Fenton/photo-Fenton oxidation [112-115], ozonation [116-119], sonolysis [120, 121], sonocatalysis [91, 122, 123], photodegradation [124, 125], hydrolysis [126], UV/chlorine process [127], persulfate process [128-130], and photocatalysis [110, 131-133]. Despite the use of individual or combined

approaches, ciprofloxacin (CIP) may still persist in aquatic environments. A study conducted by Sayed, Khan [134] demonstrated that the addition of peroxymonosulfate to a Poly(vinyl alcohol)-assisted TiO_2/Ti film resulted in the removal of 98.3% of CIP. According to a study by Igwegbe, Ahmadi [120], up to 99% removal of ciprofloxacin (CIP) using the combined use of persulfate, a nanocatalyst (ZnO), and 60 kHz. of ultrasound at a frequency. A pseudo-first-order kinetic model effectively characterized the degradation process. These results suggest that AOPs hold significant promise as powerful methods for degrading CIP in aqueous systems. However, the AOPs have a high cost and are difficult to operate. They demand a significant amount of energy, have exorbitant initial investment costs, and necessitate the presence of highly skilled operators [108, 135]. Electrocoagulation (EC) serves as an effective approach for ciprofloxacin (CIP) removal and is recognized as a highly effective treatment technique. A study by Ahmadzadeh, Asadipour [136] conducted a study that yielded a promising outcome, attaining a 90.34% removal efficiency of ciprofloxacin (CIP) from hospital wastewater through the electrocoagulation (EC) method utilizing an aluminum electrode. The test was done with a pH of 7.78 and a current density of 12.5 mA/cm^2. In a study conducted by Yoosefian, Ahmadzadeh [137], it was found that more than 99% of CIP was removed under specific conditions. The CIP concentration was 60 mg/L, the pH was 7.5, and the current density was 15 mA/cm^2. The elimination process was carried out using an iron electrode. Electrocoagulation (EC) is a process in which a sacrificial anode material undergoes oxidation to create an efficient coagulant [107]. The EC also utilizes electricity, which incurs high expenses, but it has the potential to produce hydrogen gas as a means of offsetting the operational costs involved in the EC process [138]. Additionally, it has the capability to effectively process a wide range of diverse wastewater [138]. Tasca, Clematis [139] conducted a study that found that combining ultrasonic with anodic oxidation and solid polymer electrolyte resulted in an enhanced breakdown of CIP, with a rate of 91.36%, but

only when using a low current (a lesser current is needed) within a 20-minute timeframe. Jia, Khanal [99] found a degradation rate of 28.0% for CIP during the biodegradation process using an anaerobic sulfate-reducing bacteria sludge system. This degradation occurred when the influent CIP concentration was 5000 μg/L. Carneiro, Sabatini [98] found that the anaerobic packed bed reactor achieved an 81±16% removal efficiency for CIP, while the anaerobic structured bed reactor achieved an 81±16% removal efficiency. Both reactors exhibited comparable levels of performance. The structured bed reactor is preferred due to its reduced economic and operational expenses, primarily because it necessitates less support material within the bed [98]. The observed degradation kinetics adhered to a first-order model, and these reactors operated as plug-flow systems. As reported Prieto, Möder [140] *Trametes versicolor* was able to degrade over 90% of CIP at a conc. of 2 mg/L in malt extract after seven days of incubation. These findings demonstrate the effectiveness of biological methods for CIP degradation. Typically, biological treatment approaches are applied to wastewater characterized by high biochemical oxygen demand (BOD) levels. This method is characterized by its ease of operation and cost-effectiveness. This approach is typically employed when the biochemical oxygen demand (BOD) to chemical oxygen demand (COD) ratio exceeds 0.5 [141]. However, there are certain disadvantages associated with this treatment process, primarily the lengthy detention period (often lasting several days) and the challenge of disposing of the sludge [108]. The Fe-C micro-electrolysis method has garnered considerable interest because to its efficacy, savings, and simplicity in addressing refractory organic effluent [142]. A modified biological aerated filter (BAF) combined with Fe-C micro-electrolysis was employed to reduce CIP concentrations. In this process, KH_2PO_4, $C_6H_{12}O_6$, and NH_4Cl were supplied as sources of phosphorus, carbon, and nitrogen, respectively, in a P:N:C ratio of 1:5:100. The BAF functions to remove residual organic compounds from the effluent generated by the Fe-C micro-electrolysis. At the same time, its filter

medium facilitates microbial attachment and growt.. During this treatment, hydrogen ions (H^+) and ferrous ions (Fe^{2+}) are produced, which contribute to the effective breakdown and elimination of pollutants from the water. After treatment, the method resulted in an 85% degradation of CIP. Additionally, there was a concomitant reduction of NH_4-N (95%), COD (95%), and total phosphorus (80%) in the treated sample. This approach requires many days to achieve optimal performance. Several of these techniques are prohibitively costly and lack significant efficacy in lowering the concentration of CIP in water. In addition, the adsorption method enables the use of low-cost or undervalued waste materials, as well as other inexpensive and renewable sources [143, 144]. Over the years, the application of adsorption for ciprofloxacin (CIP) removal has been extensively and effectively investigated, often in combination with advanced oxidation processes (AOPs). The adsorption separation technique is cost-effective, has a straightforward design, and is not impacted by harmful substances [145, 146], unlike the expensive AOPs, ion exchange, electrochemical, and membrane filtration methods. These methods exhibit selectivity in efficiently removing various contaminants. Adsorption proves especially effective for removing diverse pollutants, provided that an appropriate adsorbent is chosen for the specific contaminant. Unlike biological treatment methods, which are yet to be widely commercialized, adsorption is a well-established and commercially available technology [147]. However, there have been some setbacks recorded for the adsorption process, including the requirement and associated high expense of regenerating the wasted adsorbent [147, 148]. Consequently, various researchers have conducted tests on a variety of adsorbent materials. The materials used in this study include clays [149-151], magnetic adsorbents [152-155], carbon-based materials [156, 157] and polymer-based materials [158, 159]. The following section will provide a detailed explanation of adsorption as a method for mitigating and managing CIP in aqueous environments.

2.5 Adsorption of Ciprofloxacin from Water

Ciprofloxacin (CIP) is a widely used antibiotic that will remain in water sources for a long time because it is used so much and doesn't break down easily. Because of this, its presence in water poses serious ecological risks and could be harmful for human health. It is therefore important to find efficient and effective ways to get CIP out of water sources in order to protect public health and keep the environment fresh. For this purpose, many different adsorbents have been investigated, from natural materials to advanced engineered composites. Each one has its own set of properties and works better than others at removing CIP from water.

Table 2.2 illustrates a variety of adsorbents employed to remove ciprofloxacin (CIP) from aqueous environments, each offering different levels of efficiency under various conditions. These adsorbents are characterized by their synthesis methods, optimal pH levels, interaction times, temperatures, and removal performance. A significant adsorbent is composed of a composite material made from graphene oxide (GO), chitosan (CS), and polydopamine (PDA). The composite exhibited CIP removal efficiency of 95.20% at a temperature of 45°C, employing a low adsorbent concentration of 2.10 g L^{-1} [160]. This combination showcases the ability to mix substances in order to enhance the capacity for adsorption. The adsorbent $HoFeO_3/Ho_3Fe_5O_{12}$ exhibited a high removal efficiency of 91.50% at a pH of 5, utilizing the Langmuir isotherm and a pseudo-second-order kinetic model [161]. These data suggest that by manipulating the pH and utilizing an appropriate kinetic model, the efficiency of the adsorbent can be improved. Cyprus rotundas grass and wood biochar (*Syzygium cumini* L.) are natural substances that have shown great effectiveness in eliminating CIP through adsorption. Shahnaz, Priyan [162] documented a 91% elimination rate for Cyprus rotundas grass, whereas Srivastava, Dave [163] discovered that wood biochar attained a clearance rate of 96.9%. While natural materials can offer

sustainable and economical solutions, their capacity to adsorb pollutants differs. As an illustration, the grass known as Cyprus rotundas has a high adsorption capacity (227.223 mg/g), which means it can adsorb a significant number of substances. Bamboo charcoal and Moroccan oil shales have demonstrated high adsorption efficiency for ciprofloxacin (CIP), achieving removal rates of 96% and 96.1%, respectively. These adsorbents employ PSO kinetics and Langmuir isotherm models [164, 165]. The Desilicated rice husk demonstrates an impressive sorptive capacity of 454.68 mg/g, as assessed by PSO kinetics and Langmuir isotherm [166]. Grapefruit peels have a high rate of removal and possess a significant ability to absorb substances, with a sorptive capacity of 1.71 mmol g^{-1} [167]. Nevertheless, the study conducted by Najafpoor, Sani [168] revealed that γ-Al_2O_3 nanoparticles exhibit a significantly poorer efficiency in removing CIP, with a rate of just 43.78%, when the Temkin isotherm model and PSO kinetics are employed, in comparison to other adsorbents. The research conducted by Nguyen, Dao [169] discovered that PSS-modified nano alumina exhibits an impressive removal effectiveness of 97.8%, even when used in small amounts. The magnetic carbon composite has an impressive removal efficiency of 98% and has a significant sorptive capacity of 90.1 mg/g [170]. The adsorption process is well described by the Langmuir isotherm model and conforms to pseudo-second-order (PSO) kinetics. Carbon nanotubes with many valences and MCM-41 doped with iron provide alternative approaches for eliminating CIP, achieving removal rates of 73% and 90% respectively. The rates were calculated using the Freundlich isotherm and PSO kinetics [171, 172]. In addition, the $CoFe_2O_4$/activated Carbon@Chitosan combination, when combined with nanoscale zerovalent iron particles, demonstrates remarkable removal rates of 93.5% and 95.74% respectively. It also exhibits significant adsorption capacities of 188.69 mg/g and 294.67 mg/g, respectively [173, 174]. The use of gum arabic magnetic nanoparticles results in a 96.3% removal rate of CIP, accompanied by an adsorption capacity of 54.6449 mg/g. The adsorption kinetics were modeled

using both Particle Swarm Optimization (PSO) and Pattern Formation Optimization (PFO) approaches [175]. Cyclodextrin-based nanosponges demonstrate a 90% efficacy in the removal of CIP, but with a diminished sorptive capacity [176]. CIP removal efficiency of 99.2% when the pH was 3 and the temperature was 50°C using NiO nanoparticles [177]. The removal process exhibited PSO kinetics and adhered to the Langmuir isotherm. Al-Musawi, Mahvi [178] found that when iron (III) oxide is magnetized with activated carbon, it exhibits an impressive removal rate of 96.84% and an adsorption capacity of 109.833 mg/g using PSO kinetics. Amine-functionalized MCM-41 mesoporous material demonstrated an impressive 99.25% ciprofloxacin (CIP) removal efficiency within a short contact time of 2 hours. Additionally, it exhibits a notable adsorption capacity of 164.3 mg/g [179]. Red mud exhibits a CIP removal rate of 90% and possesses a sorptive capacity of 111.11 mg/g, indicating its promise as a cost-effective natural option [180]. Montmorillonite demonstrates exceptional efficacy, as demonstrated by its capacity to eliminate 99.2% of CIP during a short duration of just 1 hour. Moreover, it exhibits a notable sorptive capacity of 128 mg/g, emphasizing its efficacy [181]. The Mn-PBA/GO material exhibits an outstanding sorptive capacity of 1826.64 mg/g, suggesting its substantial potential for efficiently eliminating CIP with great efficacy [182]. The composite aerogels, consisting of graphene nanoplatelet and boron nitride, demonstrate an exceptional capacity to eliminate CIP, achieving a removal efficiency of 99% [183]. Additionally, they exhibit a significant sorptive capacity of 185 mg/g, demonstrating a strong ability to absorb substances [184].

Overall, adsorption continues to be an environmentally sustainable and cost-effective approach for ciprofloxacin removal, meriting further research for large-scale implementation and incorporation into water treatment processes.

Table 2.2 Adsorption of CIP From Water

Name of adsorbent	amount of Adsorbent	Initial conc. of CIP (mg/l)	Optimum pH	Temperature (°C)	Interaction time (min)	CIP Sorptive capacity (mg/g)	CIP Removal (%)	Kinetic study (pseudo-first order (PFO)/pseudo-second-order (PSO)	Isotherm model (Langmuir (L)/Freundlich (F))	Reference
Combining chitosan (CS), graphene oxide (GO), and polydopamine (PDA)	2.10 g/ L	90.0	6.3	45 °C	9.0 min		95.20	PSO	L	[160]
Cyprus rotundas grass	50 mg	250	12.0	40	3 h	227.223	91	PSO	F	[162]
$HoFeO_3/Ho_3Fe_5O_{12}$	700 mg/L	25 mg/L	5.0		45 min		91.50	PSO	L	[161]
Moroccan oil shales	10 mg	5	5.0	25	240	81.11	96.1	PSO	L	[165]
Desilicated rice husk	0.40	314.8	7.92	25	306.9	454.68	–	PSO	L	[166]
Grapefruit peels	3	1.5 mmol/l	7.0	45	2 h	1.71 mmol/g	96.4	PSO	L	[167]

PSS-modified nano alumina	5 mg/ml	10	6.0	–	90	34.5	97.8	PSO	Two-step	[169]
Bamboo biochar	0.5	20	7.5	35	46	78.43	96	PSO	L	[164]
Wood biochar *Syzygium cumini* L.	2	20	7.0	–	1 h	4.25	96.9	PSO	L	[163]
Potato stems and leaves	0.01 g	10	10.0	35	12 h	23.36	–	PSO	F	[185]
Magnetic carbon composite	0.02	20	7.0	30	3 h	90.1	98	PSO	L	[170]
γ -Al_2O_3 nano particles	0.78 g	20	7.5	–	32.3	–	43.78	PSO	Temkin	[168]
Multivalent carbon nanotubes	20 mg/L	20	7.0	40	30	–	73	PSO	F	[171]
$CoFe_2O_4$/activated carbon @Chitosan	100 mg/L	10	5.0	25	15	188.68	93.5	PSO	L	[173]
Gum arabic magnetic nanoparticles	20 g	60	6.0	35	48	54.6449	96.3	Both PFO & PSO	F	[175]
Fe doped-MCM-41 s	40 mg/L	20	10.0	40	2 h	83.33	90	PSO	F	[172]

Magnetic acid-activated carbons	1.5 mg/ml	100	6.0	40	–	81.97	98	PSO	L	[186]
Cyclodextrin-based nanosponges	1 g	5	6.0	90	1 h	2	90	PSO	L	[176]
Nanoscale zerovalent iron particles	$[Fe^0]$ = 0.3, [oxalate] =0.3 mM	100	7.0	25	30	294.66	95.74	PSO	F	[174]
Protein-modified nanosilica	10 mg/ml	100	7.0	–	90	85	89.86	PSO	L	[187]
TiO_2 nanotubes	20 mg	25	7.0	25	3 h	26.38	–	PSO	L	[188]
NiO nanoparticles	1	10	3.0	50	90	–	99.2	PSO	L	[177]
Amine-functionalized MCM–41 mesoporous	0.8	10	7.0	–	2 h	164.3	99.25	PSO	L	[179]
Activated carbon magnetized	1	100	7.0	25	60	109.833	96.84	PSO	L	[178]

by iron (III) oxide										
Red mud	3 g	3	6.0	25	180	111.11	90	PSO	F	[180]
Montmorillonite	2	250	7.0	45	1 h	128	99.2	PSO	Temkin	[181]
Mn-PBA/GO	20 mg/L	200	7.0	37	2 h	1826.64	98.5	PSO	L	[182]
Zn(II)-impregnated chitosan/graphene oxide composite	10 mg/L	50	6.5	–	50	210.96	99.17	PSO	L	[183]
Graphene nanoplatelet/ boron nitride composite aerogels	250 mg/L	10.5	7.0	22	–	185	99	–	F	[184]

2.6 CIP Adsorption Mechanism

This section analyses the process by which CIP is absorbed from water-based solutions. The chemical properties of the solution exert a significant impact on the adsorption mechanism [151, 189]. Researchers can gain valuable insights into solution chemistry and adsorption mechanisms by considering factors such as the adsorbate's pKa, the adsorbent's point of zero charge (pHzc), and the solution pH. The two pK_a values of CIP are known, 5.9 and 8.9 for pK_{a1} and pK_{a2}, respectively [190]. The mechanism of ciprofloxacin (CIP) uptake can be effectively elucidated by integrating data from thermodynamic, kinetic, and isotherm modeling, combined with spectroscopic techniques such as XPS, FTIR, and XRD. The adsorption process typically involves multiple mechanisms, and their identification is done systematically. Thermodynamic analysis aids in determining the adsorption mechanism by evaluating the Gibbs free energy change (ΔG^0). Larger ΔG^0 values, typically exceeding 40 kJ/mol, suggest chemisorption, whereas smaller values below 40 kJ/mol indicate physisorption. Desorption studies are also conducted to gain a deeper understanding of the adsorption mechanism. The use of eluents such as organic solvents or distilled water generally suggests that the process is physical, while the effectiveness of strong acids or bases points to chemical adsorption. Mechanistic insights can be further refined through kinetic and isotherm modeling by selecting models grounded in relevant assumptions. Additionally, spectroscopic analyses facilitate the identification of specific functional groups and precise interaction sites. It is particularly crucial to isolate the specific chemical bonds that have a role in chemical or physical interaction. Understanding solution chemistry—considering parameters such as pKa, pHzc, and pH—is crucial for determining the potential chemical reactions that may occur under specific pH conditions. The adsorption pH_{ZC} and the optimal pH uptake control mechanism are both presented in **Table 2.3** (for studies in which the researchers carried out a detailed

study of the underlying mechanisms). Other researchers just performed normal adsorption experiments without describing the process of absorption. The interactions between the adsorbate and adsorbent are influenced by the solution pH, with only the mechanism at the most favorable pH documented in **Table 2.3**. Ciprofloxacin's first pKa (pKa_1 = 5.9) corresponds to the deprotonation of the carbonyl group, while the second pKa (pKa_2 = 8.9) relates to the protonation of the amine group [191, 192]. Several studies commonly report values around 6.1 and 8.7 [149, 193, 194]. Cationic, anionic, and zwitterionic forms are the three distinct species in which ciprofloxacin (CIP) can exist. [195], as depicted in **Figure 2.2**. The colors red and green in **Figure 2.2** represent the precise locations of these functional groups. Adsorption can take place by cation exchange with the pollutant's protonated amine groups when the adsorbent surface is negatively charged. On the other hand, deprotonated carboxylic groups generate more intricate interactions across surfaces with an overall positive charge [196]. In this situation, the adsorbent point of zero charge (pHzc) is important. As demonstrated in **Figure 2.2**, electrostatic interactions, π-π interactions, hydrogen bonds, hydrophobic interactions, and pore diffusion are the main mechanisms that lead to the uptake of CIP as **Table 2.3** illustrates. Hydrophobic interactions facilitate the adsorption of ciprofloxacin (CIP) owing to its low solubility. Within the pH range of 5.90 to 8.89, CIP exhibits minimal solubility and predominantly exists as an electrically neutral zwitterion. Electrostatic interactions involve the attractive or repulsive forces between molecules carrying opposite charges [197]. Electrostatic interactions enhance ciprofloxacin (CIP) adsorption only when the adsorbent and adsorbate exhibit opposite charges, resulting in an attractive force. For this attraction to occur, CIP must carry a charge opposite to the net surface charge of the adsorbent. In the pH range of 1 to 5.59, electrostatic interactions frequently take place when the adsorbent has a net negative surface charge. They may also have some influence up to pH 8. Electrostatic attraction facilitates the uptake of CIP when the adsorbent has a positive charge greater than pH 9. The

CIP structure has a benzene ring, which means it can interact with adsorbents through π-π interactions. The benzene ring's structure, which has a lot of electrons, is what causes the stacking effect. In the acceptor-donor relationship of the π-π interaction, the CIP is usually the donor and the adsorbate is the acceptor. These elements are very important when the pH of the solution is close to neutral or when the CIP acts as a zwitterion. Hydrogen bonds and π-π interactions happen in similar pH ranges. One specific type of dipole-dipole interaction is hydrogen bonds, which are comparatively weak intermolecular interactions [198]. These interactions take place between electronegative atoms like nitrogen, fluorine, and oxygen with hydrogen at intermediate sites. Pore diffusion tends to dominate when the adsorbent has small pore diameters and ciprofloxacin (CIP) molecules stack within these pores. This behaviour can be analyzed using kinetic modeling, specifically the Weber and Morris diffusion model, originally developed by Weber Jr. and Morris in (1963) [199]. The limiting factor is usually not bulk diffusion across the solid-liquid layer. This is only true if the concentration of CIP in the solution is very low, in which case it becomes the slowest step. Electrostatic interactions, π-π interactions, H-bonds, hydrophobic interactions, and pore diffusion are the main mechanisms of CIP uptake, as shown in **Table 2.3**

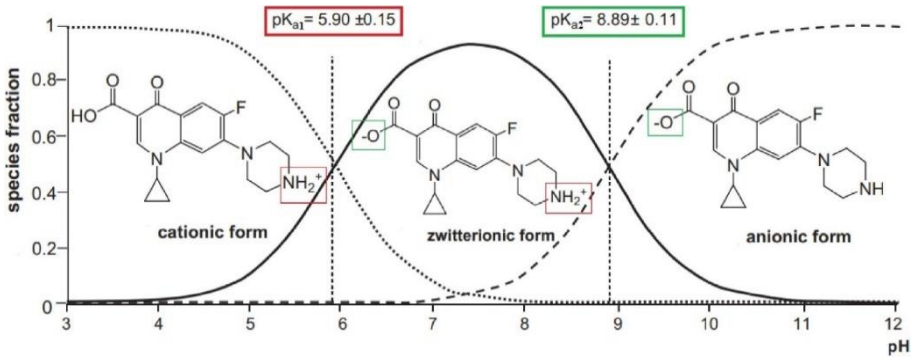


Figure 2.2 Ionic forms of CIP based on the pK_a (showing the positions of the protonation and deprotonation functional groups) [157]

Table 2.3 Mechanism of ciprofloxacin (CIP) uptake from aqueous media.

Adsorbent	Adsorption mechanism	Optimum pH	References
Chitosan/biochar hydrogel beads	H-bonds, π-π stacking interactions, hydrophobic effects	3.0	[200]
Modified hydrogel beads	H-bonds, hydrophobic effects	8.0	[201]
Activated carbon (AC) from peach stones	π-π stacking interactions	–	[202]
Bentonite-MSW biochar	Electrostatic attractions	6.5	[203]
Bentonite-chitosan	Ion exchange processes	–	[204]
Montmorillonite- MSW biochar	π-π stacking interactions	5.0	[205]
Fe_3O_4-SiO_2-Schif base composite	π-π stacking interactions	7.0	[206]
Activated carbon (AC) from hazelnut	Intra-particle diffusion	6.0	[191]
inorganic-organic modified adsorbent ICDW-APTES	Electrostatic attractions	7.0	[207]
Poly(m-phenylenediamine) grafted onto Calotropis gigantean fiber	Electrostatic attractions	6.0	[208]

AC from Prosopis juliflora	Electrostatic attractions	6.0	[209]
Montmorillonite-cellulose acetate	Intra-particle diffusion	6.0	[210]
Activated carbon (AC) from Syagrus romanzoffiana	Physisorption	7.0	[211]
Biosorbent from Dialium guineense	Physisorption	6.0	[212]
Biosorbent from grapefruit peel	Electrostatic attractions	7.0	[167]
Bentonite	π-π stacking interactions	3.0	[213]
Functionalised bio-graphene	Electrostatic attractions	–	[214]
Graphene oxide/sodium alginate	π-π stacking interactions	2.0	[215]
Montmorillonite	Electrostatic attractions	7.0	[181]
Cationic flax noil cellulose	Electrostatic attractions	7.0	[216]
Activated and zinc oxide (ZnO)-doped camphor leaf biochar.	H-bonds, Electrostatic attractions, hydrophobic effects	4.0	[217]
Activated sludge doped with biochar	Electrostatic attractions, pore diffusion effects, π-π stacking interactions,	6.0	[218]

Nickel sulphide nanomaterial	Electrostatic attractions	–	[219]
Carbon nanofibers	Electrostatic attractions, hydrophobic effects, π-π stacking interactions	5.0	[220]
Graphene oxide/nitrilotriacetic acid	H-bonds, Electrostatic attractions	–	[221]
Activated carbon (AC) from ZIF	hydrophobic effects, Electrostatic attractions,	6.0	[222]
Graphene oxide/diethylene triamine pentaacetic acid	Electrostatic attractions, H-bonds	3.0	[223]
Biochar from tea leaves	π-π stacking interactions, electrostatic attractions, H-bonds	6.0	[224]
Sodium alginate/k-carrageenan composite	Electrostatic attractions	5.1	[225]
Carbon nanotube (CNT)/GO/sodium alginate composite	π-π stacking interactions	–	[226]
Graphene hydrogel	H-bonds, π-π stacking interactions	6.0	[227]
Poly(styrenesulfonate)-modified α-alumina (α-Al_2O_3)	Electrostatic attractions	6.0	[169]

Activated carbon (AC) from bamboo	Hydrophobic effects	6.0	[228]
Ordered carbon	Hydrophobic effects	6.0	[228]
Modified ordered carbon material	Hydrophobic effects, H-bonds	6.0	[229]
Ordered carbon	Hydrophobic effects, H-bonds	6.0	[230]
Activated carbon (AC) from bamboo	Hydrophobic effects	6.0	[231]
Protein-modified nano-silica composite	Electrostatic attractions	7.0	[187]
Magnetic N-doped porous carbon	Electrostatic attractions, H-bonds, hydrophobic effects,	7.0	[232]
Magnetite–imprinted chitosan	Electrostatic attractions	6.5	[233]
Fe-based MIL-53 MOF	Electrostatic attractions, H-bonds	4.0	[234]
Magnetic chitosan/graphene oxide composite	Electrostatic attractions,	5.0	[193]
Covalent organic polymers	Electrostatic attractions, H-bonds, hydrophobic effects	6.0	[159]
MWCNT	Electrostatic attractions	4.0	[21]
Rice straw-derived biochar	π-π stacking interactions	–	[235]

g-MoS_2 coated biochar	pore diffusion, π-π stacking interactions, ion exchange processess, electrostatic attractions	–	[236]
Graphene hydrogel	π-π stacking interactions, Hydrophobic effects	–	[237]
Rice straw biochar	π-π stacking interactions, H-bonds,	7.0	[238]
Fe_3O_4/graphene oxide/biochar	Hydrophobic effects	6.0	[239]
Ni/alginate	π-π stacking interactions, H-bonds, cation bonding bridge	7.0	[240]

This study demonstrates how modern adsorbent materials can efficiently remove CIP from water, enhancing water quality and safeguarding aquatic environment.

Chapter 3: MATERIALS AND METHODOLOGY

3.1 Chemicals and Reagents

Copper (II) sulfate pentahydrate (99.5 %, Merck), sodium tungstate dihydrate (98 %, Sisco Research Laboratories), cetyltrimethylammonium bromide (99%, Sisco Research Laboratories), sodium hydroxide (Research Lab Fine Chem Industries), absolute ethanol (Sigma-Aldrich), hexadecylamine (>95%, Tokyo Chemical Industry Co Ltd), tetraethyl orthosilicate (Alfa Aesar), titanium isopropoxide (27.8-28.6% TiO_2, Sisco Research Laboratories), ammonia (25%, Merck KGaA), sulfuric acid, (ACS reagent, 95-98%, Sigma-Aldrich), methylene blue (Smart Lab), ciprofloxacin hydrocholride hydrate (98-102%, Sisco Research Laboratories). Ultrapure water (≥18.2 MΩ-cm) from a Direct-Q® 3 UV water purification system (Merck Millipore, UK) was used to make chemical solutions.

3.2 Instruments

The instruments and apparatus used for the synthesis and the photocatalytic activity of $CuWO_4$@TiO_2 are as follows: Digital balance (BEL M254Ai), Hotplate magnetic stirrer (MS-H380-Pro, USA), Direct-Q®3 UV Water purification System, Sonicator (Hwashin Powersonic 405, Korea), Centrifuge machine (CTF-TH16, China), Vortex, Hot air Oven (Memmert UN55), , UV-Vis spectrophotometer (T80+, UK), Shaking water bath (Lab House), pH meter (Hanna Instrument).

3.3 Synthesis

3.3.1 Synthesis of $CuWO_4$

For this synthesis method, we employed chemicals of analytical-grade quality. The $CuWO_4$ core was synthesized using a hydrothermal treatment process. At first, the synthesis process began with mixing copper (II) sulfate pentahydrate (0.01 M) and sodium tungstate dihydrate (0.01 M) of Milli-Q water.

Cetyltrimethylammonium bromide (CTAB), 2.5 gm, was then added to the mixture, mixed properly for 1 hour, and then added to the sodium hydroxide to keep the pH at 10 and the mixture's final volume was 150 mL. Finally, the suspension was placed in a Teflon-lined stainless-steel autoclave (250 mL) and reacted at 160°C for 24 hours. The core CuWO4 was collected once it naturally reached room temperature, cleaned with Milli-Q water and ethanol, and then dried at 70°C.

3.3.2 Synthesis of $CuWO_4@TiO_2$

After ultrasonically dispersing 0.30 g of CuWO4 core material into a solution consisting of 130 mL of ethanol and 13 mL of Milli-Q water, 12 mL of ammonia solution was added. Then, using magnetic stirring, 1 mL of tetraethyl orthosilicate (TEOS), dissolved in 9 mL of ethanol, was added to the mixture gradually at a rate of 1 mL/min. After six hours of stirring, the $CuWO_4@SiO_2$ product was collected by centrifugation, washed, and allowed to dry overnight at 70°C. For the TiO_2 coating, 0.25 g of the obtained $CuWO_4@SiO_2$ cubes was homogeneously dispersed in 9.74 mL of ethanol through ultrasonication. Following this, 0.08 g of hexadecylamine (HDA) was added and stirred at room temperature for 1 minute to form a uniform dispersion. Subsequently, 0.2 mL of titanium isopropoxide (TTIP) was introduced under stirring, and the mixture was stirred for an additional 10 minutes. The $CuWO_4@SiO_2@TiO_2$ cubes were then collected by centrifugation and dried at 70°C for 2 hours.

To prepare $CuWO_4@TiO_2$ core-shell material, a solvothermal treatment of $CuWO_4@SiO_2@TiO_2$ cubes was performed. Using ultrasonication, $CuWO_4@SiO_2@TiO_2$ precursor cubes were dispersed in a mixture of 100 mL of ethanol and 50 mL of Milli-Q water with an ammonia concentration of 0.5 M. This mixture was sealed in a 250 mL Teflon-lined autoclave and reacted for 20 hours at 160°C. After reaching ambient temperature naturally, the final products ($CuWO_4@TiO_2$) were collected, washed with absolute ethanol and Milli-Q water, and then dried at 70°C.

3.4 Characterization

Synthesized $CuWO_4@TiO_2$ nano catalyst was characterized through different physicochemical characterization processes. The $CuWO_4@TiO_2$ nanocatalyst's functional groups and chemical bonds were examined using the Fourier Transform Infrared Spectrometer (FTIR, Spectrum 100, PerkinElmer, USA). To provide a comprehensive picture of the structural integrity and homogeneity within the $CuWO_4@TiO_2$ nano catalyst, the surface morphology, lattice structure, particle size, and distribution were examined using the Field Emission Scanning Electron Microscope (FESEM, JSM 7600F, JEOL Ltd., Tokyo, Japan). Using a Micromeritics 3 Flex version 5.00 (Micromeritics, Norcross, GA, USA), the nitrogen adsorption–desorption process at 76 K was recorded using the Brunauer–Emmett–Teller (BET) technique. The crystalline structure and phase composition of synthesized nanomaterials were examined using X-ray diffraction (XRD, EMPREAL, Netherlands) in order to verify their phase purity. The surface chemical composition and oxidation states of the elements in the $CuWO_4@TiO_2$ nanocatalyst were investigated using the X-ray Photoelectron Spectrometer (XPS, Kratos Axis Supra, Kratos Analytical Ltd., UK).

3.5 Adsorption Studies

To prepare a 25 mg/L stock solution of CIP, 25.0 mg of CIP was dissolved in 1000 mL of Milli-Q water in a volumetric flask. Further, concentrations of 5–20 mg/L were also prepared by dilution from stock. 30 mL of CIP solution (5, 10, 15 mg/L) with specific amounts of adsorbent (100, 250, 400 mg/L) were added to 50 mL Falcon® conical centrifuge tubes to optimize the experiment following the Box-Behnken design. The tubes were then placed in a shaking water bath, set at 250 rpm and kept in the dark to ensure consistent shaking throughout the experiment. The required sample volume was collected after a specific interval and filtered by a syringe filter (0.22 μm). The absorbance was measured using a UV-Vis spectrophotometer (PG Instrument T80+) at the characteristic

wavelength of 272 nm. In the adsorption studies, different adsorbent dosages (i.e., 100, 250, 400 mg/L), contact times (20, 30, 40 min), pH (4, 7,10), and initial CIP concentrations (5, 10, 15 mg/L) were employed. The pH of the CIP solution was adjusted by adding sodium hydroxide base solutions or dilute sulfuric acid. A pH meter (type HI3222, Hanna Instrument, USA) was used to measure the pH. A calibration curve was created utilizing four concentrations (0, 5, 10, and 15 mg/L) in order to evaluate the adsorption percentages and adsorption capacity of CIP in an aqueous solution. This yielded an R^2 value of 0.9984.

Equations **3.1** and **3.2** were employed to calculate the adsorption capacity of Ciprofloxacin (mg/g) and the removal efficiency (%) of the adsorbent, following the methodology outlined in previous studies [241, 242].

$$\text{Q (mg/g)} = \frac{C_{i-C_f}}{m} \times V \qquad \textbf{3.1}$$

$$\text{R (\%)} = \frac{C_{i-C_f}}{C_i} \times 100 \qquad \textbf{3.2}$$

Where m and R represent the adsorbent mass (g) and the CIP removal percentage (%) in the adsorption process, respectively. C_f and C_i represent the residual (mg/L) and initial (mg/L) CIP concentrations in the solution, respectively, following the adsorption process; and V and Q represent the sample volume (L) and the adsorption capacity of the adsorbent (mg/g), respectively.

3.6 RSM-Based Modelling and Optimization

In order to maximize response, the experimental variables (adsorbent dosage, initial CIP concentration, pH, and contact time) were optimized using the Box-Behnken Design (BBD) under Response Surface Methodology (RSM). Three levels of evaluation were used for each factor (**Table 3.1**). For the development of BBD, a total of 29 experimental runs were required. Design-Expert 13.0 (trial version) software was used to create the experimental design matrix, shown in **Table 3.2**. equation **3.3** states that a second-degree polynomial model was fitted to the measured data.

$$Y = \beta_0 + \sum_{i=1}^{k} \beta_i X_i + \sum_{i=1}^{k} \sum_{j=1}^{k} \beta_{ij} X_i Y_j + \sum_{i=1}^{i} \beta_{ii} X_i^2 + \varepsilon \qquad \textbf{3.3}$$

Here, Y presents the predicted response, while X_i and X_j denote the experimental variables. The term β_0, β_i, β_{ii} and β_{ij} correspond to the regression coefficients for the intercept, linear, interaction, and quadratic terms respectively; ε defines the error [30].

Using the Box-Behnken Design (BBD), the Response Surface Methodology (RSM) was used to maximize the experimental conditions. Three different levels of evaluation were conducted on the variables that affected the adsorption process: adsorbent dosage, initial CIP concentration, pH, and contact time. This method made it possible to systematically optimize the process parameters in order to enhance the removal efficiency of ciprofloxacin (CIP).

Table 3.1 Levels of experimental variables in Box-Behnken design.

Factors	Variables	Unit	Range and coded levels		
			Low factorial (-1)	Centre point (0)	High factorial (+1)
A	Adsorbent dosage	mg/L	100	250	400
B	CIP concentration	mg/L	5	10	15
C	pH	-	4	7	10
D	Contact time	min	20	30	40

Table 3.2 Box-Behnken design matrix with actual and predicted response

	Independent variables				Response	
Run	**Adsorbent dosage (mg/L)**	**CIP Conc. (mg/L)**	**pH**	**Contact Time**	**Actual CIP removal (%)**	**Predicted CIP removal (%)**
1	100	15	7	30	59.00	58.06
2	250	15	10	30	62.00	62.92
3	250	5	4	30	94.00	92.94
4	400	10	7	20	94.80	94.09
5	250	10	10	40	82.00	81.63
6	400	10	7	40	98.10	98.55
7	400	10	10	30	80.00	78.75
8	250	15	4	30	84.00	85.09
9	250	10	7	30	95.80	95.12
10	250	10	7	30	95.80	95.12
11	250	15	7	20	77.50	76.18
12	100	5	7	30	85.00	84.16
13	250	10	7	30	96.00	95.12
14	250	10	4	20	88.00	88.28
15	400	15	7	30	95.00	95.75
16	100	10	7	40	76.60	77.17
17	250	10	7	30	92.00	95.12
18	100	10	7	20	64.20	63.60
19	100	10	4	30	67.00	68.48
20	250	5	7	20	94.40	95.13
21	250	10	4	40	90.00	88.30
22	250	5	7	40	98.00	99.55
23	250	10	7	30	96.00	95.12
24	250	5	10	30	85.00	83.77
25	100	10	10	30	54.00	54.32
26	400	5	7	30	97.50	98.35
27	250	15	7	40	90.30	89.80
28	250	10	10	20	62.00	63.61
29	400	10	4	30	96.00	95.92

To maximize the removal of emerging pollutants, such as ciprofloxacin (CIP), from urban water systems, a novel statistical technique known as RSM is employed. RSM was applied in this study using the Box-Behnken Design (BBD) to optimize the critical experimental parameters that affect the effectiveness of the TiO_2-coated $CuWO_4$ nanocatalyst, such as adsorbent dose, starting CIP concentration, pH, and contact time. This approach helps identify the best conditions for removing CIP from contaminated water. Effective experimentation with fewer trials is made possible by the Box-Behnken Design, which guarantees cost-effectiveness while capturing the nonlinear interactions between the variables. We intended to use RSM in order to better understand the process and facilitate the development of more efficient water treatment plans for antibiotic removal.

3.7 Machine Learning-Based Modelling and Optimization

3.7.1 Design of Predictive Model and Evaluation

The neural network was implemented in Python, allowing the percentage of CIP removal from aqueous solutions to be calculated. The multilayer feed-forward neural network technique, also known as the multilayer perceptron (MLP), was used to create the data-driven predictive model. An input layer, a hidden layer, and an output layer are the three or more layers that make up the MLP [[52]. A cluster of neurons makes up each layer, and these neurons are usually connected to neurons in other layers. The CIP concentration, solution pH, adsorbent dosage, and adsorption time were the study's inputs. The CIP removal percentages (%) are reflected in the output. Equation (**3.4**) was used to standardize the input and output values within the 0–1 range.

$$X_{norm} = \frac{X_i - X_{min}}{X_{max} - X_{min}} \qquad \textbf{3.4}$$

After applying equation, the normalized data, denoted as X_{norm}, is compared with the original input data X, where X_i , X_{min} and X_{max} represent the input, minimum, and maximum data, respectively.

$$X_{norm} = [X_{norm}(X_{max} - X_{min})] + X_{min} \quad \textbf{3.5}$$

Several criteria are used to determine when to stop the training process during the network's learning phase. These criteria include things like the number of steps required to implement the data into the network, computation time, and error rates [243]. Metrics like the mean correlation coefficient (R^2), mean absolute percentage error (MAPE), and mean square error (MSE) are used to evaluate the error rate. Equation **3.6** represents the correlation coefficient as follows:

$$R^2 = \frac{\sum_{i=1}^{n} (y_{di} - \acute{y}_{di})(y_i - \acute{y}_i)^2}{\sum_{i=1}^{n} (y_{di} - \acute{y}_{di})^2 (y_i - \acute{y}_i)^2} \quad \textbf{3.6}$$

where n, y_i *and* y_{di} denote the the total number of data, predicted data and the real data respectively.

To assess the predictive performance of the developed model, several statistical metrics were employed, including mean absolute error (MAE), root mean squared error (RMSE), mean squared error (MSE), and mean absolute percentage error (MAPE), defined by equations **3.7** to **3.9**.

$$\text{Mean Absolute Error (MAE)} = \frac{\sum_{i=1}^{n} |(\acute{y}_i - y_i|}{n} \quad \textbf{3.7}$$

$$\text{Root Mean Square Error (RMSE)} = \sqrt{\frac{\sum_{i=1}^{n} (\acute{y}_i - y_i)^2}{n}} \quad \textbf{3.8}$$

$$\text{Mean Absolute Percentage Error (MAPE)} = \frac{1}{n}\sum_{i=1}^{n}\left|\frac{(\acute{y}_i - y_i)}{y_i}\right| \quad \textbf{3.9}$$

Where y_i *and* $\acute{y}_i$ *denote the actual and predicted data* for the training and testing model.

3.7.2 Multilayer Perceptron (MLP) Neural Network Design

For predictive modeling, the current study used an artificial neural network (ANN) called a Multilayer Perceptron (MLP). The architecture and operation of the human brain served as the model for artificial neural networks (ANNs). They are made up of interconnected processing components, also known as artificial neurons, arranged in discrete layers. The input layer, one or more hidden layers, and the output layer are the three main layers that typically make up an ANN. The input layer of the network receives data input, with each node representing a specific feature or input variable. Through activation functions found in the hidden layers, the inputs are given weights and sent. The output layer uses the learned patterns to produce the final result or forecast. Weights represent the connections between nodes and are adjusted during training to maximize network performance.

Figure 3.1 shows and illustrates the use of a feedforward artificial neural network (ANN) with the Adam backpropagation algorithm for this investigation. A set of equations intended to calculate the network's outputs governs the forward propagation of the input data through the network during the training phase.

The output layer, on the other hand, consists of only one node, which represents the removal (%) of ciprofloxacin. The MLP neural network utilized a total of 117 experimental data points, which were obtained by systematically altering four reaction parameters. Eighty percent of the data is in the training set, and the remaining twenty percent is in the testing set. The training dataset is utilized during the optimization of hyperparameters. Once the hyperparameters have been tuned, the training dataset and optimized parameters are used to train the model. The developed model is saved and utilized to evaluate using two distinct approaches: graphical performance and performance matrices. The developed model is also used to predict the whole dataset and visualize with 95% confidence interval around the predicted values. The PSO algorithm is developed with the objective of maximizing removal efficiency, which provides optimal input parameters.

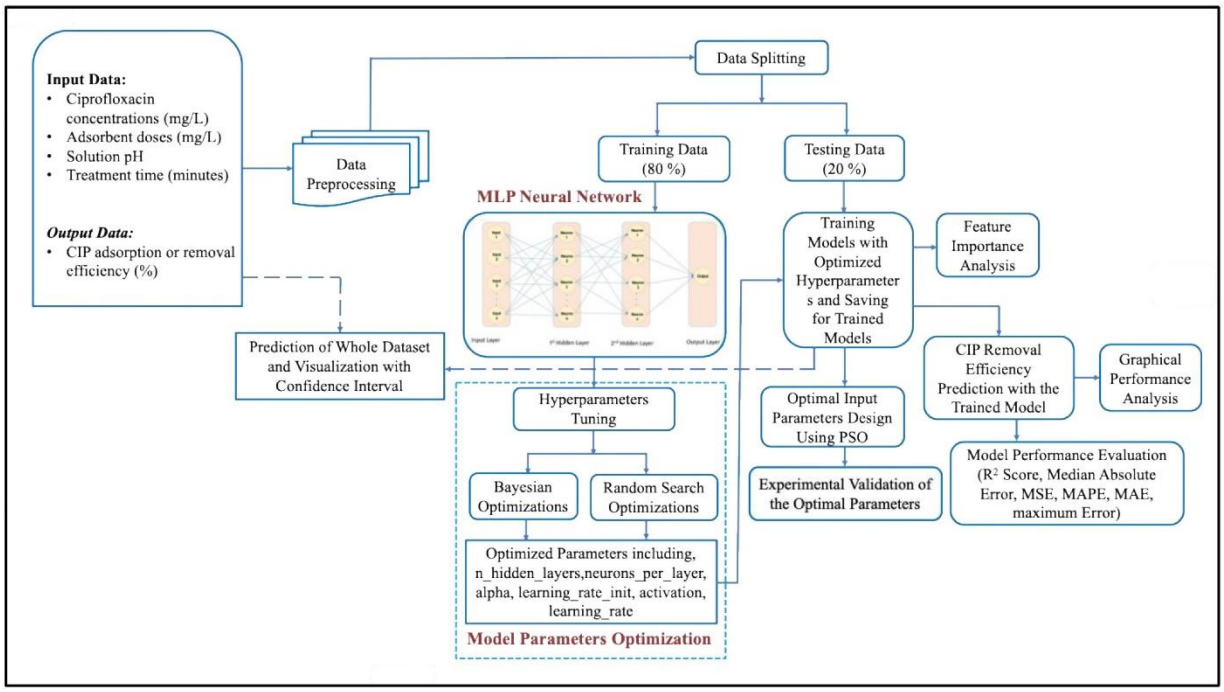


Figure 3.1 Schematic diagram of the four-layer MLP model with four input and one output layer used in this study

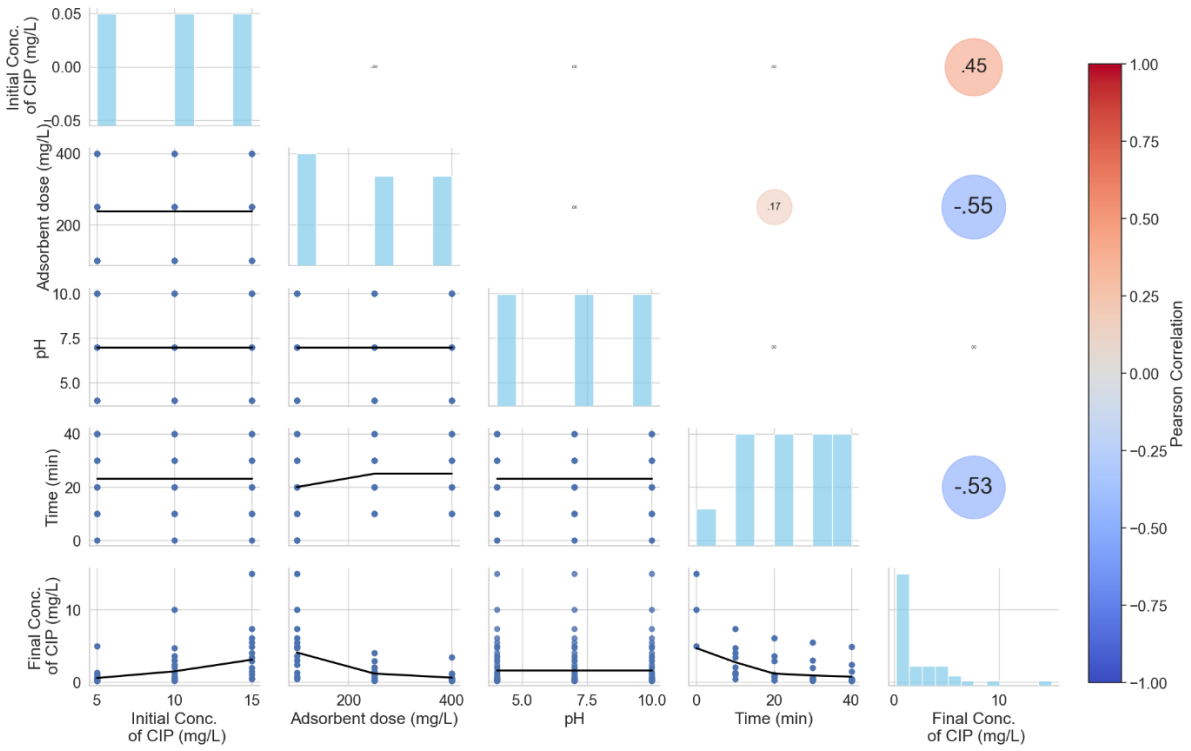


Figure 3.2 Scatter plot matrix for input and outcome variables. Red and blue circle tones indicate a positive and negative correlation with proportion, respectively.

3.7.3 Model Optimization and Its Importance

3.7.3.1 Bayesian optimization

Bayesian optimization (BO) is a method employed for solving global optimization problems, particularly those featuring black-box functions (f) that necessitate costly evaluations. BO is adept at navigating intricate search spaces and refining expensive objective functions through the iterative updating of a probabilistic posterior distribution and the utilization of an acquisition function. In the realm of Bayesian optimization, the probability distribution of this function for the global optimum is leveraged to pinpoint the optimal hyperparameters that maximize the area under the curve (AUC) [244]. Surrogate models are utilized to approximate objective functions, representing a probabilistic depiction of the objective function as $P(f(x)|x)$, where $f(x)$ denotes the score, and x denotes the hyperparameters.

The Bayesian optimization process involves the refinement of a Gaussian probabilistic model, initialized with randomly selected initial points. Acquisition, often expressed as the upper confidence bound (UCB) [245], is typically determined using the formula $UCB(x; \beta) = \mu(x) - \beta\sigma(x)$, where $\mu(x)$ denotes the predicted objective function, $\sigma(x)$ denotes uncertainty, and β governs the balance between exploration and exploitation. Through iterative iterations, the optimization evaluates objective function scores for selected hyperparameters, updates the surrogate model, and employs the acquisition function to identify the subsequent set of hyperparameters where the function achieves maximum optimization.

3.7.3.2 Random search optimization

Employing random search optimization represents a straightforward and efficient approach to hyperparameter tuning, particularly in the context of MLP

models. Unlike grid search, random search is less computationally intensive while still allowing for the exploration of a broad range of configurations [246]. By randomly selecting hyperparameter combinations, this method facilitates an effective exploration of the hyperparameter space, striking a well-balanced balance between exploration and exploitation. This pragmatic approach proves highly effective in optimizing MLP models, as it considers various parameters such as the number of hidden layers, neurons per layer, alpha, learning rate initialization, activation functions, and learning rate. It aids in the identification of optimal combinations that enhance model performance without necessitating exhaustive exploration of the entire parameter space.

3.8 Adsorption Isotherms

Adsorption isotherm models were used to understand how the adsorbate interacts with the adsorbents and to gain a comprehensive insight into the nature of this interaction. Specifically, the CIP uptake behaviour of $CuWO_4$@TiO_2 was validated using Langmuir, Freundlich and Temkin isotherm models. The experiments were conducted with a 300 mg/L fixed adsorbent dosage. Initial antibiotic concentrations ranged from 5 to 25 mg/L to observe adsorption behavior across different concentrations. The pH of the solution was kept at 7, and the experiments were performed at temperatures of 30°C, 40°C, and 50°C. Continuous shaking at 250 rpm in a water bath ensured thorough mixing and effective contact between the adsorbent and the antibiotic. After 40 minutes, the mixtures were collected, filtered, and analyzed for remaining antibiotic concentration using a UV-Vis spectrophotometer, as described in the section **0**.

The Langmuir, Freundlich and Temkin isotherm models, as illustrated in **Table 3.3**, correspond to previously reported findings [30].

A monolayer adsorption mechanism is proposed by Langmuir's model and this implies that the adsorbate molecules arrange themselves in a layer on the adsorbent surface [247].

Table 3.3 Isotherm models of Langmuir, Freundlich, and Temkin

Isotherm Model	Non-linear form	Parameters and constants	Plot	Eq. no
Langmuir	$q_e = \frac{q_m K_L C_e}{1 + K_L C_e}$	$\boldsymbol{C_e}$= the adsorbate's equilibrium concentration (mg/L) $\boldsymbol{q_e}$= amount of adsorbate adsorbed at equilibrium (mg/g) $\boldsymbol{q_m}$= maximum monolayer adsorption capacity (mg/g); $\boldsymbol{K_L}$ = Langmuir constant (L/mo1)	q_e vs C_e	**(3.10)**
Freundlich	$q_e = K_F C_e^{\frac{1}{n_F}}$	$\boldsymbol{K_F}$= Freundlich Constant (mg/g) $\boldsymbol{n_F}$= Heterogeneity factor	q_e vs C_e	**(3.11)**
Temkin	$q_e = \frac{RT}{b_T} \ln A_T C_e$	$\boldsymbol{A_T}$= Binding constant for Temkin isotherm equilibrium (Lg^{-1}) $\boldsymbol{b_T}$ = The Temkin isotherm constant correlates to the sorption heat $(Jmol^{-1})$ $\boldsymbol{R}$ = Universal gas constant $(8.314\, JK^{-1}mol^{-1})$ $\boldsymbol{T}$ = Temperature (Kelvin)	q_e vs C_e	**(3.12)**

By using the Freundlich isotherm model, the studies imply that the adsorption process is heterogeneous and has variable adsorption sites and thus forms multilayering and uneven adsorption sites for the adsorbate [248]. On the other hand, Temkin's model assumes a uniform distribution of binding energies across the adsorbent surface, where the heat of adsorption decreases linearly as the surface coverage increases [249]. The adsorption behavior—whether it aligns

with the Langmuir, Freundlich, or Temkin isotherm model—is determined based on the model that provides the best fit to the data using correlation coefficients (R^2) and other statistical parameters.

3.9 Adsorption Kinetics

Using $CuWO_4@TiO_2$, a thorough kinetic analysis was conducted to determine the kinetic parameters necessary for the design of a continuous contactor and to investigate the process of adsorptive removal of CIP. The batch contactor research used two kinetic models, pseudo first-order and pseudo second-order, to assess the experimentally collected kinetic data. The experiments employed a fixed dosage of 300 mg/L of adsorbent. The initial antibiotic concentration, temperature and pH were fixed at 10 mg/L, 30°C and 7, respectively. Continuous shaking at 250 rpm in a water-shaking bath ensured thorough mixing and contact between the adsorbent and the antibiotic. The experiments were performed over a range of 10 to 40 minutes. At specific intervals, samples were collected, filtered using a 0.22 μm syringe filter, and analyzed for remaining antibiotic concentration using a UV-Vis spectrophotometer at a characteristic wavelength of 272 nm, as described in Section **0**. The pseudo first-order and pseudo second-order kinetics models, as illustrated in **Table 3.4**, correspond to previously reported findings [30].

The fit of the data to the pseudo first-order and pseudo second-order kinetic models is used to evaluate the adsorbent's adsorption behavior. Using correlation coefficients (R^2) and other statistical measures, the model that best fits the data will show whether the adsorption process follows pseudo first-order or pseudo second-order kinetics. The pseudo first-order model suggests that the adsorption rate depends on surface reactions [250] .

The pseudo-second-order model, on the other hand, suggests that a chemisorption process is the rate-limiting phase that involves valence forces

through electron sharing or exchange between the adsorbent and the adsorbate [251]. The adsorption kinetics and mechanism are better understood as a result of this assessment.

Table 3.4 pseudo-first-order model and pseudo-second-order kinetics models

Kinetic Model	Non-linear form	Parameters and constants	Plot	Eq. no
pseudo first-order	$q_t = q_e(1 - e^{-k_1 t})$	$\boldsymbol{q_t}$ = Adsorption of antibiotics at time t (mg/g) $\boldsymbol{q_e}$= Adsorption of antibiotics at equilibrium (mg/g) $\boldsymbol{k_1}$= The pseudo-first-order kinetic model's rate constant (1/min) $\boldsymbol{t}$ = time (min)	$q_t$vs t	**(3.13)**
pseudo second-order	$q_t = \frac{k_2 q_e^2 t}{1 + k_2 q_e t}$	$\boldsymbol{k_2}$= The pseudo-second-order kinetic model's rate constant.	$q_t$vs t	**(3.14)**

3.10 Reusability Test

The $CuWO_4$@TiO_2 nanocatalyst's reusability was assessed by repeating the adsorption procedure many times. In order to renew the adsorbent after each cycle, it was dispersed in ethanol and stirred for half an hour at room temperature. Whatman filter paper was then used to separate the adsorbent, and any remaining impurities were extensively cleaned with Milli-Q water and ethanol before being dried for 12 hours at 70°C. In order to evaluate the material's capacity to sustain its adsorption over time, this regeneration process was performed for every adsorption cycle.

Chapter 4: RESULTS AND DISCUSSION

4.1 Characterization

4.1.1 X-ray Diffraction (XRD)

The $CuWO_4.2H_2O$, amorphous TiO_2, and amorphous TiO_2 coated $CuWO_4.2H_2O$ XRD patterns are displayed in **Figure 4.**. In **Figure 4.** depicts $CuWO_4.2H_2O$ nanoparticle showed five distinct peaks (2θ = 22.50, 29.52, 35.40, 52.85, and 63.36^0). This indicates that the resulting nanoparticles have a wolframite structure and are monoclinic $CuWO_4.2H_2O$ nanoparticles (JCPDS No: 330503) [252]. In **Figure 4.**, the XRD pattern of amorphous TiO_2 displays an absence of peaks, indicating its amorphous nature [253]. The XRD analysis of the TiO_2-coated $CuWO_4.2H_2O$ nanoparticles **Figure 4.** reveals no noticeable change in comparison to the uncoated $CuWO_4.2H_2O$. Specifically, there are no discernible peaks corresponding to crystalline TiO_2, indicating that the coating process did not induce TiO_2 crystallization. This result aligns with the XRD pattern obtained for TiO_2 nanoparticles synthesized under the specified conditions, except for the missing peaks of $CuWO_4{\cdot}2H_2O$. This suggests that the TiO_2 nano-shells formed on the surface of the core $CuWO_4{\cdot}2H_2O$ nanoparticles were amorphous in nature. A similar observation has been reported in [254].

4.1.2 Fourier Transform Infrared Spectroscopy (FTIR)

The FTIR spectra of $CuWO_4@TiO_2$ were collected both before **Figure 4. (blue line)** and after **Figure 4. (red line)** adsorption of ciprofloxacin (CIP) in order to analyze the changes in functional groups and confirm the adsorption mechanism. In before adsorption, a broad peak around 3400 cm^{-1} indicates O-H stretching vibrations from water molecules [255]. A sharp peak at 1100 cm^{-1} is observed for Si-O-Si bonds [256], which may indicate the use of tetraethyl orthosilicate (TEOS) in the synthesis process, while a peak around 800 cm^{-1} is due to Ti-O stretching vibrations. Characteristic bands of $CuWO_4$ occurring at around 550 cm^{-1}, 790 cm^{-1}, and 800 cm^{-1} –900 cm^{-1} for Cu-O stretching vibrations, Cu^{n+}-$O^{2-}$$W^{n+}$ vibration respectively as well as the stretching O-H vibration at around 1400 cm^{-1} confirm

the successful synthesis $CuWO_4@TiO_2$ [257]. A sharp peak around 1400 cm^{-1} in the FTIR spectrum of $CuWO_4@TiO_2$ before adsorption is attributed to C–O stretching or O–H bending vibrations, which typically arise from surface hydroxyl groups, adsorbed water, or carbonate/carboxylate species that can form on metal oxide surfaces through atmospheric CO_2 exposure or synthesis byproducts [258, 259]. After ciprofloxacin (CIP) adsorption, this peak becomes narrower, suggesting specific interactions between CIP's functional groups and the active surface sites of the adsorbent. Such interactions likely reduce the vibrational heterogeneity by forming more uniform hydrogen-bonding or electrostatic linkages. This implies the participation of –OH or –COOH groups in the adsorption mechanism. On the other hand, a distinct peak at ~2350 cm^{-1} observed before adsorption, attributed to surface-bound carbonates or adsorbed CO_2 [260], disappeared after antibiotic uptake. This suggests the replacement or masking of these species due to strong interactions between the antibiotic molecules and the $CuWO_4@TiO_2$ surface, confirming successful adsorption. Furthermore, after the adsorption of CIP, **Figure 4.** (red line) shows a new peak at 1480 cm^{-1}, attributed to the aromatic benzene ring [261], confirming the chemisorption of CIP onto $CuWO_4@TiO_2$. The emergence of this peak demonstrates the successful adsorption and provides insights into the interaction between the CIP and the $CuWO_4@TiO_2$ surface.

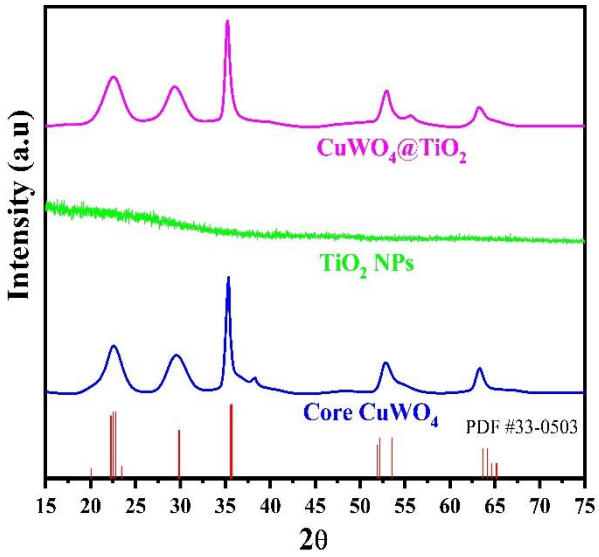


Figure 4.1 XRD pattern of $CuWO_4.2H_2O$, TiO_2 (amorphous), **and** amorphous TiO_2 coated $CuWO_4$

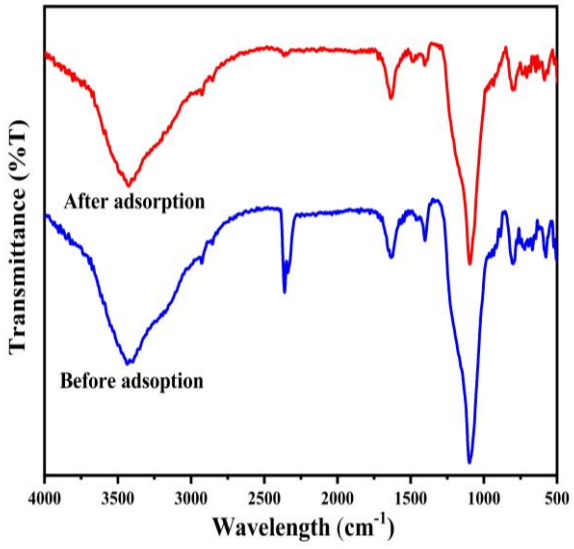


Figure 4.2 FTIR Spectra of $CuWO_4@TiO_2$: before adsorption, and after adsorption of CIP by $CuWO_4@TiO_2$

4.1.3 Field Emission Scanning Electron Microscopy (FESEM) and Average Particle Size

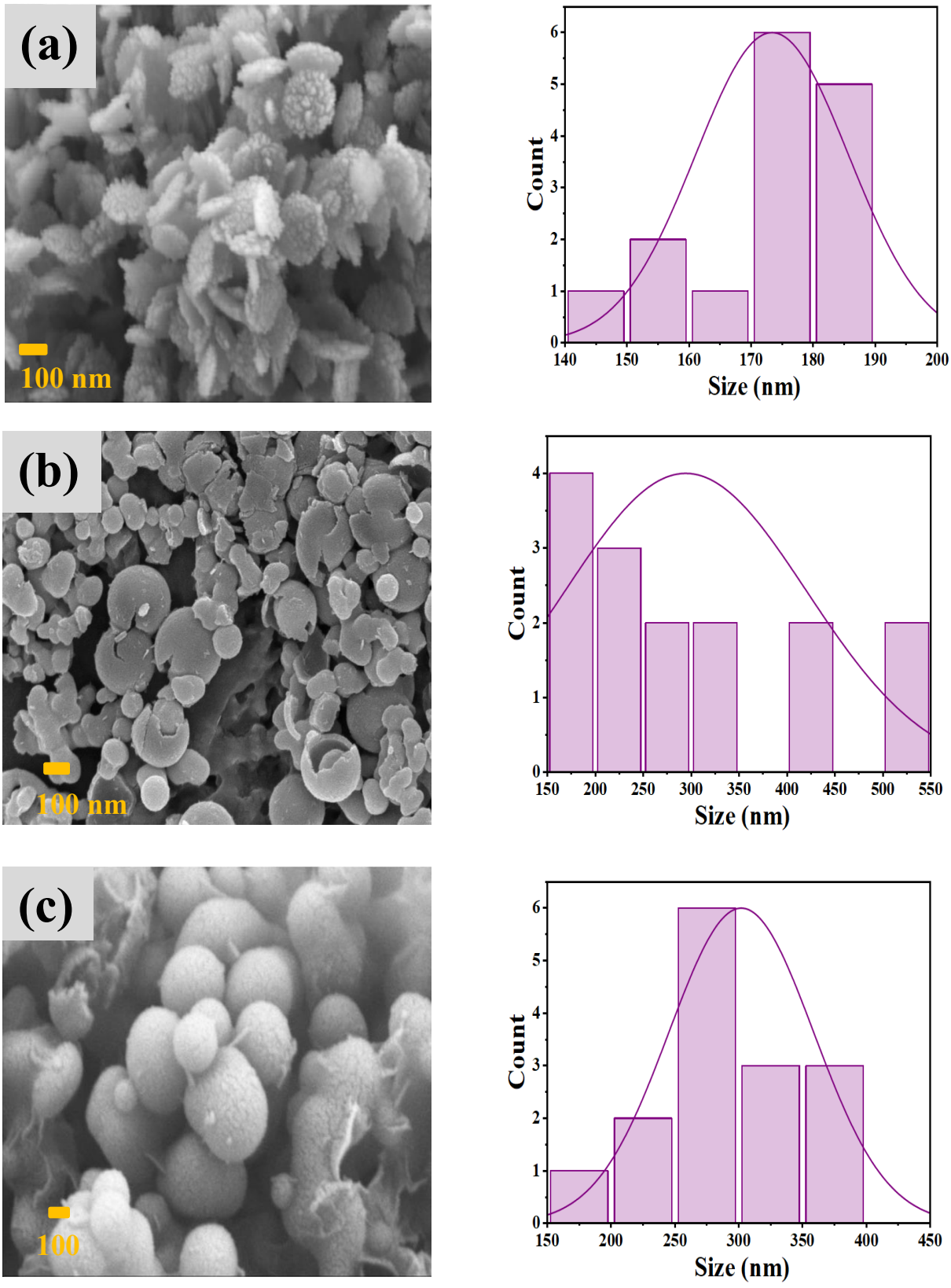


Figure 4.1 FESEM and average particle size **(a)** core $CuWO_4$ **(b)** hollow TiO_2 **(c)** TiO_2 coated $CuWO_4$ ($CuWO_4$@TiO_2)

The FESEM images in **Figure 4.1** provided detailed information on the size of the particles and morphology, confirming the successful synthesis of the desired structures, with **Figure 4.1(a)** representing the core $CuWO_4$ particles, **Figure 4.1 (b)** representing the hollow TiO_2 particles, and **Figure 4.1 (c)** representing the core-shell structured particles ($CuWO_4$@TiO_2) in this research.

The core $CuWO_4$ particles (**Figure 4.1 (a)**) exhibit well-defined spherical structures with an average size of 173 ± 12 nm (using image analysis software ImageJ and OriginPro 8.5). In contrast, the TiO_2 hollow shells (**Figure 4.1 (b)**) display a thin layer covering the hollow structure with an average size of 294 ± 126 nm. The FESEM image of the core-shell particles (**Figure 4.1 (c)**) illustrates the successful encapsulation of $CuWO_4$ cores within TiO_2 shells, forming uniform core-shell structures ($CuWO_4$@TiO_2) with an average particle size of around 302 ± 57 nm.

4.1.4 X-ray Photoelectron Spectroscopy (XPS)

The elemental composition and chemical states of the CuWO4@TiO2 core-shell nano-adsorbent was investigated using XPS analysis, as illustrated in **Figure 4.2 (a-d)** for Ti, O, Cu, and W, respectively [257]. In the high-resolution XPS spectra, the Ti 2p spectrum (4a) exhibited two characteristic peaks at binding energies of ~458.5 eV (Ti $2p_{3/2}$) and ~464.3 eV (Ti $2p_{1/2}$), corresponding to Ti^{4+} in the TiO_2 shell [262-266] (**Figure 4.2 a**). The absence of additional peaks indicated that Ti exists solely in the TiO_2 phase without any reduction to lower oxidation states. As can be seen from **Figure 4.2 b**, the O 1s spectrum showed a primary peak at ~530.1 eV, attributed to lattice oxygen in both $CuWO_4$ and TiO_2. A minor shoulder at ~531.8 eV was also observed, suggesting the presence of surface hydroxyl groups [257]. The Cu 2p spectrum (**Figure 4.2 c**) displayed two prominent peaks at ~932.6 eV (Cu $2p_{3/2}$) and ~952.3 eV (Cu $2p_{1/2}$), characteristic of Cu^{2+} in the $CuWO_4$ core [257, 265-267]. The lack of significant satellite peaks further confirms that Cu

predominantly exists in the $CuWO_4$ phase. Finally, the W 4f spectrum (**Figure 4.2 d**) exhibited peaks at ~37.8 eV and ~35.7 eV, corresponding to W $4f_{5/2}$ and W $4f_{7/2}$, respectively [257]. These binding energies are consistent with W^{6+} in the WO_4^{2-} anion of the $CuWO_4$ structure, confirming the oxidation state of tungsten in the nano adsorbent.

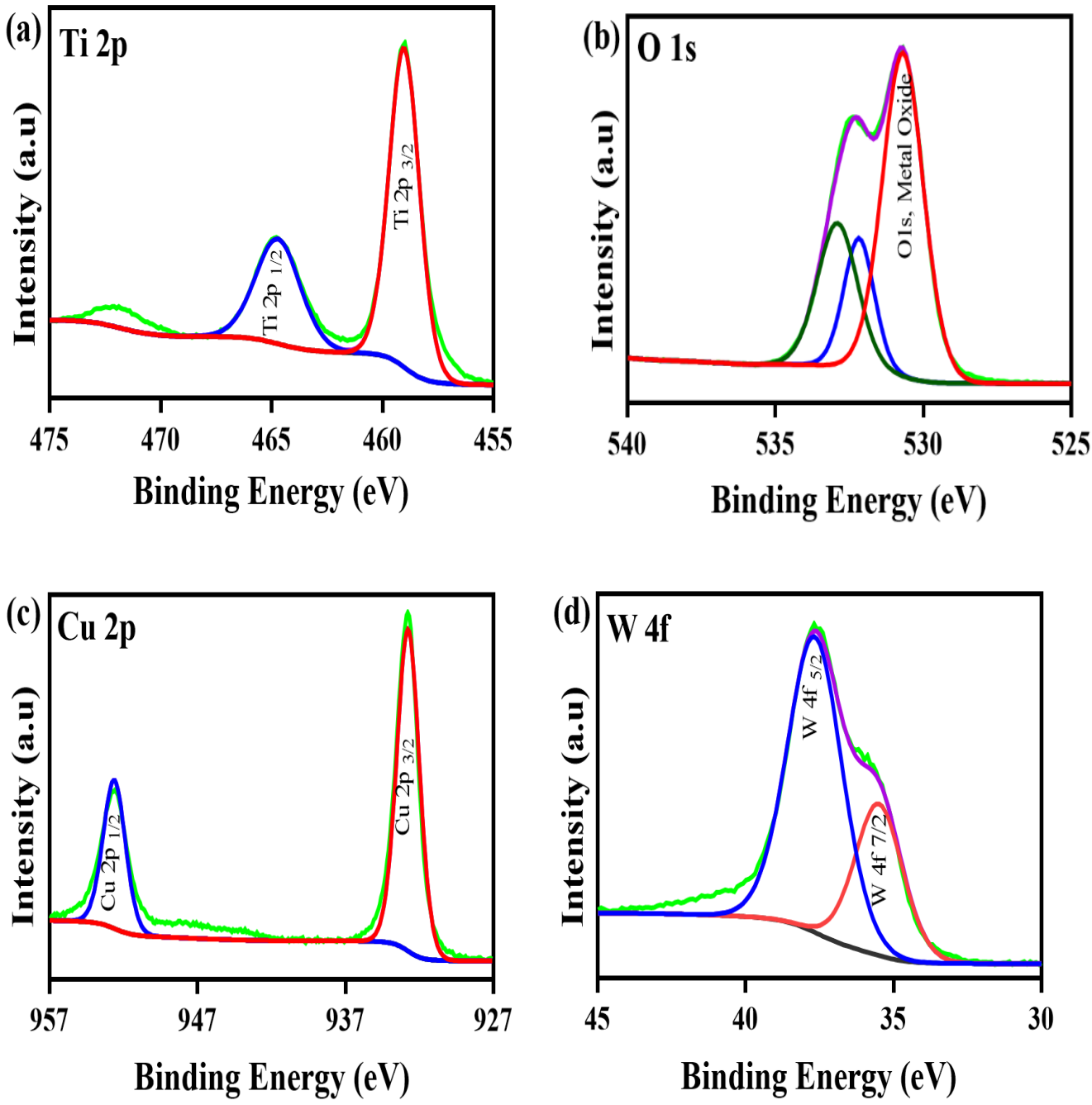


Figure 4.2 High-resolution XPS spectra of **(a)** Ti 2p, **(b)** O 1s, **(c)** Cu 2p and **(d)** W 4f for $CuWO_4@TiO_2$

4.1.5 Surface Analysis of Brunauer–Emmett–Teller (BET)

Core $CuWO_4$ and core-shell TiO_2-coated $CuWO_4$ were evaluated for their adsorption capabilities using the Brunauer-Emmett-Teller (BET) isotherm analysis. The N_2 adsorption-desorption isotherms for the core ($CuWO_4$) and core-shell ($CuWO_4$@TiO_2) structures are shown in **Figure 4.3(a)** and **(b)**, respectively. According to the International Union of Pure and Applied Chemistry (IUPAC), these isotherms are Type IV and have an H3 hysteresis loop.

The BET analysis, summarized in **Table 4.1** provides a comprehensive understanding of the surface area and pore characteristics of the TiO_2-coated $CuWO_4$ and $CuWO_4$ materials. The $CuWO_4$@TiO_2 core-shell structure demonstrates a significantly greater BET surface area of 208.1533 m^2/g, in comparison with the core $CuWO_4$, which has a surface area of 7.4373 m^2/g. Additionally, the Barrett–Joyner–Halenda (BJH) curves obtained from the adsorption branch of isotherms clearly demonstrate different pore properties for the two materials. The $CuWO_4$ material at the core (inset of **Figure 4.3 (a)**) has a significant pore width of roughly 87 nm. The highest pore volume, measured at a rate of change of pore width (dV/dlog(w)), is around 0.031 cm^3/g. The presence of smaller pores (with a width below 10 nm) has a negligible impact, suggesting a mixture of mesoporous and macroporous structures. On the other hand, the $CuWO_4$@TiO_2 material with a core-shell structure (inset of **Figure 4.3 (b)**) exhibits a narrower range of pore widths, specifically between 2 and 4 nm meanwhile, the maximum pore volume (dV/dlog(w)) is substantially greater at around 0.37 cm^3/g. The distribution of this substance highlights a mostly mesoporous structure, which offers a significant surface area that is suitable for adsorption.

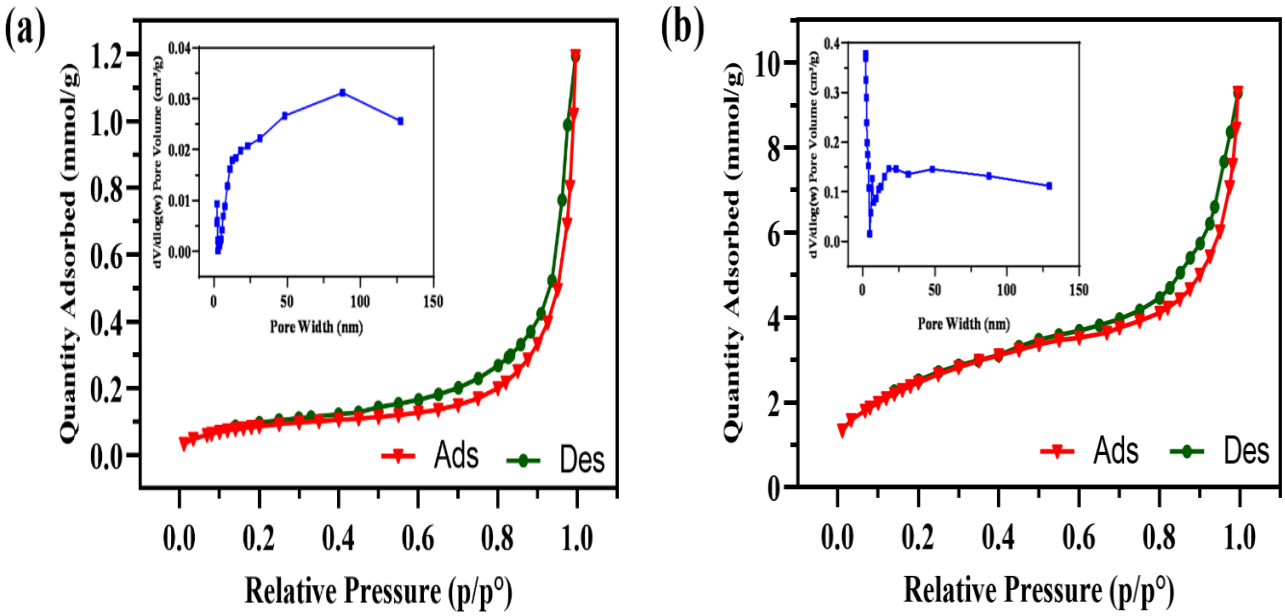


Figure 4.3 N_2 adsorption and desorption isotherms and BJH pore size distribution curves (insets) for **(a)** core $CuWO_4$ and **(b)** core-shell $CuWO_4$@TiO_2.

Table 4.1 Physiochemical properties of $CuWO_4$ and $CuWO_4$@TiO_2

Characteristics	**Value/Unit**	
	core ($CuWO_4$)	**core-shell ($CuWO_4$@TiO_2)**
Surface Area of BET	7.4373 m^2/g	208.1533 m^2/g
The surface area of Langmuir	10.7712 m^2/g	297.5842 m^2/g
Total pore volume for single point adsorption	0.023949 cm^3/g	0.245063 cm^3/g
Average pore diameter for adsorption (BET)	12.88030 nm	4.70928 nm
BJH pore width	87 nm	2-4 nm
BJH pore Volume	0.031 cm^3/g	0.37 cm^3/g

4.2 Response Surface Methodology-Based Optimization Results

4.2.1 Box Behnken Statistical Analysis and Model Fitting

Table 4.3 presents the Box-Behnken design matrix, which includes factors such as adsorbent dosage (A), ciprofloxacin concentration (B), pH (C), and contact time (D). The experimental response, expressed as percentage removal, was evaluated using polynomial models—linear, quadratic and two-factor interaction. **Table 4.2** provides a summary of the model statistics and corresponding regression equations.

By comparing the model statistics, it was determined that the quadratic model yielded the highest R^2 value (0.9931). In comparison to the other models that were evaluated, the quadratic model also showed a smaller standard deviation (1.60), a higher F-value (119.68), and a p-value of less than 0.0001. The quadratic model best explained the experimental data, and Eq. **(4.1)** demonstrates how the response to the four variables was correlated with a second-order polynomial equation.

$$\text{CIP Removal} = +95.12 +12.97A -7.18B -7.83C +4.51D +5.88AB -0.7500AC -2.27AD -3.25BC +2.30BD +4.50CD -8.93A^2 -2.11B^2 -11.83C^2 -2.84D^2 \quad \textbf{(4.1)}$$

Table 4.2 Model statistics for the removal of CIP using $CuWO_4$ @TiO_2.

Model	Std Dev.	F-value	p-value	R^2	Adj. R^2	Pre. R^2	PRESS	Remark
Linear	8.06	13.91	< .0001	0.6986	0.6484	0.5829	2158.38	
2-factor interaction	8.35	0.7305	0.6313	0.7576	0.6230	0.4464	2865.12	
Quadratic	**1.60**	**119.68**	**< .0001**	**0.9931**	**0.9862**	**0.9702**	**154.04**	**Suggested**

Table 4.3 ANOVA for the response surface quadratic model for removal of CIP by $CuWO_4@TiO_2$

Source	Sum of Squares	df	Mean Square	F-value	p-value	
Model	5139.68	14	367.12	144.22	< 0.0001	significant
A-adsorbent dose	2017.61	1	2017.61	792.58	< 0.0001	
B-CIP conc	617.77	1	617.77	242.68	< 0.0001	
C-pH	736.33	1	736.33	289.25	< 0.0001	
D-Time	243.90	1	243.90	95.81	< 0.0001	
AB	138.06	1	138.06	54.24	< 0.0001	
AC	2.25	1	2.25	0.8839	0.3631	
AD	20.70	1	20.70	8.13	0.0128	
BC	42.25	1	42.25	16.60	0.0011	
BD	21.16	1	21.16	8.31	0.0120	
CD	81.00	1	81.00	31.82	< 0.0001	
A^2	516.88	1	516.88	203.05	< 0.0001	
B^2	28.99	1	28.99	11.39	0.0045	
C^2	907.27	1	907.27	356.40	< 0.0001	
D^2	52.29	1	52.29	20.54	0.0005	
Residual	35.64	14	2.55			not significant
Lack of Fit	23.43	10	2.34	0.7677	0.6668	
Pure Error	12.21	4	3.05			
Cor Total	5175.32	28				
Std. Dev.	1.60		R^2	0.9931		
Mean	84.48		Adjusted R^2	0.9862		
C.V. %	1.89		Predicted R^2	0.9702		
			Adeq Precision	39.4198		

A, D, AB, BD, and CD were the model terms that had positive effects on the removal efficiency. In contrast, negative coefficients for the interaction terms (B, C, AC, AD, and BC) and the quadratic terms (A^2, B^2, C^2, and D^2) suggested these factors adversely influenced ciprofloxacin removal. Data points were uniformly distributed around the diagonal line in the plot of experimental vs projected responses (**Figure 4.4**), demonstrating the quadratic model's applicability and sufficiency for assessing and optimizing CIP removal by $CuWO_4$@TiO_2.

Additionally, a crucial statistical tool for assessing the model's suitability is the residuals' Normal Probability Plot (NPP) [268].

The model's acceptability is confirmed by the Normal Probability Plot (NPP) of the residuals for CIP removal (%) in **Figure 4.5 (a)**, which displays the residuals dispersed tightly around the diagonal line, suggesting a normal distribution. A strong fit of the model is further demonstrated by the residuals vs expected CIP removal plot in **Figure 4.5 (b)**, which shows points grouped close to the diagonal.

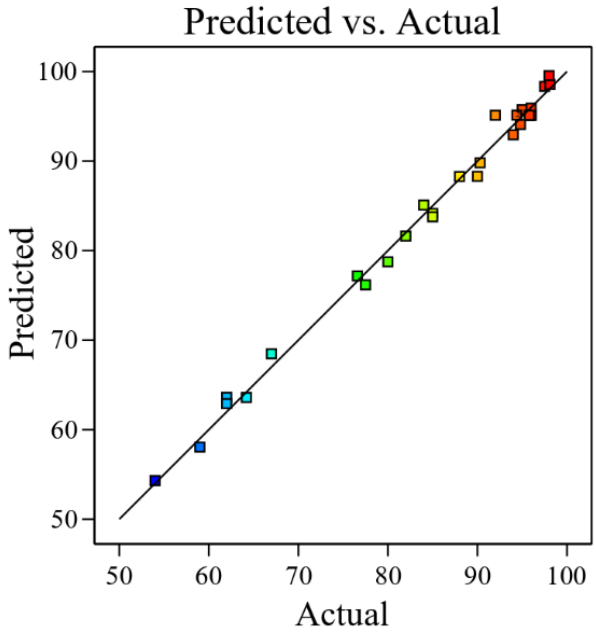


Figure 4.4 Plot of actual vs. predicted responses for removal of CIP by $CuWO_4$@TiO_2

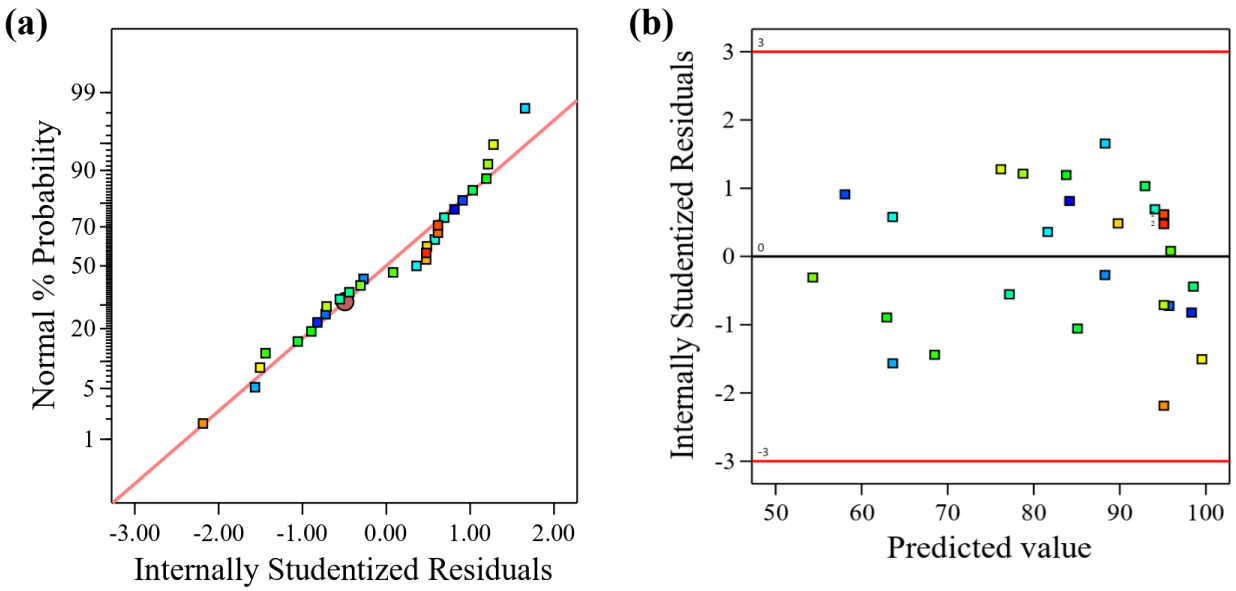


Figure 4.5 (a) Plot of the internally studentized residual with normal probability, **(b)** plot of the predicted value against the internally studentized residuals of the CIP adsorption by $CuWO_4$@TiO_2

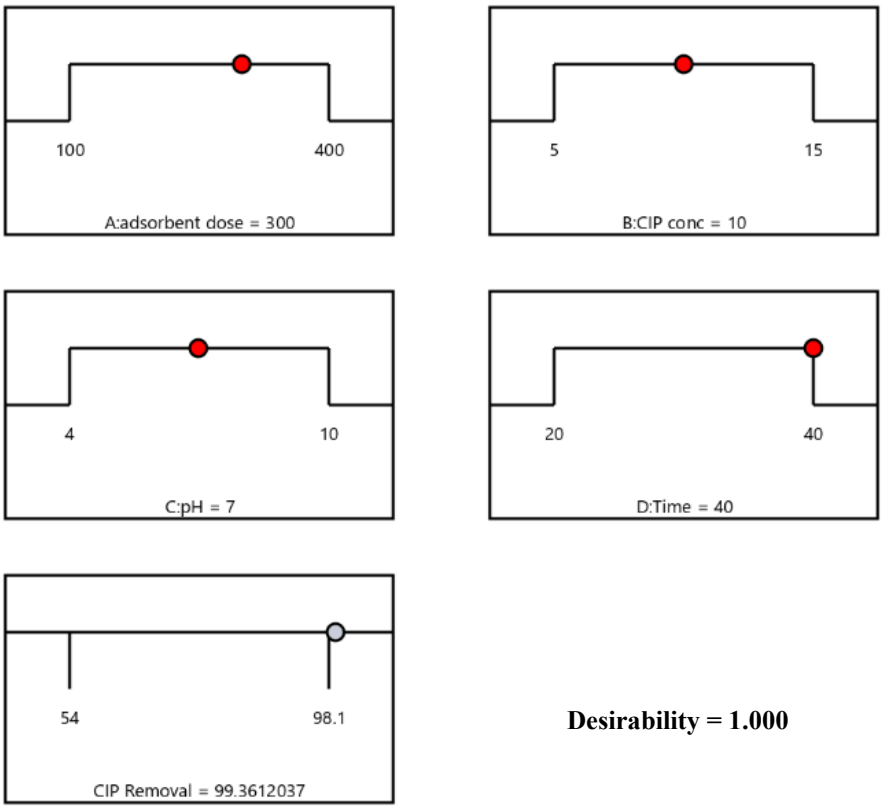


Figure 4.6 The graph of optimization displays the best-predicted values for the maximum removal of CIP (%) and desirability function.

4.2.2 Verification of the Model Using the Desirability Function

The optimal conditions for the highest response were estimated during the optimization process using the desirability function. This function has a range of 0 (unwanted) to 1 (very desirable). The desirability value is maximized under the circumstances provided by the numerical optimization technique [33]. **Figure 4.6**. displays the optimisation plot of the best projected values for maximal ciprofloxacin removal and their associated desirability.

Numerical optimization was performed with independent variables maintained within specified ranges: adsorbent dosage (100 mg/L to 400 mg/L), initial concentration (5–15 mg/L), pH (4–10), and contact time (20–40 min) to achieve the maximum response. According to the desirability function, the optimal parameters for obtaining the maximum CIP removal % were 300 mg/L of adsorbent, 10 mg/L of initial CIP concentration, 7.0 pH, and 40 minutes of contact time. A removal effectiveness of 99.36% was predicted by the RSM fitting model.

Triplicate experiments conducted at the optimal conditions showed results closely matching the predicted values, confirming that Response Surface Methodology (RSM) accurately predicts the removal efficiency of CIP by $CuWO_4$@TiO_2.

The minimal deviation between experimental and predicted values confirms the model's reliability and robustness. Hence, the RSM-based model can be confidently applied for process optimization and scale-up in real-world water treatment applications.

4.2.3 Interaction Effects of Variables and Response Surface

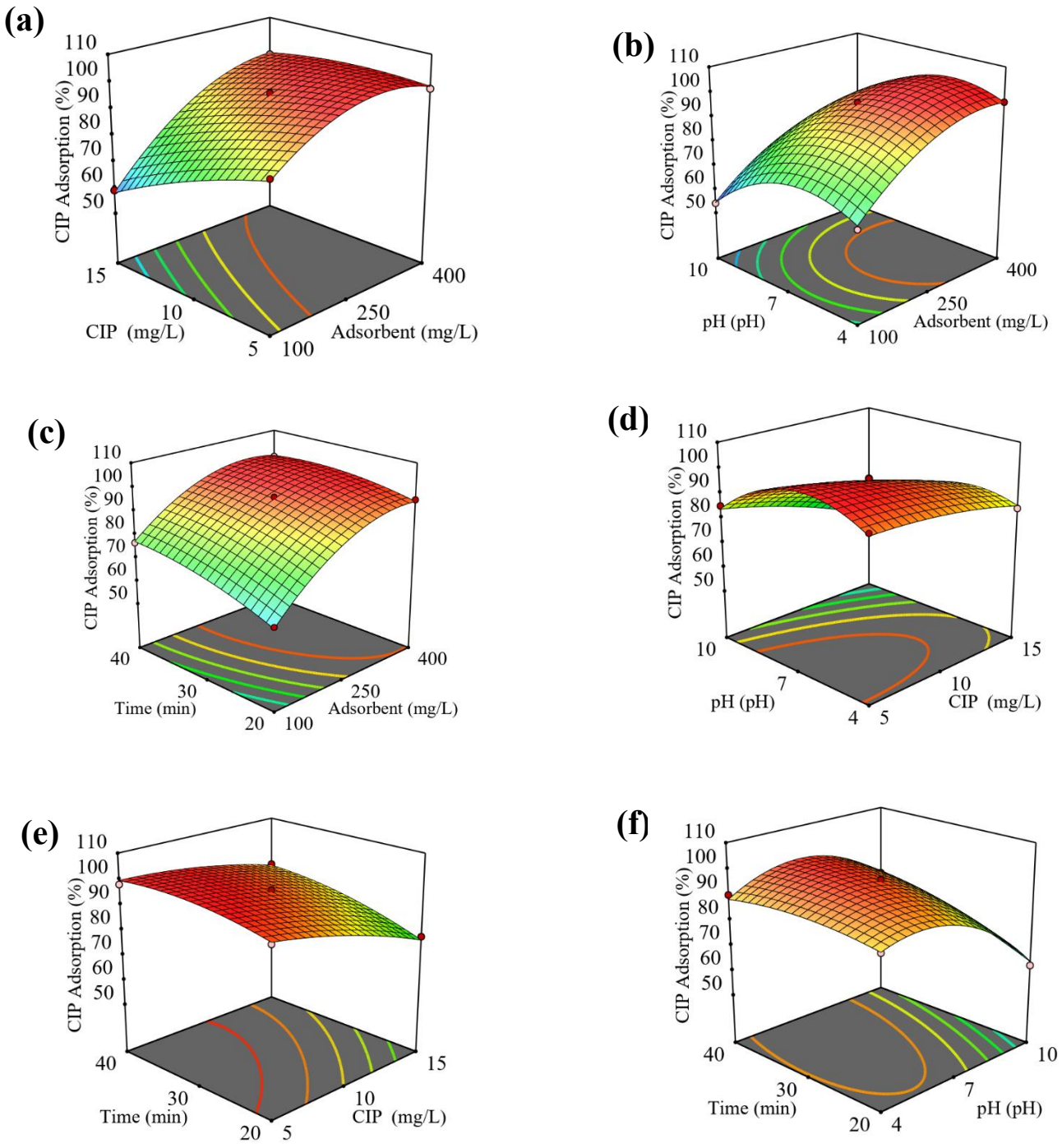


Figure 4.7 3D surface plots illustrating the impact of four factors on the adsorption of CIP by using $CuWO_4$@TiO_2 (a-f).

Response surface plots (3D) were used to see how important the binary interactions between the chosen variables were while controlling for other factors. These plots showed how two variables worked together to affect the CIP removal efficiency. The combined effect of the adsorbent dose and the CIP concentration on how well it is taken up (**Figure 4.7 (a)**). It was discovered that an increase in adsorbent dose corresponded with enhanced removal efficiency. The removal efficiency, on the other hand, goes down when the concentration of CIP goes up. **Figure 4.7 (b)** shows that the removal efficiency increased as the adsorbent dose increased at any constant pH. This pattern makes sense because a higher dose of adsorbent gives more active sites for CIP to attach to, which raises the percentage of removal. At pH = 7, the highest removal efficiency was over 99%.

Figure 4.7 (c) showed how the amount of adsorbent and the amount of time it was in contact with the surface affected how well it worked. The plot showed that efficiency dropped at lower adsorbent dosages because there were fewer active sites available for CIP to stick to. As the adsorbent dose went up, the removal effectiveness went up too because there were more active sites for CIP to bind to. Also, the adsorbent and CIP interacted more when they were in contact for longer periods of time, which made removal even more effective. **Figure 4.7 (d)**, a 3D plot, shows how pH and CIP concentration work together to affect removal efficiency (%). $CuWO_4@TiO_2$'s ability to adsorb and remove CIP was very much affected by the pH of the solution. The pH of the solution changed the surface charges of the adsorbent and CIP molecules, which had a big effect on how they interacted and behaved during adsorption.

The literature shows that CIP has two p_{Ka} values: 5.90 ± 0.15 for the carboxylic acid group and 8.89 ± 0.11 for the basic N moiety. As a result, CIP can be an anion, zwitterion, or cation depending on the pH level [22]. Cationic (CIP^+) is the most common form of CIP when the pH is less than 5.90 ± 0.15. CIP exists mostly as a

zwitterion (CIP°) in the pH range of 5.90 ± 0.15 to 8.89 ± 0.11. Above 8.89 ± 0.11, the anionic form (CIP^-) is more common [269]. This speciation highlights the significance of pH regulation in enhancing the adsorption process. pH changes the charge distribution of both the adsorbent and the adsorbate, which in turn changes how much they like each other. $CuWO_4@TiO_2$'s ability to adsorb was significantly lower at acidic pH levels (<7). This is because there are mostly positively charged species on the adsorbent surface because functional groups are protonated. At the same time, CIP molecules tend to have a positive charge (CIP^+) when the pH is low, which causes the adsorbent and adsorbate to repel each other. This repulsion made it harder for CIP to stick to the positively charged surface of $CuWO_4@TiO_2$, which in turn made it less effective at removing it.

In contrast, the adsorption efficiency of $CuWO_4@TiO_2$ improved a lot as the pH of the solution got closer to neutral, around pH 7. At this pH, the surface charge of the adsorbent is usually more neutral, which makes it easier for CIP molecules to stick to it. Also, the main form of CIP changes to its zwitterionic form (CIP°) when the pH is between 5.90 ± 0.15 and 8.89 ± 0.11. This makes the interaction between the adsorbate and adsorbent stronger by making favorable electrostatic and hydrogen bonding interactions. So, the best pH for the $CuWO_4@TiO_2$ nano catalyst to work best at removing CIP was 7. As the pH of the solution went above neutral and into the alkaline range (pH > 7), the adsorption efficiency went down. This drop in value is because the surface functional groups lost their protons, which made the surface negatively charged. At higher pH levels, CIP mostly exists as an anion (CIP^-), which makes it repel the negatively charged adsorbent surface. This repulsion made it harder for CIP to stick to $CuWO_4@TiO_2$, which made it less effective at removing it in alkaline conditions.

To sum up, the pH has a big effect on how well $CuWO_4@TiO_2$ can adsorb CIP. The observed preference for neutral pH (pH = 7) conditions in enhancing CIP removal is consistent with multiple reports in the literature [269-271]. Numerous

studies have consistently demonstrated that neutral pH conditions are more effective in eliminating CIP from water compared to acidic or alkaline environments. This preference for neutral pH highlights the importance of our findings and supports the idea that adjusting pH levels is important for effective water treatment strategies that use $CuWO_4$@TiO_2 as an adsorbent to remove CIP. **Figure 4.7** (e) shows the interactive effect of CIP concentration and contact time. It shows that when the CIP concentration stayed the same, longer contact times made removal more efficient. This trend is because the contact time is longer, which lets the adsorbent and CIP interact more fully. This means that more CIP can stick to the active sites that are already there, which makes the overall removal process more effective. On the other hand, higher initial CIP concentrations led to lower removal efficiency at any set contact time. This is likely due to the saturation of the adsorbent's active sites, which diminishes the efficacy of adsorption. These results show how important it is to find the right balance between CIP concentration and contact time for the best removal performance. **Figure 4.7** (f) shows how pH and contact time affect how well CIP removal works. Increasing the contact time made CIP removal more effective at any given pH. After 40 minutes, the most CIP (>99%) was taken out at a pH of 7.

4.3 Machine Learning-Based Optimization Result

4.3.1 Data Processing and Analysis

This research conducted a series of batch adsorption experiments to assess the efficacy of a nano adsorbent in removing ciprofloxacin under diverse operational conditions. The dataset, comprising ciprofloxacin concentrations, adsorbent dosages, solution pH levels, treatment time, and adsorption efficiency, were utilized to train and validate the MLPNN model. Statistical methodologies and machine learning algorithms were applied to analyze the data, evaluate model performance, and refine the MLPNN framework for predicting ciprofloxacin removal efficiency. A total of 117 observations related to the removal of CIP were recorded, as detailed in **Table 4.4**. The initial CIP concentrations ranged between 5 and 15 mg/L, with an average concentration of 10 mg/L and a standard deviation of 4.1 mg/L. Adsorbent dosages varied from 100 to 400 mg/L, with average and standard deviation values of 238.46 mg/L and 124.81 mg/L, respectively. The measured pH levels during the experiments exhibited a standard deviation of 2.46 and a mean of 7, spanning pH from 4 to 10. Adsorption times ranged from 0 to 40 minutes, with an average duration of 23.08 minutes and a standard deviation of 12.69 minutes. Post-catalytic process, the average concentration of CIP was 2.45 mg/L, with a standard deviation of 3.09 mg/L and a concentration range of 0.2 to 15 mg/L. Skewness values ranged from 0 to 2.2321, while kurtosis values for each variable varied from -1.5431 to 5.7595. These statistical metrics provide insights into the distribution characteristics of the data, aiding in comprehending their behavior and potential biases. Furthermore, a scatter plot of experimental data in

highlights a significant correlation between initial CIP concentration and final concentration, with adsorbent dosages and treatment time demonstrating a marginal correlation.

Table 4.4 Summarized results of the statistics of the experimental data

Statistics	Initial conc. of CIP (mg/L)	Adsorbent dose (mg/L)	Solution pH	Adsorption time (min)	Final conc. of CIP (mg/L)
Mean	10	238.4615	7	23.0769	2.4462
Standard Deviation	4.1	124.8075	2.46	12.6941	3.0854
Minimum	5	100	4	0	0.2
25%	5	100	4	10	0.4
50%	10	250	7	20	1
75%	15	400	10	30	3.6
Maximum	15	400	10	40	15
Skewness	0	0.146	0	-0.137	2.2321
Kurtosis	-1.513	-1.5431	-1.513	-1.114	5.7595

4.3.2 Performance of Prediction Model and Optimization

The dataset consists of 117 data points, where the primary output is the removal efficiency of ciprofloxacin. The input variables for this output include solution pH, antibiotic concentration, adsorption time, and dosages of adsorbent. A maximum ciprofloxacin elimination efficiency exceeding 97% was achieved. To address scaling disparities, a normalization rescaling technique was employed to transform all input values into o to 1 range [50]. As no references were available to substantiate the normalization of the single column of experimental output data, it was determined to maintain it unchanged.

Prior to simulations, a random seed was assigned to each probabilistic aspect of the project to ensure the replicability of outcomes. The testing dataset was

composed of 20% of the total data points, chosen randomly from the entire dataset. Two hidden layers were employed, with the number of neurons and activation function of each layer regarded as decision variables for hyperparameter adjustment. Commonly employed activation functions for regression tasks in each layer include exponential linear unit (ELU), rectified linear unit (ReLU), or Tanh [272]. ELU includes a hyperparameter known as alpha, which governs the threshold at which negative inputs become saturated. A linear activation function was utilized for the output layer.

Bayesian optimization and random search optimization were both utilized in the configuration of the multilayer perceptron (MLP) neural network to refine hyperparameter values. Both configurations feature a network design comprising 2 hidden layers, although the number of neurons in each layer differs. Bayesian optimization selects 89 neurons per layer, while random search optimization uses 17 neurons per layer. The regularization parameter (alpha) in the Bayesian-optimized MLP is set at 0.0003, compared to 0.0021 in the random search-optimized MLP. Notably, the two systems vary in their learning rate initialization, with Bayesian optimization utilizing a value of 0.0809 and random search optimization employing a value of 0.042. Additionally, Bayesian optimization utilizes the logistic function as its activation function, while random search optimization employs ReLU. The learning rate in the MLP optimized using Bayesian optimization was set at 0.0104, whereas in the MLP optimized with random search, it was slightly lower at 0.0024. **Table 4.5** provides the hyperparameters' range and optimal values calculated by BO and RSO. These combinations of hyperparameters illustrate the delicate decisions taken in optimizing the MLP for certain tasks, balancing the network's complexity with regularization to maximize its learning performance. Fig. S3 depicts the plot of mean squared error (MSE) against the number of epochs. It was evident from the graph that the lowest MSE values for training, validation, and testing were

observed within 120 epochs. Notably, there was no significant improvement in performance beyond 50 epochs for Bayesian optimization and 5 epochs for random search optimization, as illustrated in the **Figure 4.8**. Training and testing losses for the MLP regressor with Bayesian and random search optimization are presented in **Figure 4.8 (a)** and **Figure 4.8 (b)**, respectively. While both losses initially fluctuate for Bayesian optimization, they tend to converge to zero around 50 epochs. In contrast, training and testing losses approach zero at approximately 5 epochs for random search optimization.

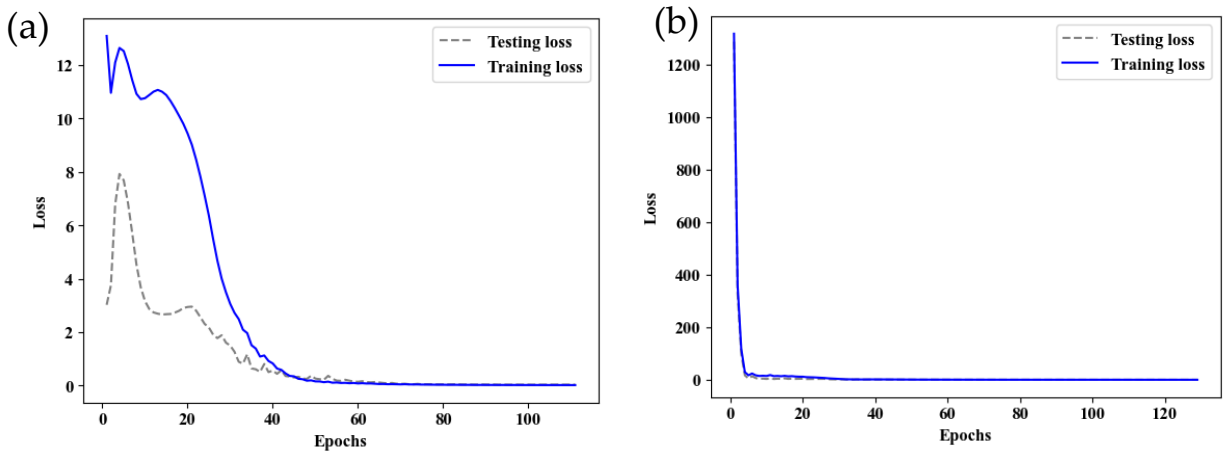


Figure 4.8 Training and testing loss (a) Bayesian optimization (b) Random search optimization.

Table 4.5 Hyper-parameters' range and optimal values

MLP hyperparameters	**Bayesian Optimization**	**Random Search Optimization**
n hidden layers	3	3
neurons per layer	89	17
alpha	0.0003	0.0021
Learning rate init	0.0809	0.042
activation	logistic	ReLU
Learning rate	0.0104	0.0024

The feature ranking analysis derived from both Bayesian optimization and random search optimization techniques (**Figure 4.9**) for the MLP model offers insights into the relative importance of various input features in predicting the target variable. Bayesian optimization identifies 'Adsorption time (min)' as the most significant feature, with a weight of 0.524737, closely followed by 'Adsorption dose (mg/L)' with a weight of 0.390007, and 'Initial antibiotic concentration (mg/L)' with a weight of 0.075537. Conversely, the random search optimization algorithm assigns the highest importance to the feature 'Adsorption dose (mg/L)' with a weight of 0.611459, followed by 'Adsorption time (min)' with a weight of 0.367455, and 'Initial antibiotic concentration' with a weight of 0.018206. Notably, the variable 'pH' appears to exert minimal influence in both optimization techniques, with extremely low weights of 0.009719 in Bayesian and 0.002880 in random search, respectively. These findings offer valuable insights into the variations in feature relevance between optimization strategies, aiding in feature selection for the MLP model in the provided dataset.

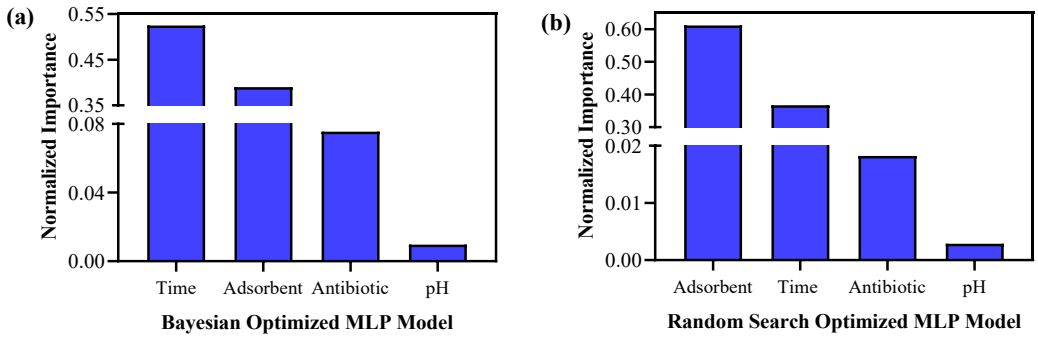


Figure 4.9 Feature importance of MLP model (a) Bayesian optimization (b) Random search optimization

The scatter plot depicting the training and testing datasets for the MLP regressor with Bayesian and random search optimizations is presented in **Figure 4.10** Both the experimental and predicted training datasets closely align, clustering near the 45-degree lines for both Bayesian and random search optimization, as shown in **Figure 4.10 (a)** and **Figure 4.10 (b)**. Furthermore, both Bayesian and random search optimization MLP models demonstrate superior performance on the testing data compared to the training data, as depicted in **Figure 4.10 (c)** and **Figure 4.10 (d)**. Additionally, both models predict a maximum removal efficiency exceeding 97%, closely mirroring the experimental result of over 97.71%. This highlights the effectiveness of the ANN based Bayesian optimized MLP model in accurately predicting the concentration of ciprofloxacin from a liquid solution.

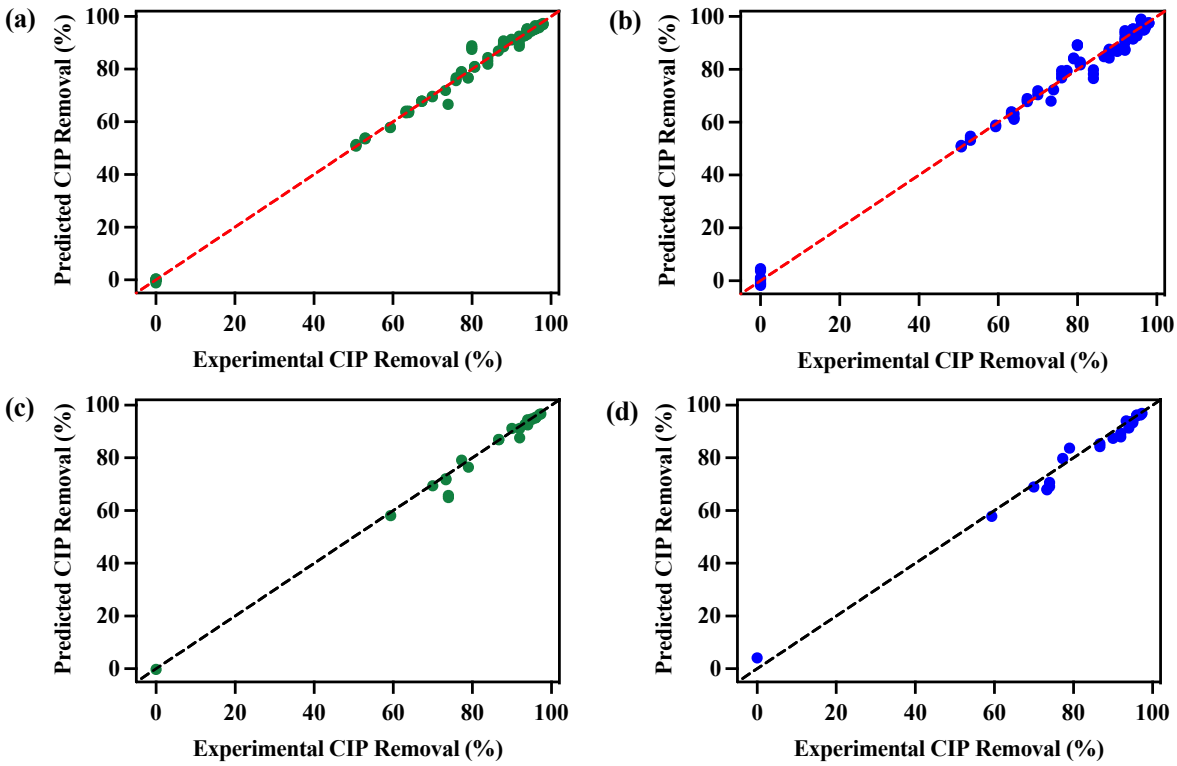


Figure 4.10 The scatter plot represents the predictive results of the MLP model with training and testing dataset (a) Training dataset with Bayesian optimization (b) Training dataset with random search optimization (c) Testing dataset with Bayesian optimization (d) Testing dataset with random search optimization.

The radar plots showcasing the statistical performance of the MLP model highlight its outstanding predictive capabilities for CIP removal across various scenarios (**Figure 4.12**). Both Bayesian and random search optimization methods demonstrate excellence in training and testing datasets, affirming the robustness and generalization capacity of the MLP model in accurately forecasting CIP removal. The Area under the curve (AUC) for the models optimized using Bayesian and random search methods is 0.894 and 0.879, respectively, indicating excellent performance in predicting CIP removal (**Figure 4.14**).

The optimization outcomes for the MLP model based on a variety of performance metrics using Bayesian and random search methods are summarized in **Table 4.6**. The Bayesian optimization model exhibits exceptional performance on both the training and testing datasets, as evidenced by its respective R^2 scores of 0.9985 and 0.9856. Both datasets display low MAE, indicating precise predictions. The MSE is also negligible, further corroborating the model's accuracy. Additionally, the maximal error and MAPE metrics demonstrate low values, indicating excellent prediction performance. The random search optimization yields slightly lower but still impressive results, with R^2 scores of 0.9958 for training and 0.9650 for testing. The model demonstrates the ability to generalize, performing admirably on unseen data. Overall, the MLP model's efficacy in precisely forecasting the target variable is demonstrated by both optimization methods; however, Bayesian optimization exhibits marginally superior performance. The MLP model's performance with the full dataset is illustrated in **Figure 4.12** for Bayesian optimization. The prediction interval plot elucidates the relationship between actual and predicted values, demonstrating a 95% confidence interval around the predicted values. Out of 117 data points, only 8 fall outside the prediction interval, indicating that the model provides reasonably accurate predictions with few instances of significant deviation from the expected range. The model performance for random optimization is depicted in **Figure 4.13**.

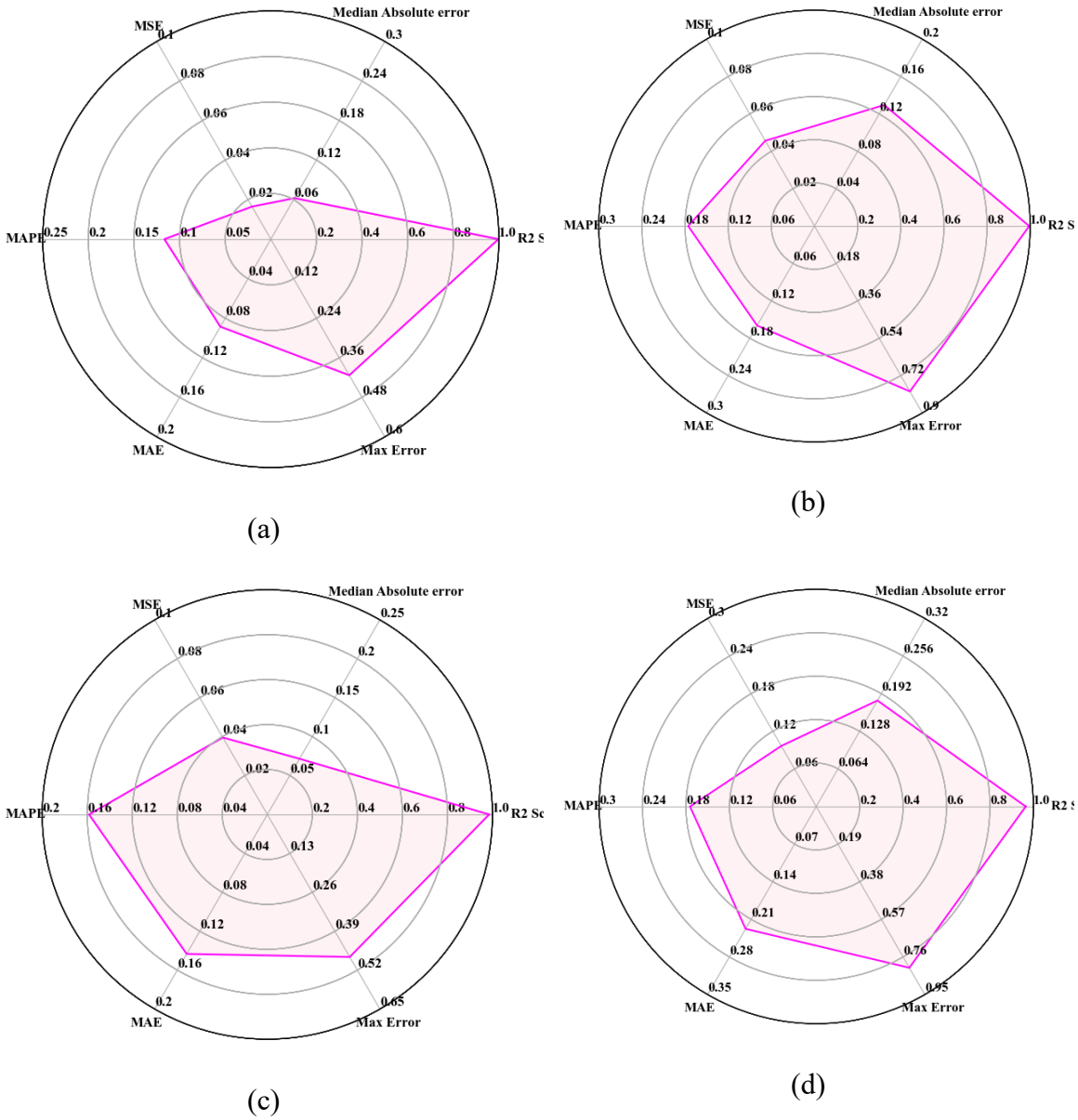


Figure 4.11 Radar plots illustrating the statistical performance of the MLP model on (a) the training dataset utilizing Bayesian optimization, (b) the training dataset employing random search optimization, (c) the testing dataset with Bayesian optimization, and (d) the testing dataset with random search optimization.

Table 4.6 Statistical performance measures for training and testing data with two algorithms

Optimization	Data	R^2 Score	Median Absolute Error	MSE	MAPE	MAE
Bayesian MLP model	Training	0.9985	0.0623	0.0165	0.1168	0.0886
	Testing	0.9856	0.0716	0.0396	0.1585	0.1434
Random Search MLP model	Training	0.9958	0.1296	0.0457	0.1758	0.1597
	Testing	0.9650	0.1805	0.0967	0.1745	0.2278

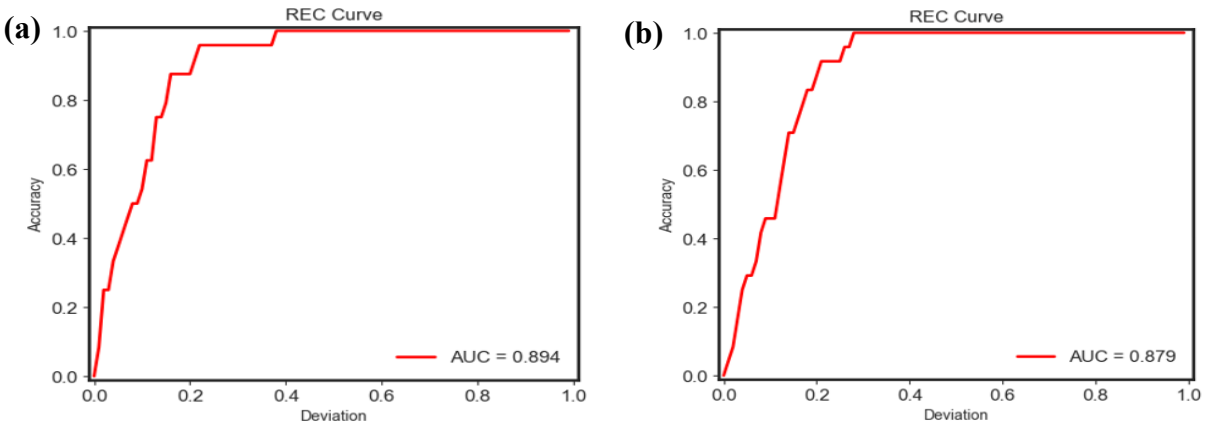


Figure 4.12 Regression error characteristic curves illustrating the performance of the MLP model under (a) Bayesian optimization and (b) Random search optimization.

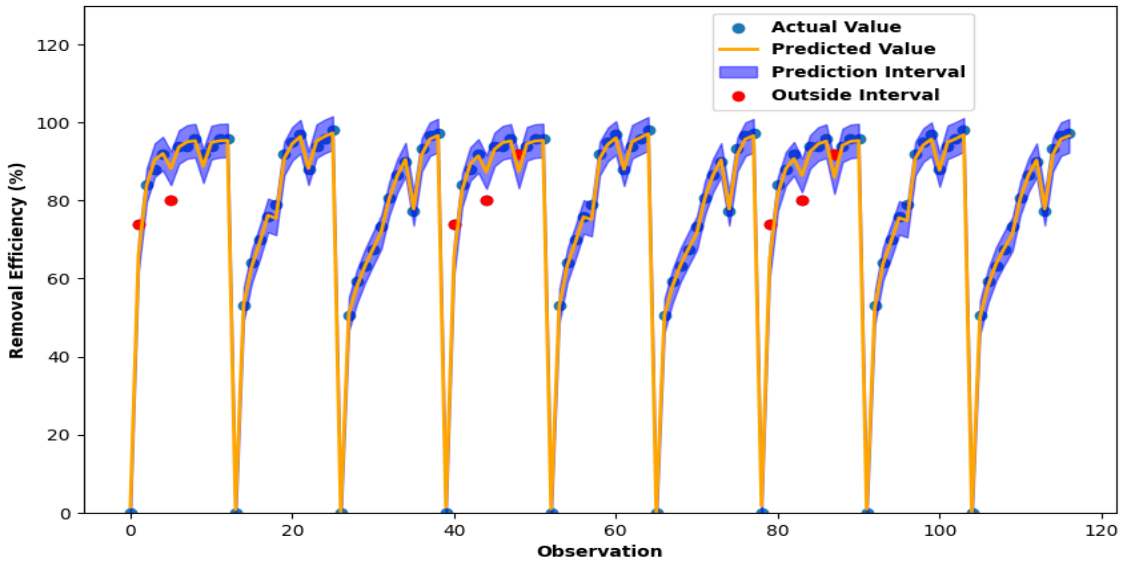


Figure 4.13 Model performance realization for full dataset with Bayesian optimization.

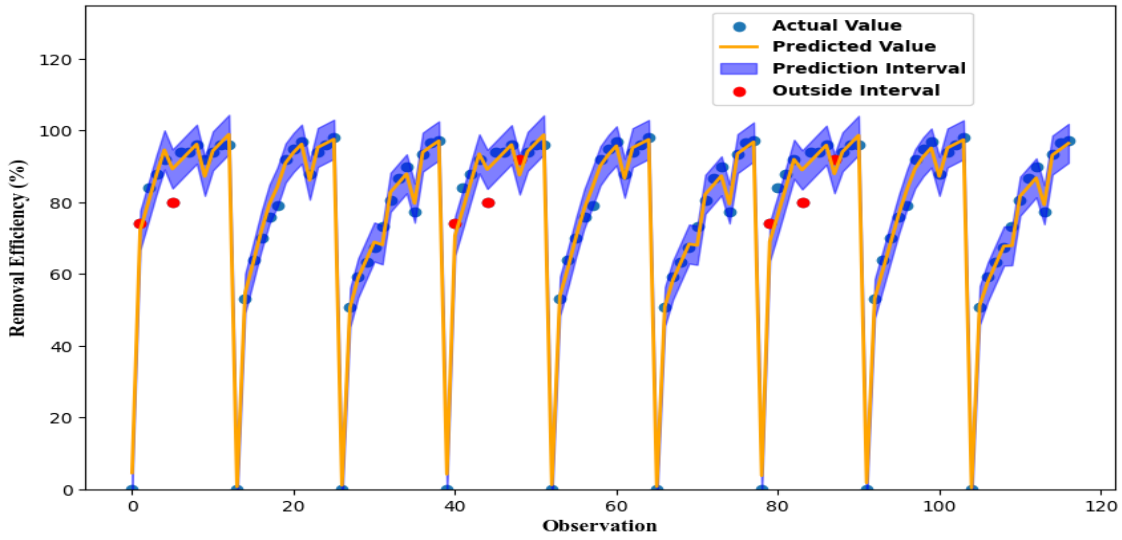


Figure 4.14 Model performance realization for full dataset with Random search optimization.

4.3.3 PSO Optimization of Input Parameters and Experimental Validations

The developed Bayesian optimized, and random search models are utilized to optimize the input parameters using PSO algorithms. An optimization algorithm is formulated to minimize the final concentration of CIP (mg/L). The obtained results are then used to calculate the corresponding removal efficiency. The optimization process provides optimal values of initial concentration of CIP (mg/L), adsorbent dose (mg/L), pH, and adsorption time (min) shown in **Table 4.7** and **Figure 4.15**.

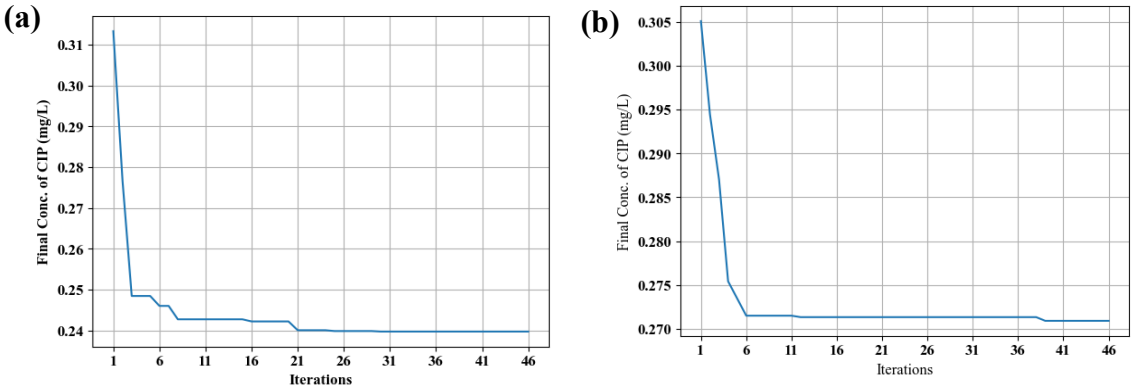


Figure 4.15 PSO algorithm convergence for optimal input parameters design under (a) Bayesian optimization and (b) Random search optimization MLP model

Table 4.7 Input parameters optimization using the novel framework.

Model	Initial Conc. of CIP (mg/L)	Adsorbent dose (mg/L)	Solution pH	Adsorption time (min)	Final conc. of CIP (mg/L)	Removal efficiency (%)
Bayesian approach	9.6	400	6.50	40	0.2394	97.51
Random Search Approach	9.6	400	7.04	40	0.2731	97.16

The **Table 4.7** compares the performance of two machine learning models, MLP with Bayesian and Random Search approaches, in removing ciprofloxacin (CIP) from a solution. Each row details the initial CIP concentration, adsorbent dose, pH level, duration of the experiment, and the resulting final CIP concentration. Lower final concentrations indicate better removal. In this case, the MLP with Bayesian approach achieved a final concentration of 0.2394 mg/L that means the CIP removal efficiency 97.51%, while the MLP with random search approach yielded a higher concentration of 0.2731 mg/L (97.16%) as shown in Fig. 5. Hence, the Bayesian approach demonstrated superior efficacy in reducing CIP concentration.

Figure 4.16 displays the comparison between the experimental data and the data obtained via Bayesian and random search MLP optimisation. This comparison was conducted to evaluate the effectiveness of ciprofloxacin antibiotic removal utilising a synthesised $CuWO_4@TiO_2$ nano adsorbent. The Bayesian optimised MLP model accurately predicted a CIP removal efficiency of 97.51% (Final CIP concentration 0.2393 mg/L)., which closely matched the experimental result of 97.45% (CIP =0.2444 mg/L). This result was obtained by using an initial CIP concentration of 9.6 mg/L, 400 mg/L of $CuWO_4@TiO_2$ adsorbent, an adsorption time of 40 minutes at room temperature, and a pH of 6.5. However, the MLP model optimised using random search also accurately predicted a CIP removal efficiency of 97.16% (Final CIP conc. 0.2731 mg/L), which is very similar to the experimental result of 97.18% (CIP=0.271 mg/L). This result was obtained by using 9.6 mg/L of CIP, 400 mg/L of same adsorbent, a contact time of 40 minutes at room temperature, and a pH of 7.0. The results suggest that the Bayesian optimised model outperformed the random search optimised model in accurately forecasting the ultimate concentration of CIP in wastewater and its removal efficiency.

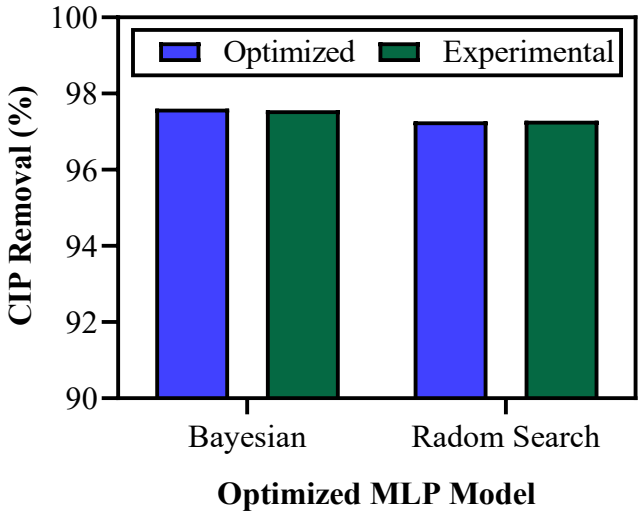


Figure 4.16 Experimental validation for removal of ciprofloxacin under optimum condition (9.6 mg/L of initial CIP, 400 mg/L of $CuWO_4$@TiO_2 adsorbent, 40 minutes of adsorption time at room temperature and neutral pH).

4.3.4 Effect of Factors on Adsorption and Comparison with the MLP Optimized Model

4.3.4.1 Effect of ciprofloxacin concentration

The antibiotic concentration in wastewater systems significantly influences the adsorption process. To assess the impact of antibiotic concentration and contact time on CIP removal, experiments were conducted for durations ranging from 0 to 40 minutes. Antibiotic concentrations of 5, 10, and 15 mg/L were used, while the nano adsorbent dosages and solution pH remained constant at 400 mg/L and pH 7 respectively. **Figure 4.17** demonstrates that the antibiotic under investigation was quickly taken in by the adsorbent's surface because of the existence of large empty active sites. Over time, the quantity of active sites diminishes, resulting in a decline in the rate of adsorption until it reaches a state of equilibrium. Extending the contact period has no impact on the adsorption capacity. Based on the results shown in **Figure 4.17**, there is a direct relationship

between the adsorption of CIP and the duration of contact. Specifically, there is an upward trend in adsorption up to 20 minutes, after which the adsorption rate stabilizes at a constant level. The removal efficiency of the antibiotic gradually increases until it saturates the surface of the adsorbent. Upon comparing the adsorption capacities at antibiotic concentrations of 5, 10, and 15 mg/L, it was observed that at a concentration of 10 mg/L, the adsorption capacity is higher compared to that at 5 mg/L. However, the removal rate slightly decreases at a ciprofloxacin concentration of 15 mg/L. Two potential factors contributing to this phenomenon are the adsorbent shielding effect and excessive occupancy of catalyst active sites at the 15 mg/L concentration [273].

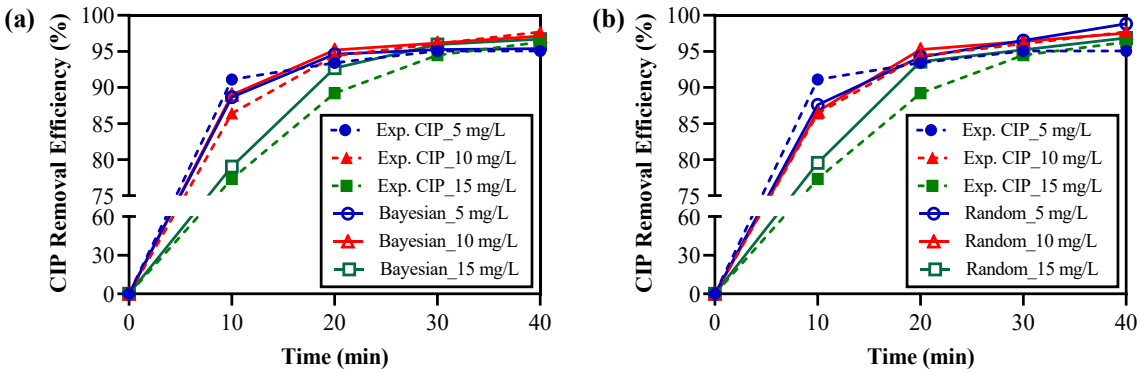


Figure 4.17 The effect of antibiotic concentration on the removal of ciprofloxacin with the $CuWO_4@TiO_2$ adsorbent at a dosage of 400 mg/L and pH 7, and the comparison of the experimental data with a) Bayesian optimisation and b) Random search optimisation MLP model.

4.3.4.2 Effect of adsorbent dosage

The adsorbent dosage plays a critical role in determining the capacity and efficacy of the adsorbent in removing antibiotics at a specific initial concentration. To evaluate the impact of the adsorbent ($CuWO_4@TiO_2$) dosages, an experiment was conducted wherein 100, 250, and 400 mg/L of the adsorbent were added to a solution with a pH of 7. The solution contained CIP at a concentration of 10 mg/L

and was maintained at a temperature of 25 ± 3°C. The adsorption process was monitored by collecting samples of the solution at regular intervals ranging from 0 to 40 minutes. As depicted in **Figure 4.18**, the adsorption capacities of adsorbent doses of 100, 250, and 400 mg/L within a 40-minute timeframe were 76.06%, 97.30%, and 97.71%, respectively. Notably, the CIP removal rate was slightly higher for the Bayesian optimization than the random search algorithm. A substantial increase in the CIP removal rate was observed from 76.06% to 97.30% when the adsorbent dosage was increased from 100 to 250 mg/L, as depicted in **Figure 4.18**, while maintaining an initial CIP concentration of 10 mg/L. This enhancement can be attributed to the increased surface area and availability of functional groups resulting from the higher mass of the adsorbent. However, further increasing the adsorbent dosage beyond 250 mg/L did not lead to a significant change in the ciprofloxacin adsorption capacity (97.71%). This phenomenon may be elucidated by the accumulation of available antibiotics in the solution and the surface characteristics of the adsorbent particles.

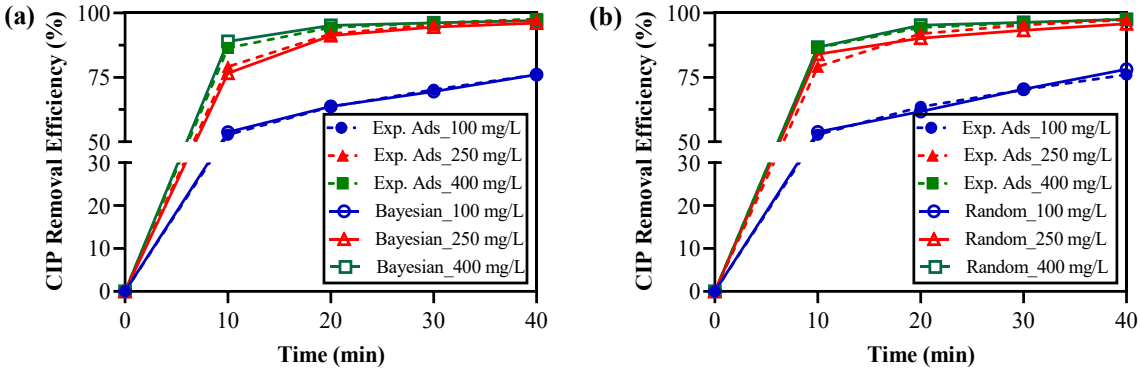


Figure 4.18 The effect of adsorbent dosage ($CuWO_4$@TiO_2) on the removal of ciprofloxacin with an initial ciprofloxacin concentration of 10 mg/L and pH 7, and the comparison of the experimental data with a) Bayesian optimisation and b) Random search optimisation MLP model.

4.3.4.3 Effect of solution pH

The pH level significantly influences the adsorption process, affecting both the surface charge of the adsorbent and the speciation of adsorbates in the solution [274]. To assess the impact of solution pH on ciprofloxacin removal, a series of experiments were conducted at three distinct pH levels (4, 7, and 10). The relevant outcomes are illustrated in **Figure 4.19** The percentage of CIP removal increased from 95.44% to 97.77% when the solution pH was increased from 4 to 7 with 10 mg/L of initial CIP concentration and 400 mg/L of $CuWO_4@TiO_2$ nano adsorbent.

Determining the point of zero charge (pH_{PZC}) is essential to anticipate the surface charge of nanoparticles throughout the adsorption process accurately. In this study, minimal activity of the $CuWO_4$ material on CIP was observed even after a 1-hour treatment at the tested pH (data not shown). Unlike $CuWO_4@TiO_2$ material, the adsorption efficiency of $CuWO_4$ over CIP is not influenced by pH (**Figure 4.19**). This suggests that the pH_{PZC} of material systems may influenced by the TiO_2 phase. According to Watanabe et al. (2005), the pH_{PZC} of TiO_2 is approximately 6.0 ± 0.7. Consequently, TiO_2 carries a positive charge below pH 6.7 and a negative charge above pH 6.7 [275]. The nano adsorbent exhibits higher CIP removal efficiency in the adsorption process at pH 7, reaching over 97.71%. However, there is a decline in CIP removal efficiency as the pH decreases from 7.0 to 4.0, as shown in **Figure 4.19** Nevertheless, a significant decrease in CIP removal was observed from pH 7.0 to 10.0. This decline may be associated with zeta potentials (ZPs) and the present species of CIP in the reaction solution.

The literature states that ciprofloxacin has two pKa values of 5.90 ± 0.15 and 8.89 ± 0.11, which correspond to the carboxylic acid group and the basic N moiety, respectively. As a result, CIP can exist as a cation, zwitterion, or anion at different pH levels [22]. At a pH of less than 5.90 ± 0.15, the main form of CIP is cationic

(CIP⁺). In this acidic condition, there is a high concentration of H^+ ions due to protonation of the $–NH_2$ group. The H^+ ions have a smaller ionic radius and are more likely to be adsorbed. Nevertheless, the TiO_2 coated $CuWO_4$ adsorbent may increase the positive charge when the pH was decreased from 7 to below. This positive charge leads to electrostatic repulsion between the cationic species of CIP and positive charge of adsorbent. At a pH greater than 8.89 ± 0.11, where anionic CIP is the main species, there was a significant drop in CIP removal. This can be attributed to the electrostatic repulsion between the negatively charged adsorbent and the anionic CIP ($CIP^–$). Consequently, adsorption at pH 10 showed lower adsorption efficiency for CIP (88.98%) as compared to neural and acidic pH and is depicted in **Figure 4.19** Antonelli et al. [274] and Zheng et al. [276] have noticed similar behaviour. Hence, the electrostatic interaction between synthesized $CuWO_4$@TiO_2 nano adsorbent and the CIP antibiotic plays a significant role in influencing the adsorption process.

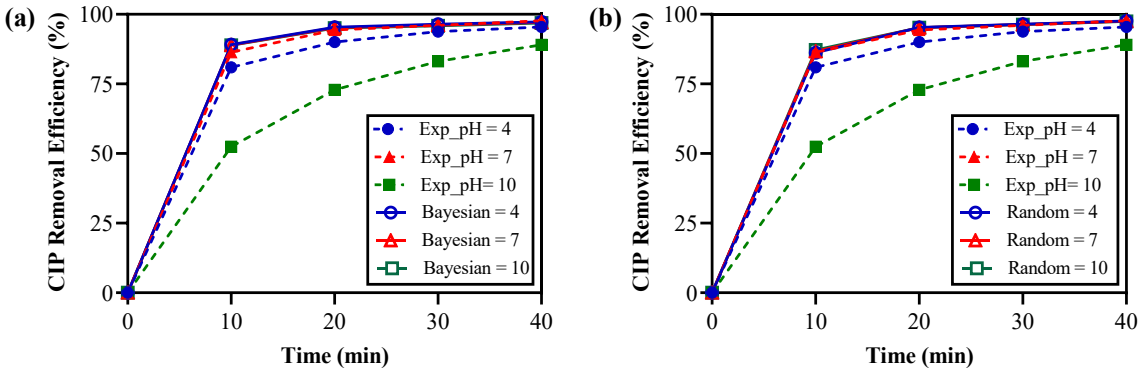


Figure 4.19 The effect of the pH of the solution on the removal of ciprofloxacin, with an initial antibiotic concentration of 10 mg/L and 400 mg/L of $CuWO_4$@TiO_2 adsorbent, and the comparison of the experimental data with a) Bayesian optimisation and b) Random search optimisation MLP model.

4.4 Adsorption Isotherms

The nature of the interaction between CIP and the CuWO4@TiO2 adsorbent at equilibrium was determined by applying the isotherm models to the adsorption data [30]. As shown in **Table 4.8** and **Figure 4.20 (a-c)**, Langmuir, Freundlich, and Temkin's models were investigated in this study at three distinct temperatures (30, 40, and 50 ºC) and various starting concentrations. The non-linear parameters (R_L, q_m, K_F , $\frac{1}{n_F}$, A_T, B_T *and* R^2) were determined employing OriginPro 8.5 software, with the isotherm models detailed in **Table 4.8** as the foundation for the corresponding equations [277]. The characteristic of the Langmuir isotherm is typically described as the dimensionless parameter R_L, which can be calculated using Eq. **(4.2)**

$$R_L = \frac{1}{1 + K_L C_0} \qquad \textbf{(4.2)}$$

Adsorption process type is shown by the R_L value, with (i) R_L = 0 suggesting irreversibility, (ii) 0 < R_L < 1 indicating favorability, (iii) R_L = 1 representing linearity, and (iv) R_L > 1 signifying unfavourability [30]. According to the R_L values in the present study, CIP's adsorption onto the $CuWO_4$@TiO_2 surface was favourable (0 < R_L < 1). It was also shown that the adsorption of ciprofloxacin from an aqueous solution onto produced NiO exhibited comparable properties [177]. Additionally, at all temperatures examined, the $\frac{1}{n_F}$ values derived from the Freundlich isotherm plot were consistently less than 1, showing the favorable adsorption of CIP onto $CuWO_4$@TiO_2 [30]. Similarly, for the adsorption of CIP onto thermally modified bentonite clay, the $\frac{1}{n_F}$ value was also reported to be less than 1 [274], in agreement with the results of this study. Furthermore, the R_L values were larger at lower temperatures than at higher ones, with all values lying between 0 and 1, suggesting that the adsorption process is more likely to be chemical in nature rather than physical [278].

Table 4.8 Non-linear fitting of the adsorption of CIP onto $CuWO_4$@TiO_2 yielded the adsorption isotherm values. pH=7, contact period of 40 minutes, CIP concentration of 5–25 mg/L, and adsorbent dose of 300 mg/L

Isotherm Model	30^0 C	40^0 C	50^0 C
Langmuir			
$q_m(mg\ g^{-1})$	109.58	99.69	96.14
$K_L(L\ mg^{-1})$	1.93	2.21	2.33
R^2	0.9949	0.9923	0.9913
R_L	0.047	0.043	0.041
Freundlich			
$K_F\ (mg\ g^{-1})$	70.38	64.01	62.70
$\frac{1}{n_F}$	0.54	0.48	0.46
R^2	0.9447	0.9204	0.9193
Temkin			
A_T	19.76	21.34	22.13
B_T	23.94	22.09	21.40
R^2	0.9944	0.9975	0.9961

Table 4.8 indicates that the Langmuir isotherm model is most suited to describe the absorption of CIP onto $CuWO_4$@TiO_2 due to its greatest R^2 and other parameters.

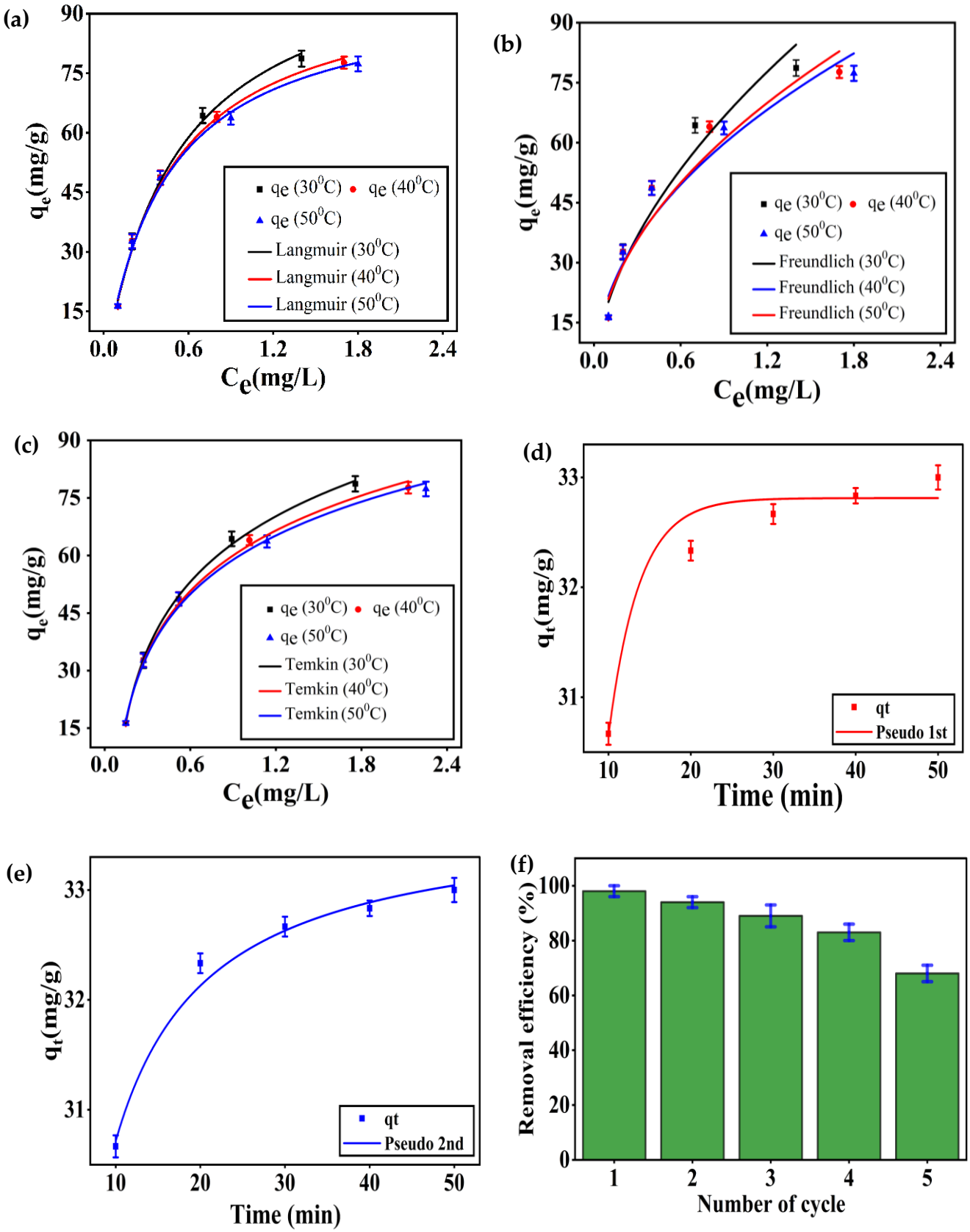


Figure 4.20 (a–c) Isotherm models: Langmuir, Freundlich, and Temkin; (d–e) kinetic models: pseudo-first and pseudo-second order; (f) reusability of the TiO_2-coated $CuWO_4$ nanocatalyst.

4.5 Adsorption Kinetics

The experimental kinetic data have been analyzed using two kinetic models in order to comprehend the process of ciprofloxacin absorption onto $CuWO_4@TiO_2$ [30]. **Table 4.9** summarizes the pseudo first-order (PFO) and pseudo second-order (PSO) kinetic models' nonlinear equations. **Figure 4.20 (d,e)** displays nonlinear plots of q_t (mg/g)vs. t (min) for PFO and PSO models at 303k. **Table 4.9** provides a summary of the non-linear form's parameters, which were computed using the OriginPro8.5 software [277].

Table 4.9 Non-linear fitting was employed to figure out the adsorption kinetics parameters for CIP on $CuWO_4@TiO_2$ (adsorbent dose 300 mg/L, CIP concentration 10 mg/L, and pH 7).

Kinetic Model	**CIP adsorption onto $CuWO_4@TiO_2$**
Pseudo first-order	
$q_{e.cal}(mg\ g^{-1})$	32.7543
$k_1(min^{-1})$	0.27351
R^2	0.94244
Pseudo second-order	
$q_{e.cal}(mg\ g^{-1})$	33.69373
$k_2(min^{-1})$	0.03089
R^2	0.98213

A correlation coefficient (R^2) of 0.94244 is found in the pseudo first-order model. The PFO model did not fit the measured data well, as these results showed. The PSO kinetic model's k^2 and $q_{e\,cal}$ values were calculated using nonlinear regression analysis and are displayed in **Table 4.9**.. According to the figure, the correlation coefficient (R^2) is 0.98213. In contrast to the PFO kinetic model, it was shown that the PSO model suited the adsorption data well. Therefore, the adsorption of ciprofloxacin onto $CuWO_4@TiO_2$ was favoured by the chemisorption process [30]. A similar finding has been reported in previous studies [279, 280].

4.6 Reusability Test

In order to reduce the cost of the adsorption process, the reusability of the adsorbent material is an important consideration for the material's practical and commercial use in actual samples [281]. Determining the percentage removal of CIP over four consecutive cycles was the goal of the experiment. The solution was dissolved in 100% ethanol and stirred for half an hour at room temperature following each adsorption cycle. After that, the adsorbent was separated using Whatman filter paper, thoroughly cleaned with ethanol and Milli-Q water, and dried for 12 hours at 70°C. Every cycle underwent this regeneration process. **Figure 4.20 (f)** shows the data from the nano-adsorbent reuse procedure following CIP adsorption. After two cycles, the adsorption rate surpasses 94%, but after four cycles, it progressively drops to 68%. These results imply that $CuWO_4@TiO_2$ is a useful adsorbent for CIP removal.

Chapter 5: CONCLUSION

5.1 General

In this study, the removal of emerging contaminants from urban water systems was investigated using TiO_2-coated $CuWO_4$ nanocatalysts. The core-shell nanomaterial was successfully synthesized using a variety of physicochemical techniques, and its surface and structural properties were thoroughly examined. The material's performance was assessed through adsorption experiments carried out in a variety of conditions, and both kinetic and isotherm models were used to analyze the adsorption mechanisms. Additionally, machine learning techniques were used for precise predictive modeling, and RSM was used for statistical optimization. The potential of the nanocatalyst as an effective and sustainable solution for urban water treatment applications was highlighted by its good reusability across several cycles.

5.2 Key Findings

- TiO_2-coated $CuWO_4$ nanocatalysts were successfully synthesized with a core–shell structure and confirmed through detailed physicochemical characterization.
- The nanocatalyst exhibited high adsorption efficiency for emerging contaminants under neutral pH conditions.
- The Langmuir isotherm model successfully described the behavior in adsorption experiments carried out under various conditions.
- The pseudo-second-order model, which chemisorption is the predominant mechanism, is best fitted by kinetic data.

- RSM identified optimal operating conditions for maximum removal efficiency.
- Machine learning (Multilayer Perceptron) provided accurate predictive modeling of the removal performance, complementing the statistical approach.
- The nanocatalyst demonstrated good reusability over several adsorption–desorption cycles, confirming its stability and practical applicability.

5.3 Limitations of the Study

- **Real-World Application:** The study was carried out using model contaminants in a controlled laboratory setting, which might not accurately represent the complexity of wastewater with a variety of pollutants in the real world.
- **Long-Term Reusability:** The long-term stability and performance of the nanocatalyst in realistic, practical applications have not been fully examined, despite the fact that reusability was tested over a number of cycles.
- **Scalability and Cost:** The study did not assess the scalability or the cost-effectiveness of synthesizing TiO_2-coated $CuWO_4$ nanocatalysts at a commercial scale, which is essential for evaluating its practical viability in large-scale water treatment systems.

5.4 Recommendation for Further Study

- **Real-World Water Treatment:** Further investigations should focus on testing TiO_2-coated $CuWO_4$ nanocatalysts in real wastewater environments containing a mixture of emerging contaminants, including complex organic and inorganic compounds, to better understand their performance under practical conditions.
- **Continuous Flow Systems:** Future studies should explore the performance of the nanocatalysts in continuous flow systems to simulate more realistic treatment scenarios and assess their efficiency under dynamic conditions.
- **Long-Term Stability and Reusability:** Extended studies on reusability, the long-term stability, and structural integrity of the nanocatalyst over multiple cycles and under different environmental factors would provide a deeper understanding of its practical applications.
- **Scale-Up Studies:** Research on the scalability of the synthesis process and cost analysis should be conducted to evaluate the feasibility of large-scale production and the economic viability of TiO_2-coated $CuWO_4$ nanocatalysts for commercial water treatment applications.
- **Hybrid Systems and Modifications:** Investigating the modification of the nanocatalyst by incorporating other materials or creating hybrid systems with advanced oxidation processes (AOPs) could further enhance its adsorption and catalytic performance.

REFERENCES

1. Ahmed, Y., et al., *Roles of reactive oxygen species in antibiotic resistant bacteria inactivation and micropollutant degradation in Fenton and photo-Fenton processes.* Journal of Hazardous Materials, 2022. **430**: p. 128408.
2. Ahmed, Y., et al., *Efficient inactivation of antibiotic resistant bacteria and antibiotic resistance genes by photo-Fenton process under visible LED light and neutral pH.* Water Research, 2020. **179**: p. 115878.
3. Ahmed, Y., et al., *Simultaneous removal of antibiotic resistant bacteria, antibiotic resistance genes, and micropollutants by a modified photo-Fenton process.* Water Research, 2021. **197**: p. 117075.
4. Zhong, J., et al., *Simultaneous removal of micropollutants, antibiotic resistant bacteria, and antibiotic resistance genes using graphitic carbon nitride under simulated solar irradiation.* Chemical Engineering Journal, 2022. **433**: p. 133839.
5. Guo, J., et al., *Control strategies to combat dissemination of antibiotic resistance in urban water systems*, in *Antibiotic Resistance in the Environment : A Worldwide Overview*, C.M. Manaia, et al., Editors. 2020, Springer International Publishing: Cham. p. 147-187.
6. Pirsaheb, M., N. Moradi, and H. Hossini, *Sonochemical processes for antibiotics removal from water and wastewater: A systematic review.* Chemical Engineering Research and Design, 2023. **189**: p. 401-439.
7. European Commission, E., et al., *State of the art on the contribution of water to antimicrobial resistance*. 2018, Publications Office.
8. Alharbi, O.A., et al., *Assessment of selected pharmaceuticals in Riyadh wastewater treatment plants, Saudi Arabia: Mass loadings, seasonal variations, removal efficiency and environmental risk.* Science of The Total Environment, 2023. **882**: p. 163284.

9. Akhtar, P., et al., *Efficiency of effluent treatment plants and threat to human health and aquatic environment in Bangladesh.* Asian Journal of Chemistry, 2016. **28**(1).
10. Tasho, R.P. and J.Y. Cho, *Entry routes of veterinary antibiotics in the environment*, in *Antibiotics and Antibiotics Resistance Genes in Soils: Monitoring, Toxicity, Risk Assessment and Management*, M.Z. Hashmi, V. Strezov, and A. Varma, Editors. 2017, Springer International Publishing: Cham. p. 55-70.
11. Indu, M. Sharma, and K. Kumar Dubey, *Chapter 3 - Leaking of antibiotics in the aquatic environment*, in *Contemporary Chemical Approaches for Green and Sustainable Drugs*, M. Török, Editor. 2022, Elsevier. p. 47-67.
12. Manyi-Loh, C., et al., *Antibiotic use in agriculture and its consequential resistance in environmental sources: Potential public health implications.* Molecules, 2018. **23**(4): p. 795.
13. Mondal, S.K., A.K. Saha, and A. Sinha, *Removal of ciprofloxacin using modified advanced oxidation processes: kinetics, pathways and process optimization.* Journal of cleaner production, 2018. **171**: p. 1203-1214.
14. An, T., et al., *Kinetics and mechanism of advanced oxidation processes (AOPs) in degradation of ciprofloxacin in water.* Applied Catalysis B: Environmental, 2010. **94**(3): p. 288-294.
15. Nguyen, T.-T., et al., *Effect of ciprofloxacin dosages on the performance of sponge membrane bioreactor treating hospital wastewater.* Bioresource Technology, 2019. **273**: p. 573-580.
16. Qalyoubi, L., A. Al-Othman, and S. Al-Asheh, *Removal of ciprofloxacin antibiotic pollutants from wastewater using nano-composite adsorptive membranes.* Environmental Research, 2022. **215**: p. 114182.
17. Sayin, F., S.T. Akar, and T. Akar, *From green biowaste to water treatment applications: Utilization of modified new biochar for the efficient removal of ciprofloxacin.* Sustainable Chemistry and Pharmacy, 2021. **24**: p. 100522.

18. Yousefi, M., et al., *Photocatalytic degradation of ciprofloxacin using a novel carbohydrate-based nanocomposite from aqueous solutions.* Chemosphere, 2024. **349**: p. 140972.
19. Wang, Y., et al., *The electrochemical degradation of ciprofloxacin using a SnO_2-Sb/Ti anode: Influencing factors, reaction pathways and energy demand.* Chemical Engineering Journal, 2016. **296**: p. 79-89.
20. Staudt, J., et al., *Ciprofloxacin desorption from gel type ion exchange resin: Desorption modeling in batch system and fixed bed column.* Separation and Purification Technology, 2020. **230**: p. 115857.
21. Yu, F., et al., *Adsorption removal of ciprofloxacin by multi-walled carbon nanotubes with different oxygen contents from aqueous solutions.* Chemical engineering journal, 2016. **285**: p. 588-595.
22. Carabineiro, S.A.C., et al., *Adsorption of ciprofloxacin on surface-modified carbon materials.* Water Research, 2011. **45**(15): p. 4583-4591.
23. Haider Jaffari, Z., et al., *Machine-learning-based prediction and optimization of emerging contaminants' adsorption capacity on biochar materials.* Chemical Engineering Journal, 2023. **466**: p. 143073.
24. Farzinmanesh, O., M. Hosseini Sabzevari, and M.R. Asghari, *Efficient removal of ciprofloxacin and ofloxacin from aqueous solutions using a novel nano-scale adsorbent: Modeling, optimization, and characterization.* Chemosphere, 2024: p. 141640.
25. Rahman, N., S. Sameen, and M. Kashif, *Spectroscopic study of charge transfer complexation between doxepin and π–acceptors and its application in quantitative analysis.* Journal of Molecular Liquids, 2016. **222**: p. 944-952.
26. Rahman, N. and U. Haseen, *Development of polyacrylamide chromium oxide as a new sorbent for solid phase extraction of As(iii) from food and environmental water samples.* RSC Advances, 2015. **5**(10): p. 7311-7323.

27. Rahman, N. and M. Nasir, *Effective removal of acetaminophen from aqueous solution using Ca (II)-doped chitosan/β-cyclodextrin composite.* Journal of Molecular Liquids, 2020. **301**: p. 112454.

28. Rahman, N., M.F. Khan, and M. Nasir, *Experimental design approach for optimization of Pb(II) removal from aqueous solution using poly-o-toluidine/stannic(IV) triethanolamine as adsorbent.* Environmental Technology & Innovation, 2020. **17**: p. 100634.

29. Rahman,N. and M. Nasir, *N-(((2-((2-Aminoethyl)amino)ethyl)amino)methyl)-4-sulfamoylbenzamide Impregnated Hydrous Zirconium Oxide as a Novel Adsorbent for Removal of Ni(II) from Aqueous Solutions: Optimization of Variables Using Central Composite Design.* ACS Omega, 2019. **4**(2): p. 2823-2832.

30. Rahman, N. and P. Varshney, *Assessment of ampicillin removal efficiency from aqueous solution by polydopamine/zirconium(iv) iodate: optimization by response surface methodology.* RSC Advances, 2020. **10**(34): p. 20322-20337.

31. Khedmati, M., A. Khodaii, and H.F. Haghshenas, *A study on moisture susceptibility of stone matrix warm mix asphalt.* Construction and Building Materials, 2017. **144**: p. 42-49.

32. Behbahani, M., M.R.A. Moghaddam, and M. Arami, *Techno-economical evaluation of fluoride removal by electrocoagulation process: Optimization through response surface methodology.* Desalination, 2011. **271**(1): p. 209-218.

33. Kumari, S., et al., *Application of RSM for Bioremoval of Methylene Blue Dye from Industrial Wastewater onto Sustainable Walnut Shell (Juglans regia) Biomass.* Water, 2022. **14**(22): p. 3651.

34. Khoshraftar, Z., H. Masoumi, and A. Ghaemi, *Experimental, response surface methodology (RSM) and mass transfer modeling of heavy metals elimination using dolomite powder as an economical adsorbent.* Case Studies in Chemical and Environmental Engineering, 2023. **7**: p. 100329.

35. Khakbaz, M., A. Ghaemi, and G. Mir Mohamad Sadeghi, *Heavy metal elimination using hyper-cross-linked waste polycarbonate resin as an effective adsorbent: experimental and RSM optimization.* Iranian Polymer Journal, 2023. **32**(8): p. 947-968.

36. Das, T. and D.K. Patel, *Efficient removal of cationic dyes using lemon peel-chitosan hydrogel composite: RSM-CCD optimization and adsorption studies.* International Journal of Biological Macromolecules, 2024. **275**: p. 133561.

37. Rose, P.K., et al., *Congo red dye adsorption onto cationic amino-modified walnut shell: Characterization, RSM optimization, isotherms, kinetics, and mechanism studies.* Groundwater for Sustainable Development, 2023. **21**: p. 100931.

38. Cheikh, S., et al., *Adsorption behavior and mechanisms of the emerging antibiotic pollutant norfloxacin on eco-friendly and low-cost hydroxyapatite: Integrated experimental and response surface methodology optimized adsorption process.* Journal of Molecular Liquids, 2023. **392**: p. 123424.

39. Kim Ngan Tran, T., et al., *Optimization of ciprofloxacin adsorption onto CoFe-MOF aerogel cylinders based on response surface methodology: Adsorption kinetics, isotherm models.* Materials Science and Engineering: B, 2023. **297**: p. 116694.

40. Nezhad, N.T., et al., *Vanadium dioxide nanoparticles as a promising sorbent for controlled removal of waterborne fluoroquinolone ciprofloxacin.* Materials Chemistry and Physics, 2021. **259**: p. 123993.

41. Ghadami, F., et al., *Synthesis of a novel $HoFeO_3$/$Ho_3Fe_5O_{12}$ nanoadsorbent for efficient absorption of ciprofloxacin from liquid-phase: Modeling and optimization using response surface methodology.* Journal of Industrial and Engineering Chemistry, 2024. **129**: p. 143-157.

42. Yousefi, M., et al., *Comparison of LSSVM and RSM in simulating the removal of ciprofloxacin from aqueous solutions using magnetization of functionalized multi-walled carbon nanotubes: Process optimization using GA and RSM*

techniques. Journal of Environmental Chemical Engineering, 2021. **9**(4): p. 105677.

43. Zhong, S., et al., *Machine learning: New ideas and tools in environmental science and engineering.* Environmental Science & Technology, 2021. **55**(19): p. 12741-12754.
44. Zhu, M., et al., *A review of the application of machine learning in water quality evaluation.* Eco-Environment & Health, 2022. **1**(2): p. 107-116.
45. Shafiullah, M., K.A. AlShumayri, and M.S. Alam, *Machine learning tools for active distribution grid fault diagnosis.* Advances in Engineering Software, 2022. **173**: p. 103279.
46. Rahman, M.M., et al., *Decision tree-based ensemble model for predicting national greenhouse gas emissions in Saudi Arabia.* Applied Sciences, 2023. **13**(6): p. 3832.
47. Alam, M.S., S.P. Tiwari, and S.M. Rahman, *Optimized ensemble machine learning models for predicting Phytoplankton absorption coefficients.* IEEE Access, 2024. **12**: p. 5760-5769.
48. Torabi Fard, N., et al., *Esterification modification of graphene oxide for metronidazole release: Optimization and modelling using response surface methodology and artificial neural networks.* Journal of Molecular Liquids, 2024. **399**: p. 124393.
49. Dolatabadi, M., et al., *Adsorption of tetracycline antibiotic onto modified zeolite: Experimental investigation and modeling.* MethodsX, 2020. **7**: p. 100885.
50. Khazaie, A., et al., *Adsorption modeling of tetracycline removal by multi-walled carbon nanotube functionalized with aspartic acid and poly-pyrrole using Bayesian optimized artificial neural network.* Journal of the Taiwan Institute of Chemical Engineers, 2023. **144**: p. 104743.
51. Shang, Q., et al., *Photocatalytic degradation of ofloxacin antibiotic wastewater using TS-1/C_3N_4 composite photocatalyst: Reaction performance optimisation and estimation of wastewater component synergistic effect by artificial neural*

network and genetic algorithm. Chemical Engineering Journal, 2022. **443**: p. 136354.

52. Samadi-Maybodi, A. and M. Nikou, *Removal of sarafloxacin from aqueous solution by a magnetized metal-organic framework; Artificial neural network modeling.* Polyhedron, 2020. **179**: p. 114342.
53. Bennemla, M., M. Chabani, and A. Amrane, *Photocatalytic degradation of oxytetracycline in aqueous solutions with TiO_2 in suspension and prediction by artificial neural networks.* International Journal of Chemical Kinetics, 2016. **48**(8): p. 464-473.
54. Tkaczyk, A., K. Mitrowska, and A. Posyniak, *Synthetic organic dyes as contaminants of the aquatic environment and their implications for ecosystems: A review.* Science of The Total Environment, 2020. **717**: p. 137222.
55. Li, M., et al., *Occurrence, risk, and treatment of ciprofloxacin and clarithromycin in drainage.* Chemical Engineering Journal, 2023. **466**: p. 142968.
56. Nguyen, M.-K., et al., *Occurrence and fate of pharmaceutical pollutants in wastewater: Insights on ecotoxicity, health risk, and state–of–the-art removal.* Chemosphere, 2024. **354**: p. 141678.
57. Ren, L., et al., *One-step solvothermal synthesis of Fe_3O_4@Carbon composites and their application in removing of Cr (VI) and Congo red.* Ceramics International, 2019. **45**(7, Part B): p. 9646-9652.
58. Mishra, S., et al., *Cobalt ferrite nanoparticles prepared by microwave hydrothermal synthesis and adsorption efficiency for organic dyes: Isotherms, thermodynamics and kinetic studies.* Advanced Powder Technology, 2020. **31**(11): p. 4552-4562.
59. Rahimi, Z., et al., *Hydrothermal synthesis of magnetic $CoFe_2O_4$ nanoparticles and $CoFe_2O_4$/MWCNTs nanocomposites for U and Pb removal from aqueous solutions.* Journal of Radioanalytical and Nuclear Chemistry, 2018. **317**(1): p. 431-442.

60. Prasannamedha, G., P. Senthil Kumar, and V. Shankar, *Facile route for synthesis of $Fe^0/Fe_3C/\gamma$-Fe_2O_3 carbon composite using hydrothermal carbonization of sugarcane bagasse and its use as effective adsorbent for sulfamethoxazole removal.* Chemosphere, 2022. **289**: p. 133214.

61. Habibi, M.K., et al., *Synthesis of $ZnFe_2O_4$: 1 wt% Ce^{3+}/Carbon fibers composite and investigation of its adsorption characteristic to remove Congo red dye from aqueous solutions.* Journal of Alloys and Compounds, 2022. **890**: p. 161901.

62. Patra, T., et al., *Effect of calcination temperature on morphology and phase transformation of MnO_2 nanoparticles: A step towards green synthesis for reactive dye adsorption.* Chemosphere, 2022. **288**: p. 132472.

63. Irawan, C., I.F. Nata, and C.-K. Lee, *Removal of Pb(II) and As(V) using magnetic nanoparticles coated montmorillonite via one-pot solvothermal reaction as adsorbent.* Journal of Environmental Chemical Engineering, 2019. **7**(2): p. 103000.

64. Mpelane, S., et al., *Synthesis of mesoporous iron oxide nanoparticles for adsorptive removal of levofloxacin from aqueous solutions: Kinetics, isotherms, thermodynamics and mechanism.* Alexandria Engineering Journal, 2022. **61**(11): p. 8457-8468.

65. Bhavsar, K.S., et al., *Solvothermal synthesis of activated carbon loaded CdS nanoflowers: Boosted photodegradation of dye by adsorption and photocatalysis synergy.* Chemical Physics Letters, 2020. **744**: p. 137202.

66. Zhang, X., et al., *Efficient adsorptive elimination of organic pollutants from aqueous solutions on ZIF-8/MWCNTs-COOH nanoadsorbents: Adsorption kinetics, isotherms, and thermodynamic study.* Journal of Industrial and Engineering Chemistry, 2022. **111**: p. 155-167.

67. Sangor, F.I.M.S. and M.A. Al-Ghouti, *Waste-to-value: Synthesis of nano-aluminum oxide (nano-γ-Al_2O_3) from waste aluminum foils for efficient adsorption of methylene blue dye.* Case Studies in Chemical and Environmental Engineering, 2023. **8**: p. 100394.

68. Han, X.-W., et al., *γ-AlOOH decorated 3D-reduce graphene oxide: An effective adsorbent for removal of methylene blue and ciprofloxacin.* Colloids and Surfaces A: Physicochemical and Engineering Aspects, 2024. **685**: p. 133244.

69. Rajendran, J., et al., *Methylene blue and methyl orange removal from wastewater by magnetic adsorbent based on activated carbon synthesised from watermelon shell.* Desalination and Water Treatment, 2024. **317**: p. 100040.

70. Eyni Gavabari, S., et al., *Preparation of novel polyurethane/activated carbon/cellulose nano-whisker nanocomposite film as an efficient adsorbent for the removal of methylene blue and basic violet 16 dyes from wastewater.* Separation and Purification Technology, 2024. **330**: p. 125285.

71. Luong, H.V.T., et al., *A graphene oxide based composite granule for methylene blue separation from aqueous solution: Adsorption, kinetics and thermodynamic studies.* Heliyon, 2024. **10**(7): p. e28648.

72. Soudagar, S., et al., *Adsorption of methylene blue dye on nano graphene oxide-thermodynamics and kinetic studies.* Materials Today: Proceedings, 2022. **59**: p. 667-672.

73. Kim Ngan Tran, T., et al., *Co-doped Fe-MOF bimetallic organic framework applied as adsorbent to treat methylene blue dye in wastewater.* Materials Today: Proceedings, 2023.

74. Khooni, M.A.-K., H. Ahmadzadeh, and M. Davardoostmanesh, *Magnetic graphene oxide/Mg-Al layered double hydroxide nanocomposite as an efficient adsorbent for removal of methylene blue: A study of equilibrium isotherms, kinetics, thermodynamic and reusability.* Materials Science and Engineering: B, 2024. **300**: p. 117123.

75. salah omer, A., et al., *Adsorption of crystal violet and methylene blue dyes using a cellulose-based adsorbent from sugercane bagasse: characterization, kinetic and isotherm studies.* Journal of Materials Research and Technology, 2022. **19**: p. 3241-3254.

76. Geranmayeh, S., S. Mastali, and M. Mohammadnejad, *Functionalized iron Oxide/MOF nanocomposite exhibiting excellent performance for methylene blue adsorption.* Inorganic Chemistry Communications, 2024. **162**: p. 112222.

77. Smart, A., et al., *Sniffing out resistance–rapid identification of urinary tract infection-causing bacteria and their antibiotic susceptibility using volatile metabolite profiles.* Journal of pharmaceutical and biomedical analysis, 2019. **167**: p. 59-65.

78. Wagenlehner, F., et al., *Explorative randomized phase II clinical study of the efficacy and safety of finafloxacin versus ciprofloxacin for treatment of complicated urinary tract infections.* Antimicrobial agents and chemotherapy, 2018. **62**(4): p. 10.1128/aac. 02317-17.

79. Lee, S.-H., et al., *Detection status and removal characteristics of pharmaceuticals in wastewater treatment effluent.* Journal of Water Process Engineering, 2019. **31**: p. 100828.

80. Ebert, I., et al., *Toxicity of the fluoroquinolone antibiotics enrofloxacin and ciprofloxacin to photoautotrophic aquatic organisms.* Environmental toxicology and chemistry, 2011. **30**(12): p. 2786-2792.

81. Gupta, A. and A. Garg, *Degradation of ciprofloxacin using Fenton's oxidation: Effect of operating parameters, identification of oxidized by-products and toxicity assessment.* Chemosphere, 2018. **193**: p. 1181-1188.

82. Almomani, F., et al., *Potential use of solar photocatalytic oxidation in removing emerging pharmaceuticals from wastewater: A pilot plant study.* Solar Energy, 2018. **172**: p. 128-140.

83. Stuart, M., et al., *Review of risk from potential emerging contaminants in UK groundwater.* Science of the Total Environment, 2012. **416**: p. 1-21.

84. Nie, X., et al., *Response of the freshwater alga Chlorella vulgaris to trichloroisocyanuric acid and ciprofloxacin.* Environmental Toxicology and Chemistry: An International Journal, 2008. **27**(1): p. 168-173.

85. González-Pleiter, M., et al., *Toxicity of five antibiotics and their mixtures towards photosynthetic aquatic organisms: implications for environmental risk assessment.* Water research, 2013. **47**(6): p. 2050-2064.

86. Magdaleno, A., et al., *Effects of six antibiotics and their binary mixtures on growth of Pseudokirchneriella subcapitata.* Ecotoxicology and Environmental Safety, 2015. **113**: p. 72-78.

87. Shen, R., et al., *The cardiovascular toxicity induced by high doses of gatifloxacin and ciprofloxacin in zebrafish.* Environmental Pollution, 2019. **254**: p. 112861.

88. Maul, J.D., et al., *Effects of the antibiotic ciprofloxacin on stream microbial communities and detritivorous macroinvertebrates.* Environmental Toxicology and Chemistry: An International Journal, 2006. **25**(6): p. 1598-1606.

89. Johansson, C.H., L. Janmar, and T. Backhaus, *Toxicity of ciprofloxacin and sulfamethoxazole to marine periphytic algae and bacteria.* Aquatic toxicology, 2014. **156**: p. 248-258.

90. Näslund, J., J.E. Hedman, and C. Agestrand, *Effects of the antibiotic ciprofloxacin on the bacterial community structure and degradation of pyrene in marine sediment.* Aquatic toxicology, 2008. **90**(3): p. 223-227.

91. Ahmadi, S., et al., *Efficacy of persulfate-based advanced oxidation process (US/PS/Fe_3O_4) for ciprofloxacin removal from aqueous solutions.* Applied Water Science, 2020. **10**(8): p. 1-6.

92. Wang, W., et al., *Effect of humic acid on ciprofloxacin removal by magnetic multifunctional resins.* Scientific reports, 2016. **6**(1): p. 30331.

93. Bajpai, S. and M. Bhowmik, *Poly (acrylamide-co-itaconic acid) as a potential ion-exchange sorbent for effective removal of antibiotic drug-ciprofloxacin from aqueous solution.* Journal of Macromolecular Science, Part A, 2010. **48**(2): p. 108-118.

94. Wang, C.-J., et al., *Cation exchange interaction between antibiotic ciprofloxacin and montmorillonite.* Journal of Hazardous Materials, 2010. **183**(1-3): p. 309-314.

95. Barisci, S. and O. Turkay. *Applications of response surface methodology (RSM) for the optimization of ciprofloxacin removal by electrocoagulation*. in *Proceedings of the IWA Balkan Young Water Professionals Conference*. 2015.

96. Hannmann, L., et al., *Removal of ciprofloxacin from water with chemical oxidation.* Worcester Polytechnic Institute (WPI), Worcester, MA, 2012.

97. Hom-Diaz, A., et al., *Ciprofloxacin removal during secondary domestic wastewater treatment in high rate algal ponds.* Chemosphere, 2017. **180**: p. 33-41.

98. Carneiro, R.B., et al., *Feasibility of anaerobic packed and structured-bed reactors for sulfamethoxazole and ciprofloxacin removal from domestic sewage.* Science of the total environment, 2019. **678**: p. 419-429.

99. Jia, Y., et al., *Ciprofloxacin degradation in anaerobic sulfate-reducing bacteria (SRB) sludge system: mechanism and pathways.* Water research, 2018. **136**: p. 64-74.

100. Al-Ahmad, A., F. Daschner, and K. Kümmerer, *Biodegradability of cefotiam, ciprofloxacin, meropenem, penicillin G, and sulfamethoxazole and inhibition of waste water bacteria.* Archives of environmental contamination and toxicology, 1999. **37**: p. 158-163.

101. Do, M.T. and D.C. Stuckey, *Fate and removal of Ciprofloxacin in an anaerobic membrane bioreactor (AnMBR).* Bioresource technology, 2019. **289**: p. 121683.

102. Eccles, H., *Ion exchange-future challenges/opportunities in environmental clean-up*, in *Progress in Ion Exchange*. 1997, Elsevier. p. 245-259.

103. Banerjee, S., et al. *Synthesis of Hydrophobic Ceramic Ultrafiltration Membrane and Performance Evaluation for Removal of Ciprofloxacin in Water*. in *Waste Water Recycling and Management: 7th IconSWM–ISWMAW 2017, Volume 3*. 2019. Springer.

104. Alonso, J.J.S., et al., *Removal of ciprofloxacin from seawater by reverse osmosis.* Journal of environmental management, 2018. **217**: p. 337-345.

105. Shuang, C., et al., *Quaternized magnetic microspheres for the efficient removal of reactive dyes.* Water research, 2012. **46**(14): p. 4417-4426.

106. Reverberi, A., et al., *Membrane processes for water recovery and decontamination.* Current opinion in chemical engineering, 2014. **6**: p. 75-82.

107. Nwabanne, J.T., C.A. Igwegbe, and S.O. Okpo. *Removal of copper, nickel, and chromium from simulated wastewater using electrocoagulation technique*. in *International conference proceedings: faculty of engineering, Unizik*. 2018.

108. Lippi, M., et al., *State of art of landfill leachate treatment: literature review and critical evaluation.* Ciência e Natura, 2018: p. e78-e78.

109. Ahmadi, S., C.A. Igwegbe, and S. Rahdar, *The application of thermally activated persulfate for degradation of Acid Blue 92 in aqueous solution.* International Journal of Industrial Chemistry, 2019. **10**: p. 249-260.

110. An, T., et al., *Kinetics and mechanism of advanced oxidation processes (AOPs) in degradation of ciprofloxacin in water.* Applied Catalysis B: Environmental, 2010. **94**(3-4): p. 288-294.

111. Matavos-Aramyan, S. and M. Moussavi, *Advances in Fenton and Fenton based oxidation processes for industrial effluent contaminants control-a review.* Int. J. Environ. Sci. Nat. Resour, 2017. **2**(4): p. 1-18.

112. Sun, S.-P., et al., *Degradation of antibiotic ciprofloxacin hydrochloride by photo-Fenton oxidation process.* Environmental Engineering Science, 2009. **26**(4): p. 753-759.

113. Salari, M., G.R. Rakhshandehroo, and M.R. Nikoo, *Degradation of ciprofloxacin antibiotic by Homogeneous Fenton oxidation: Hybrid AHP-PROMETHEE method, optimization, biodegradability improvement and identification of oxidized by-products.* Chemosphere, 2018. **206**: p. 157-167.

114. Mi, X., et al., *Electro-Fenton degradation of ciprofloxacin with highly ordered mesoporous $MnCo_2O_4$-CF cathode: Enhanced redox capacity and accelerated electron transfer.* Chemical Engineering Journal, 2019. **358**: p. 299-309.

115. Matzek, L.W., et al., *Understanding electrochemically activated persulfate and its application to ciprofloxacin abatement.* Environmental science & technology, 2018. **52**(10): p. 5875-5883.

116. Sani, O.N., M. Yazdani, and M. Taghavi, *Catalytic ozonation of ciprofloxacin using γ-Al_2O_3 nanoparticles in synthetic and real wastewaters.* Journal of Water Process Engineering, 2019. **32**: p. 100894.

117. Sui, M., et al., *Heterogeneous catalytic ozonation of ciprofloxacin in water with carbon nanotube supported manganese oxides as catalyst.* Journal of hazardous materials, 2012. **227**: p. 227-236.

118. De Witte, B., et al., *Ozonation and advanced oxidation by the peroxone process of ciprofloxacin in water.* Journal of hazardous materials, 2009. **161**(2-3): p. 701-708.

119. Rhmani, A., et al., *Efficiency of ciprofloxacin removal by ozonation process with calcium peroxide from aqueous solutions.* Journal of Inflammatory Diseases, 2015. **19**(2): p. 55-64.

120. Igwegbe, C.A., et al., *Efficiency comparison of advanced oxidation processes for ciprofloxacin removal from aqueous solutions: Sonochemical, sono-nano-chemical and sono-nano-chemical/persulfate processes.* Environmental engineering research, 2020. **25**(2): p. 178-185.

121. De Bel, E., et al., *Sonolysis of ciprofloxacin in aqueous solution: Influence of operational parameters.* Ultrasonics sonochemistry, 2011. **18**(1): p. 184-189.

122. Banach, A.M., A. Mollazehi, and S. Ahmadi, *Survey on the removal of ciprofloxacin from aqueous solutions by nano-sono-catalytic process.* Desalination and Water Treatment, 2018. **136**: p. 207-211.

123. Hassani, A., et al., *Sonocatalytic degradation of ciprofloxacin using synthesized TiO_2 nanoparticles on montmorillonite.* Ultrasonics sonochemistry, 2017. **35**: p. 251-262.

124. Guo, H.-G., et al., *Photochemical degradation of ciprofloxacin in UV and UV/H_2O_2 process: kinetics, parameters, and products.* Environmental Science and Pollution Research, 2013. **20**: p. 3202-3213.

125. Belden, J., J. Maul, and M. Lydy, *Partitioning and photodegradation of ciprofloxacin in aqueous systems in the presence of organic matter.* Chemosphere, 2007. **66**(8): p. 1390-1395.

126. Rahdar, S., et al., *Efficiency of sono-nano-catalytic process of magnesium oxide nano particle in removal of penicillin G from aqueous solution.* Desalination and Water Treatment, 2018. **106**: p. 330-335.

127. Yang, H., et al., *Comparison of ciprofloxacin degradation in reclaimed water by UV/chlorine and UV/persulfate advanced oxidation processes.* Water Environment Research, 2019. **91**(12): p. 1576-1588.

128. Deng, J., et al., *Degradation of ciprofloxacin using α-MnO_2 activated peroxymonosulfate process: effect of water constituents, degradation intermediates and toxicity evaluation.* Chemical Engineering Journal, 2017. **330**: p. 1390-1400.

129. Ji, Y., et al., *Degradation of ciprofloxacin and sulfamethoxazole by ferrous-activated persulfate: implications for remediation of groundwater contaminated by antibiotics.* Science of the total environment, 2014. **472**: p. 800-808.

130. Mahdi-Ahmed, M. and S. Chiron, *Ciprofloxacin oxidation by UV-C activated peroxymonosulfate in wastewater.* Journal of hazardous materials, 2014. **265**: p. 41-46.

131. Durán-Álvarez, J.C., et al., *Photocatalytic degradation of ciprofloxacin using mono-(Au, Ag and Cu) and bi-(Au–Ag and Au–Cu) metallic nanoparticles supported on TiO_2 under UV-C and simulated sunlight.* Catalysis Today, 2016. **266**: p. 175-187.

132. Ye, S., et al., *Facile assembled biochar-based nanocomposite with improved graphitization for efficient photocatalytic activity driven by visible light.* Applied Catalysis B: Environmental, 2019. **250**: p. 78-88.

133. Zhang, X., et al., *Degradation of ciprofloxacin in aqueous bismuth oxybromide (BiOBr) suspensions under visible light irradiation: a direct hole oxidation pathway*. Chemical Engineering Journal, 2015. **274**: p. 290-297.

134. Sayed, M., et al., *Solar light responsive poly (vinyl alcohol)-assisted hydrothermal synthesis of immobilized TiO_2/Ti film with the addition of peroxymonosulfate for photocatalytic degradation of ciprofloxacin in aqueous media: a mechanistic approach.* The Journal of Physical Chemistry C, 2018. **122**(1): p. 406-421.

135. Naje, A.S., et al., *A review of electrocoagulation technology for the treatment of textile wastewater.* Reviews in Chemical Engineering, 2017. **33**(3): p. 263-292.

136. Ahmadzadeh, S., et al., *Removal of ciprofloxacin from hospital wastewater using electrocoagulation technique by aluminum electrode: Optimization and modelling through response surface methodology.* Process Safety and Environmental Protection, 2017. **109**: p. 538-547.

137. Yoosefian, M., et al., *Optimization of electrocoagulation process for efficient removal of ciprofloxacin antibiotic using iron electrode; kinetic and isotherm studies of adsorption*. Journal of Molecular Liquids, 2017. **225**: p. 544-553.

138. Igwegbe, C.A., O.D. Onukwuli, and P.C. Onyechi, *Optimal Route for Turbidity removal from Aquaculture Wastewater by Electrocoagulation-flocculation process.* UNIZIK Journal of Engineering and Applied Sciences, 2019. **15**(1): p. 99-108.

139. Tasca, A.L., et al., *Ciprofloxacin removal: BDD anode coupled with solid polymer electrolyte and ultrasound irradiation.* Journal of Water Process Engineering, 2020. **33**: p. 101074.

140. Prieto, A., et al., *Degradation of the antibiotics norfloxacin and ciprofloxacin by a white-rot fungus and identification of degradation products.* Bioresource technology, 2011. **102**(23): p. 10987-10995.

141. Igwegbe, C.A. and O.D. Onukwuli, *Removal of total dissolved solids (TDS) from aquaculture wastewater by coagulation-flocculation process using Sesamum indicum extract: effect of operating parameters and coagulation-flocculation kinetics.* Pharm Chem J, 2019. **6**(4): p. 32-45.

142. Zhang, L., et al., *Enhanced phosphorus and ciprofloxacin removal in a modified BAF system by configuring Fe-C micro electrolysis: Investigation on pollutants removal and degradation mechanisms.* Journal of hazardous materials, 2018. **342**: p. 705-714.

143. Choi, H.-J., *Agricultural bio-waste for adsorptive removal of crude oil in aqueous solution.* Journal of Material Cycles and Waste Management, 2019. **21**: p. 356-364.

144. Umembamalu, C.J., et al., *Packed bed column adsorption of oil and grease from refinery desalter effluent, using rice husks derived carbon as the adsorbent: Influence of process parameters and Bohart–Adams kinetics study.* World News of Natural Sciences, 2020. **31**: p. 155-174.

145. Ahmadi, S., et al., *Removal of Remazol Black B from aqueous solution using P-γ-Fe_2O_3 nanoparticles: synthesis, physical characterization, isotherm, kinetic and thermodynamic studies.* Desalination and water treatment, 2019. **152**: p. 401-410.

146. Pathania, D., S. Sharma, and P. Singh, *Removal of methylene blue by adsorption onto activated carbon developed from Ficus carica bast.* Arabian journal of chemistry, 2017. **10**: p. S1445-S1451.

147. Ariffin, N., et al. *Review on adsorption of heavy metal in wastewater by using geopolymer*. in *MATEC Web of Conferences*. 2017. EDP Sciences.

148. Banerjee, S., et al., *Study on adsorption behavior of Acid Orange 10 onto modified wheat husk.* Desalination and Water Treatment, 2016. **57**(26): p. 12302-12315.

149. Wu, Q., et al., *Adsorption and intercalation of ciprofloxacin on montmorillonite.* Applied Clay Science, 2010. **50**(2): p. 204-211.

150. Duan, W., et al., *Ciprofloxacin adsorption onto different micro-structured tourmaline, halloysite and biotite.* Journal of Molecular Liquids, 2018. **269**: p. 874-881.

151. Li, Z., et al., *A mechanistic study of ciprofloxacin removal by kaolinite.* Colloids and Surfaces B: Biointerfaces, 2011. **88**(1): p. 339-344.

152. Ahmadi, S., et al., *Study survey of cupric oxide nanoparticles in removal efficiency of ciprofloxacin antibiotic from aqueous solution: adsorption isotherm study.* 2017.

153. Dhiman, N. and N. Sharma, *Batch adsorption studies on the removal of ciprofloxacin hydrochloride from aqueous solution using ZnO nanoparticles and groundnut (Arachis hypogaea) shell powder: a comparison.* Indian Chemical Engineer, 2019. **61**(1): p. 67-76.

154. Khoshnamvand, N., S. Ahmadi, and F.K. Mostafapour, *Kinetic and isotherm studies on ciprofloxacin an adsorption using magnesium oxide nanopartices.* Journal of Applied Pharmaceutical Science, 2017. **7**(11): p. 079-083.

155. Rahdar, S., et al., *Synthesis and physical characterization of nickel oxide nanoparticles and its application study in the removal of ciprofloxacin from contaminated water by adsorption: equilibrium and kinetic studies.* Desalination and water treatment, 2019. **141**: p. 386-393.

156. Sun, Y., et al., *Adsorption and cosorption of ciprofloxacin and Ni (II) on activated carbon-mechanism study.* Journal of the Taiwan Institute of Chemical Engineers, 2014. **45**(2): p. 681-688.

157. Carabineiro, S., et al., *Comparison between activated carbon, carbon xerogel and carbon nanotubes for the adsorption of the antibiotic ciprofloxacin.* Catalysis today, 2012. **186**(1): p. 29-34.

158. Zhang, X., et al., *Selective adsorption of micro ciprofloxacin by molecularly imprinted functionalized polymers appended onto ZnS.* Environmental technology, 2012. **33**(17): p. 2019-2025.

159. Yang, Q., et al., *Porous three-component hybrid hydrogen-bonded covalent organic polymers: Design, synthesis and ciprofloxacin adsorption.* European Polymer Journal, 2020. **123**: p. 109445.

160. Farzinmanesh, O., M.H. Sabzevari, and M.R. Asghariganjeh, *Efficient removal of ciprofloxacin and ofloxacin from aqueous solutions using a novel nano-scale adsorbent: Modeling, optimization, and characterization.* Chemosphere, 2024. **354**: p. 141640.

161. Ghadami, F., et al., *Synthesis of a novel $HoFeO_3$/$Ho_3Fe_5O_{12}$ nanoadsorbent for efficient absorption of ciprofloxacin from liquid-phase: Modeling and optimization using response surface methodology.* Journal of Industrial and Engineering Chemistry, 2024. **129**: p. 143-157.

162. Shahnaz, T., et al., *Use of Nanocellulose extracted from grass for adsorption abatement of Ciprofloxacin and Diclofenac removal with phyto, and fish toxicity studies.* Environmental Pollution, 2021. **268**: p. 115494.

163. Srivastava, A., et al., *Low cost iron modified syzygium cumini l. Wood biochar for adsorptive removal of ciprofloxacin and doxycycline antibiotics from aqueous solution.* Inorganic Chemistry Communications, 2022. **144**: p. 109895.

164. Wakejo, W.K., et al., *Enhanced ciprofloxacin removal from aqueous solution using a chemically modified biochar derived from bamboo sawdust: adsorption process optimization with response surface methodology.* Adsorption Science & Technology, 2022. **2022**: p. 1-23.

165. Chafyq, E.H., et al., *Adsorption of ciprofloxacin antibiotic on materials prepared from Moroccan oil shales.* Chemical Physics Letters, 2021. **778**: p. 138707.

166. Zhang, B., et al., *Response surface methodology approach for optimization of ciprofloxacin adsorption using activated carbon derived from the residue of desilicated rice husk.* Journal of Molecular Liquids, 2017. **238**: p. 316-325.

167. Fu, Y., et al., *Adsorption of ciprofloxacin pollutants in aqueous solution using modified waste grapefruit peel.* Energy Sources, Part A: Recovery, Utilization, and Environmental Effects, 2021. **43**(2): p. 225-234.

168. Najafpoor, A.A., et al., *Optimization of ciprofloxacin adsorption from synthetic wastewaters using γ-Al_2O_3 nanoparticles: An experimental design based on response surface methodology.* Colloid and Interface Science Communications, 2019. **33**: p. 100212.

169. Nguyen, N.T., et al., *Adsorption characteristic of ciprofloxacin antibiotic onto synthesized alpha alumina nanoparticles with surface modification by polyanion.* Journal of Molecular Liquids, 2020. **309**: p. 113150.

170. Mao, H., et al., *Modification of a magnetic carbon composite for ciprofloxacin adsorption.* Journal of environmental sciences, 2016. **49**: p. 179-188.

171. Sharifpour, N., et al., *Evaluation of the activated carbon coated with multiwalled carbon nanotubes in removal of ciprofloxacin from aqueous solutions.* Applied Water Science, 2020. **10**(6): p. 1-17.

172. Wu, Y., et al., *The correlation of adsorption behavior between ciprofloxacin hydrochloride and the active sites of Fe-doped MCM-41.* Frontiers in chemistry, 2018. **6**: p. 17.

173. Malakootian, M., A. Nasiri, and H. Mahdizadeh, *Preparation of $CoFe_2O_4$/activated carbon@ chitosan as a new magnetic nanobiocomposite for adsorption of ciprofloxacin in aqueous solutions.* Water Science and Technology, 2018. **78**(10): p. 2158-2170.

174. Falyouna, O., et al., *Promotion of ciprofloxacin adsorption from contaminated solutions by oxalate modified nanoscale zerovalent iron particles.* Journal of Molecular Liquids, 2022. **359**: p. 119323.

175. Birniwa, A.H., et al., *Synthesis of gum Arabic magnetic nanoparticles for adsorptive removal of ciprofloxacin: equilibrium, kinetic, thermodynamics studies, and optimization by response surface methodology.* Separations, 2022. **9**(10): p. 322.

176. Rizzi, V., et al., *Cyclodextrin nanosponges as adsorbent material to remove hazardous pollutants from water: The case of ciprofloxacin.* Chemical Engineering Journal, 2021. **411**: p. 128514.

177. Balarak, D., et al., *Adsorption of ciprofloxacin from aqueous solution onto synthesized NiO: isotherm, kinetic and thermodynamic studies.* Desalin Water Treat, 2021. **212**: p. 390-400.

178. Al-Musawi, T.J., et al., *Effective adsorption of ciprofloxacin antibiotic using powdered activated carbon magnetized by iron (III) oxide magnetic nanoparticles.* Journal of porous materials, 2021. **28**: p. 835-852.

179. Rumman, G.A., et al., *Adsorption performance of an amine-functionalized MCM–41 mesoporous silica nanoparticle system for ciprofloxacin removal.* Environmental Nanotechnology, Monitoring & Management, 2021. **16**: p. 100536.

180. Aydin, S., et al., *Removal of antibiotics from aqueous solution by using magnetic Fe_3O_4/red mud-nanoparticles.* Science of the total environment, 2019. **670**: p. 539-546.

181. Gulen, B. and P. Demircivi, *Adsorption properties of flouroquinolone type antibiotic ciprofloxacin into 2:1 dioctahedral clay structure: Box-Behnken experimental design.* Journal of Molecular Structure, 2020. **1206**: p. 127659.

182. Khan, N.A., et al., *Development of Mn-PBA on GO sheets for adsorptive removal of ciprofloxacin from water: kinetics, isothermal, thermodynamic and mechanistic studies.* Materials chemistry and physics, 2020. **245**: p. 122737.

183. Rahman, N. and P. Varshney, *Facile synthesis and characterization of Zn (II)-impregnated chitosan/graphene oxide: evaluation of its efficiency for removal of ciprofloxacin from aqueous solution.* Journal of Inorganic and Organometallic Polymers and Materials, 2021. **31**(8): p. 3595-3612.

184. Han, L., et al., *Graphene-boron nitride composite aerogel: a high efficiency adsorbent for ciprofloxacin removal from water.* Separation and Purification Technology, 2021. **278**: p. 119605.

185. Li, R., et al., *Enhanced adsorption of ciprofloxacin by KOH modified biochar derived from potato stems and leaves.* Water Science and Technology, 2018. **77**(4): p. 1127-1136.

186. Kumar, A., et al., *Effect of magnetization on the adsorptive removal of an emerging contaminant ciprofloxacin by magnetic acid activated carbon.* Environmental Research, 2022. **206**: p. 112604.

187. Pham, T.D., et al., *Adsorptive removal of antibiotic ciprofloxacin from aqueous solution using protein-modified nanosilica.* Polymers, 2020. **12**(1): p. 57.

188. Zheng, K., et al., *Removal of ciprofloxacin from aqueous solution using long TiO_2 nanotubes with a high specific surface area.* RSC advances, 2016. **6**(5): p. 3625-3631.

189. Zide, D., et al., *Zeolite 'adsorption'capacities in aqueous acidic media; The role of acid choice and quantification method on ciprofloxacin removal.* Microporous and Mesoporous Materials, 2018. **255**: p. 226-241.

190. Li, X., et al., *Adsorption of ciprofloxacin, bisphenol and 2-chlorophenol on electrospun carbon nanofibers: in comparison with powder activated carbon.* Journal of colloid and interface science, 2015. **447**: p. 120-127.

191. Balarak, D., F.K. Mostafapour, and H. Azarpira, *Adsorption kinetics and equilibrium of ciprofloxacin from aqueous solutions using Corylus avellana (Hazelnut) activated carbon.* British journal of pharmaceutical research, 2016. **13**(3): p. 1-14.

192. Bizi, M. and F. El Bachra, *Evaluation of the ciprofloxacin adsorption capacity of common industrial minerals and application to tap water treatment.* Powder technology, 2020. **362**: p. 323-333.

193. Wang, F., et al., *Removal of ciprofloxacin from aqueous solution by a magnetic chitosan grafted graphene oxide composite.* Journal of Molecular Liquids, 2016. **222**: p. 188-194.

194. Sun, Y., et al., *Characterization and ciprofloxacin adsorption properties of activated carbons prepared from biomass wastes by H_3PO_4 activation.* Bioresource technology, 2016. **217**: p. 239-244.

195. Carabineiro, S., et al., *Adsorption of ciprofloxacin on surface-modified carbon materials.* Water research, 2011. **45**(15): p. 4583-4591.

196. Li, H., et al., *Adsorption of antibiotic ciprofloxacin on carbon nanotubes: pH dependence and thermodynamics.* Chemosphere, 2014. **95**: p. 150-155.

197. Borkovec, M. and G. Papastavrou, *Interactions between solid surfaces with adsorbed polyelectrolytes of opposite charge.* Current opinion in colloid & interface science, 2008. **13**(6): p. 429-437.

198. Steiner, T., *The hydrogen bond in the solid state.* Angewandte Chemie International Edition, 2002. **41**(1): p. 48-76.

199. Weber Jr, W.J. and J.C. Morris, *Kinetics of adsorption on carbon from solution.* Journal of the sanitary engineering division, 1963. **89**(2): p. 31-59.

200. Afzal, M.Z., et al., *Enhancement of ciprofloxacin sorption on chitosan/biochar hydrogel beads.* Science of the Total Environment, 2018. **639**: p. 560-569.

201. Afzal, M.Z., et al., *Enhanced removal of ciprofloxacin using humic acid modified hydrogel beads.* Journal of colloid and interface science, 2019. **543**: p. 76-83.

202. Álvarez-Torrellas, S., et al., *Effective adsorption of non-biodegradable pharmaceuticals from hospital wastewater with different carbon materials.* Chemical Engineering Journal, 2017. **320**: p. 319-329.

203. Ashiq, A., et al., *Municipal solid waste biochar-bentonite composite for the removal of antibiotic ciprofloxacin from aqueous media.* Journal of environmental management, 2019. **236**: p. 428-435.

204. Arya, V. and L. Philip, *Adsorption of pharmaceuticals in water using Fe_3O_4 coated polymer clay composite.* Microporous and Mesoporous Materials, 2016. **232**: p. 273-280.

205. Ashiq, A., et al., *Sorption process of municipal solid waste biochar-montmorillonite composite for ciprofloxacin removal in aqueous media.* Chemosphere, 2019. **236**: p. 124384.

206. Amirmahani, N., et al., *Evaluating nanoparticles decorated on Fe_3O_4@SiO_2-Schiff base (Fe_3O_4@SiO_2-APTMS-HBA) in adsorption of ciprofloxacin from aqueous environments.* Journal of Inorganic and Organometallic Polymers and Materials, 2020. **30**: p. 3540-3551.

207. Caicedo, D.F., et al., *Efficient adsorbent based on construction and demolition wastes functionalized with 3-aminopropyltriethoxysilane (APTES) for the removal ciprofloxacin from hospital synthetic effluents.* Journal of Environmental Chemical Engineering, 2020. **8**(4): p. 103875.

208. Cao, E., et al., *Oriented growth of poly (m-phenylenediamine) on Calotropis gigantea fiber for rapid adsorption of ciprofloxacin.* Chemosphere, 2017. **171**: p. 223-230.

209. Chandrasekaran, A., et al., *Adsorptive removal of Ciprofloxacin and Amoxicillin from single and binary aqueous systems using acid-activated carbon from Prosopis juliflora.* Environmental Research, 2020. **188**: p. 109825.

210. Das, S., A. Barui, and A. Adak, *Montmorillonite impregnated electrospun cellulose acetate nanofiber sorptive membrane for ciprofloxacin removal from wastewater.* Journal of Water Process Engineering, 2020. **37**: p. 101497.

211. de Oliveira Carvalho, C., et al., *Kinetic, equilibrium, and thermodynamic studies on the adsorption of ciprofloxacin by activated carbon produced from Jerivá (Syagrus romanzoffiana).* Environmental Science and Pollution Research, 2019. **26**: p. 4690-4702.

212. Ezekoye, O.M., et al., *Biosorptive interaction of alkaline modified Dialium guineense seed powders with ciprofloxacin in contaminated solution: central composite, kinetics, isotherm, thermodynamics, and desorption.* International journal of phytoremediation, 2020. **22**(10): p. 1028-1037.

213. Genç, N., E. Can Dogan, and M. Yurtsever, *Bentonite for ciprofloxacin removal from aqueous solution.* Water science and technology, 2013. **68**(4): p. 848-855.

214. Ghadiri, S.K., et al., *Valorization of biomass into amine-functionalized bio graphene for efficient ciprofloxacin adsorption in water-modeling and optimization study.* Plos one, 2020. **15**(4): p. e0231045.

215. Fei, Y., et al., *Adsorptive removal of ciprofloxacin by sodium alginate/graphene oxide composite beads from aqueous solution.* Journal of colloid and interface science, 2016. **484**: p. 196-204.

216. Hu, D. and L. Wang, *Adsorption of ciprofloxacin from aqueous solutions onto cationic and anionic flax noil cellulose.* Desalination and Water Treatment, 2016. **57**(58): p. 28436-28449.

217. Hu, Y., et al., *An efficient adsorbent: Simultaneous activated and magnetic ZnO doped biochar derived from camphor leaves for ciprofloxacin adsorption.* Bioresource technology, 2019. **288**: p. 121511.

218. Kim, D.G., et al., *Addition of biochar into activated sludge improves removal of antibiotic ciprofloxacin.* Journal of Water Process Engineering, 2020. **33**: p. 101019.

219. Kumari, S., et al., *Efficient and highly selective adsorption of cationic dyes and removal of ciprofloxacin antibiotic by surface modified nickel sulfide nanomaterials: Kinetics, isotherm and adsorption mechanism.* Colloids and Surfaces A: Physicochemical and Engineering Aspects, 2020. **586**: p. 124264.

220. Li, X., et al., *Dynamic adsorption of ciprofloxacin on carbon nanofibers: quantitative measurement by in situ fluorescence.* Journal of water process engineering, 2016. **9**: p. e14-e20.

221. Li, M.-f., et al., *Cu(II)-influenced adsorption of ciprofloxacin from aqueous solutions by magnetic graphene oxide/nitrilotriacetic acid nanocomposite: competition and enhancement mechanisms.* Chemical Engineering Journal, 2017. **319**: p. 219-228.

222. Li, S., X. Zhang, and Y. Huang, *Zeolitic imidazolate framework-8 derived nanoporous carbon as an effective and recyclable adsorbent for removal of ciprofloxacin antibiotics from water.* Journal of hazardous materials, 2017. **321**: p. 711-719.

223. Li,M.-f.,etal., *Performance of magnetic graphene oxide/diethylenetriaminepentaacetic acid nanocomposite for the tetracycline and ciprofloxacin adsorption in single and binary systems.* Journal of colloid and interface science, 2018. **521**: p. 150-159.

224. Li, J., et al., *Study of ciprofloxacin removal by biochar obtained from used tea leaves.* Journal of Environmental Sciences, 2018. **73**: p. 20-30.

225. Li, L., et al., *Ionically cross-linked sodium alginate/κ-carrageenan double-network gel beads with low-swelling, enhanced mechanical properties, and excellent adsorption performance.* Chemical Engineering Journal, 2019. **372**: p. 1091-1103.

226. Ma, J., et al., *Enhanced adsorption for the removal of antibiotics by carbon nanotubes/graphene oxide/sodium alginate triple-network nanocomposite hydrogels in aqueous solutions.* Chemosphere, 2020. **242**: p. 125188.

227. Ma, J., et al., *Comparative study of graphene hydrogels and aerogels reveals the important role of buried water in pollutant adsorption.* Environmental science & technology, 2017. **51**(21): p. 12283-12292.

228. Peng, X., et al., *Adsorption behavior and mechanisms of ciprofloxacin from aqueous solution by ordered mesoporous carbon and bamboo-based carbon.* Journal of colloid and interface science, 2015. **460**: p. 349-360.

229. Peng, X., et al., *Preparation of a graphitic ordered mesoporous carbon and its application in sorption of ciprofloxacin: Kinetics, isotherm, adsorption mechanisms studies.* Microporous and Mesoporous Materials, 2016. **228**: p. 196-206.

230. Peng, X., et al., *Study of the adsorption mechanisms of ciprofloxacin antibiotics onto graphitic ordered mesoporous carbons.* Journal of the Taiwan Institute of Chemical Engineers, 2016. **65**: p. 472-481.

231. Peng, X., et al., *Amine-functionalized magnetic bamboo-based activated carbon adsorptive removal of ciprofloxacin and norfloxacin: A batch and fixed-bed column study.* Bioresource technology, 2018. **249**: p. 924-934.

232. Tang, Y., et al., *Engineering magnetic N-doped porous carbon with super-high ciprofloxacin adsorption capacity and wide pH adaptability.* Journal of hazardous materials, 2020. **388**: p. 122059.

233. Rasoulzadeh, H., et al., *Mechanistic investigation of ciprofloxacin recovery by magnetite–imprinted chitosan nanocomposite: isotherm, kinetic, thermodynamic and reusability studies.* International journal of biological macromolecules, 2019. **133**: p. 712-721.

234. Van Tran, T., et al., *MIL-53 (Fe)-directed synthesis of hierarchically mesoporous carbon and its utilization for ciprofloxacin antibiotic remediation.* Journal of Environmental Chemical Engineering, 2019. **7**(1): p. 102881.

235. Yang, Z., R. Xing, and W. Zhou, *Adsorption of ciprofloxacin and Cu^{2+} onto biochars in the presence of dissolved organic matter derived from animal manure.* Environmental Science and Pollution Research, 2019. **26**: p. 14382-14392.

236. Yang, Z., et al., *Adsorption characteristics of ciprofloxacin onto g-MoS_2 coated biochar nanocomposites.* Frontiers of environmental science & engineering, 2020. **14**: p. 1-10.

237. Yu, F., et al., *Adsorption mechanism and effect of moisture contents on ciprofloxacin removal by three-dimensional porous graphene hydrogel.* Journal of hazardous materials, 2019. **374**: p. 195-202.

238. Zeng, Z.-w., et al., *Comprehensive adsorption studies of doxycycline and ciprofloxacin antibiotics by biochars prepared at different temperatures.* Frontiers in chemistry, 2018. **6**: p. 80.

239. Zhou, Y., et al., *A novel Fe_3O_4/graphene oxide/citrus peel-derived bio-char based nanocomposite with enhanced adsorption affinity and sensitivity of ciprofloxacin and sparfloxacin.* Bioresource Technology, 2019. **292**: p. 121951.

240. Zhang, X., et al., *Novel alginate particles decorated with nickel for enhancing ciprofloxacin removal: characterization and mechanism analysis.* Ecotoxicology and environmental safety, 2019. **169**: p. 392-401.

241. Raji, Y., et al., *High adsorption capacities of crystal violet dye by low-cost activated carbon prepared from Moroccan Moringa oleifera wastes: Characterization, adsorption and mechanism study.* Diamond and Related Materials, 2023. **135**: p. 109834.

242. Bulin, C., *Adsorption mechanism and removal efficiency of magnetic graphene oxide-chitosan hybrid on aqueous Zn(II).* International Journal of Biological Macromolecules, 2023. **241**: p. 124588.

243. Aldoseri, A., K.N. Al-Khalifa, and A.M. Hamouda, *Re-thinking data strategy and Integration for artificial intelligence: Concepts, opportunities, and challenges.* Applied Sciences, 2023. **13**(12): p. 7082.

244. Islam, M.S.S., et al., *Optimizing short-term photovoltaic power forecasting: A novel approach with Gaussian process regression and Bayesian hyperparameter tuning.* Processes, 2024. **12**(3): p. 546.

245. Garnett, R., *Bayesian optimization*. 2023: Cambridge University Press.

246. Bergstra, J. and Y. Bengio, *Random search for hyper-parameter optimization.* Journal of machine learning research, 2012. **13**(2).

247. Wang, J., et al., *Adsorption Process Optimization and Adsorbent Evaluation Based on Langmuir Isotherm Model.* Langmuir, 2023. **39**(46): p. 16404-16414.

248. Pereira, S.K., et al., *A simplified modeling procedure for adsorption at varying pH conditions using the modified Langmuir–Freundlich isotherm.* Applied Water Science, 2022. **13**(1): p. 29.

249. Khan, A.S.A., *Evaluation of thermodynamic parameters of cadmium adsorption on sand from Temkin adsorption isotherm.* Turkish journal of chemistry, 2012. **36**(3): p. 437-443.

250. Cortés, J.C., et al., *Statistical analysis of randomized pseudo-first/second order kinetic models. Application to study the adsorption on cadmium ions onto tree fern.* Chemometrics and Intelligent Laboratory Systems, 2023. **240**: p. 104910.

251. Tran, H.N., *Applying Linear Forms of Pseudo-Second-Order Kinetic Model for Feasibly Identifying Errors in the Initial Periods of Time-Dependent Adsorption Datasets.* Water, 2023. **15**(6): p. 1231.

252. Douqin, M., et al., *Hydrothermal Synthesis of Nano-sized Cupric Tungstate (VI) Dihydrate and Its Synthesis Mechanism.* Rare Metal Materials and Engineering, 2014. **43**(12): p. 2917-2920.

253. Jalali, E., S. Maghsoudi, and E. Noroozian, *A novel method for biosynthesis of different polymorphs of TiO_2 nanoparticles as a protector for Bacillus thuringiensis from Ultra Violet.* Scientific Reports, 2020. **10**(1): p. 426.

254. Liao, M.-H., C.-H. Hsu, and D.-H. Chen, *Preparation and properties of amorphous titania-coated zinc oxide nanoparticles.* Journal of Solid State Chemistry, 2006. **179**(7): p. 2020-2026.

255. My Hang, T.T., et al., *Facile synthesis of copper tungstate ($CuWO_4$) for novel photocatalytic degradation of tetracycline under visible light.* Sustainable Chemistry and Pharmacy, 2021. **21**: p. 100407.

256. Borrajo, J.P., et al., *Influence of the network modifier content on the bioactivity of silicate glasses.* Key Engineering Materials, 2004. **254**: p. 23-26.

257. Anucha, C.B., et al., *Enhanced Photocatalytic Activity of $CuWO_4$ Doped TiO_2 Photocatalyst Towards Carbamazepine Removal under UV Irradiation.* Separations, 2021. **8**(3): p. 25.

258. Mecozzi, M. and E. Sturchio, *Computer Assisted Examination of Infrared and Near Infrared Spectra to Assess Structural and Molecular Changes in Biological Samples Exposed to Pollutants: A Case of Study.* Journal of Imaging, 2017. **3**(1): p. 11.

259. Janardhan, E., et al., *Synthesis of SnO Nanopatricles—A Hydrothermal Approach.* World Journal of Nano Science and Engineering, 2018. **8**: p. 33-37.

260. Yamakawa, K., Y. Sato, and K. Fukutani, *Asymmetric and symmetric absorption peaks observed in infrared spectra of CO_2 adsorbed on TiO_2 nanotubes.* The Journal of Chemical Physics, 2016. **144**(15).

261. Nandiyanto, A.B.D., R. Ragadhita, and M. Fiandini, *Interpretation of Fourier transform infrared spectra (FTIR): A practical approach in the polymer/plastic thermal decomposition.* Indonesian Journal of Science and Technology, 2023. **8**(1): p. 113-126.

262. Turkten, N., et al., *Copper-doped TiO_2 photocatalysts: application to drinking water by humic matter degradation.* Environmental Science and Pollution Research, 2019. **26**(36): p. 36096-36106.

263. Sajjad, A.K.L., et al., *One step activation of WO_x/TiO_2 nanocomposites with enhanced photocatalytic activity.* Applied Catalysis B: Environmental, 2009. **91**(1-2): p. 397-405.

264. Srinivasan, M. and T. White, *Degradation of methylene blue by three-dimensionally ordered macroporous titania.* Environmental science & technology, 2007. **41**(12): p. 4405-4409.

265. Hasan, M.R., et al., *A sol–gel derived, copper-doped, titanium dioxide–reduced graphene oxide nanocomposite electrode for the photoelectrocatalytic reduction of CO_2 to methanol and formic acid.* RSC Advances, 2015. **5**(95): p. 77803-77813.

266. Mathew, S., et al., *Cu-doped TiO_2: visible light assisted photocatalytic antimicrobial activity.* Applied Sciences, 2018. **8**(11): p. 2067.

267. He, D., et al., *Synergistic effect of TiO_2-$CuWO_4$ on the photocatalytic degradation of atrazine.* Environmental Science and Pollution Research, 2019. **26**: p. 12359-12367.

268. El-Naggar, N.E.-A., A.A. El-Bindary, and N.S. Nour, *Statistical optimization of process variables for antimicrobial metabolites production by Streptomyces anulatus NEAE-94 against some multidrug-resistant strains.* International Journal of Pharmacology, 2013. **9**(6): p. 322-334.

269. Ahmed, Y., et al., *Harnessing neural network model with optimization for enhanced ciprofloxacin antibiotic adsorption from contaminated water: A transparent and objective framework.* Journal of Water Process Engineering, 2024. **65**: p. 105724.

270. Salari, M., et al., *Optimizing Fenton-like process, homogeneous at neutral pH for ciprofloxacin degradation: Comparing RSM-CCD and ANN-GA.* Journal of Environmental Management, 2022. **317**: p. 115469.

271. He, F., et al., *Efficient decontamination of ciprofloxacin at neutral pH via visible light assisted Fenton–like process mediated by Fe(III)–GLDA complexation.* Chemosphere, 2022. **289**: p. 133199.

272. Dubey, S.R., S.K. Singh, and B.B. Chaudhuri, *Activation functions in deep learning: A comprehensive survey and benchmark.* Neurocomputing, 2022. **503**: p. 92-108.

273. Das, S., et al., *Sunlight assisted photocatalytic degradation of ciprofloxacin in water using Fe doped ZnO nanoparticles for potential public health applications.* International Journal of Environmental Research and Public Health, 2018. **15**(11): p. 2440.

274. Antonelli, R., et al., *Adsorption of ciprofloxacin onto thermally modified bentonite clay: Experimental design, characterization, and adsorbent regeneration.* Journal of Environmental Chemical Engineering, 2020. **8**(6): p. 104553.

275. Watanabe, N., et al., *On the recalcitrant nature of the triazinic ring species, cyanuric acid, to degradation in Fenton solutions and in UV-illuminated TiO_2 (naked) and fluorinated TiO_2 aqueous dispersions.* Journal of Photochemistry and Photobiology A: Chemistry, 2005. **174**(3): p. 229-238.

276. Zheng, C., et al., *Structural design of magnetic biosorbents for the removal of ciprofloxacin from water.* Bioresource Technology, 2020. **296**: p. 122288.

277. Shafiq, M., A.A. Alazba, and M.T. Amin, *Kinetic and Isotherm Studies of Ni^{2+} and Pb^{2+} Adsorption from Synthetic Wastewater Using Eucalyptus camdulensis—Derived Biochar.* Sustainability, 2021. **13**(7): p. 3785.

278. Gouda, M.H., N.A. Elessawy, and A. Toghan, *Development of hybrid green nanocomposite polymeric beads doped with nano sulfated zirconia for effective removal of Cefotaxime antibiotic from aqueous solution.* Scientific Reports, 2022. **12**(1): p. 12701.

279. Shi, J., et al., *Ciprofloxacin Removal via Acid-Modified Red Mud: Optimizing the Process, Analyzing the Adsorption Features, and Exploring the Underlying Mechanism.* Molecules, 2024. **29**(12): p. 2928.

280. da Silva de Assis, D.A., E.G. dos Santos, and D. Eiras, *Efficient and reusable mesoporous silica structures for ciprofloxacin removal from water media.* Journal of Water Process Engineering, 2024. **60**: p. 105144.

281. Zaman, H.G., et al., *Post Synthetic Modification of NH_2-(Zr-MOF) via Rapid Microwave-promoted Synthesis for Effective Adsorption of Pb(II) and Cd(II).* Arabian Journal of Chemistry, 2023. **16**(1): p. 104122.